PUBLICATIONS OF
THE UNIVERSITY OF EASTERN FINLAND

Dissertations in Forestry and Natural Sciences

CAROLINA VOIGT

EFFECTS OF CLIMATE WARMING AND PERMAFROST THAW ON GREENHOUSE GAS DYNAMICS IN SUBARCTIC ECOSYSTEMS

Carolina Voigt

EFFECTS OF CLIMATE WARMING AND PERMAFROST THAW ON GREENHOUSE GAS DYNAMICS IN SUBARCTIC ECOSYSTEMS

Publications of the University of Eastern Finland
Dissertations in Forestry and Natural Sciences
No 301

University of Eastern Finland
Kuopio
2018

Academic dissertation
To be presented by permission of the Faculty of Science and Forestry
for public examination in the Auditorium TTA in Tietoteknia Building
at the University of Eastern Finland, Kuopio, on 9th February 2018,
at 12 o'clock noon

Department of Environmental and Biological Sciences

Grano Oy
Jyväskylä, 2018
Editors: Pertti Pasanen, Matti Vornanen,
Jukka Tuomela, Matti Tedre

Distribution:
University of Eastern Finland / Sales of publications
www.uef.fi/kirjasto

ISBN: 978-952-61-2720-0 (Print)
ISBN: 978-952-61-2721-7 (PDF)
ISSNL: 1798-5668
ISSN: 1798-5668
ISSN: 1798-5676 (PDF)

Author's address: Carolina Voigt
University of Eastern Finland
Department of Environmental and Biological Sciences
P.O. Box 1627
70211 KUOPIO, FINLAND
email: carolina.voigt@uef.fi

Supervisors: Adj. Professor Christina Biasi
University of Eastern Finland
Department of Environmental and Biological Sciences
P.O. Box 1627
70211 KUOPIO, FINLAND
email: christina.biasi@uef.fi

Maija E. Marushchak, Ph.D.
University of Eastern Finland
Department of Environmental and Biological Sciences
P.O. Box 1627
70211 KUOPIO, FINLAND
email: maija.marushchak@uef.fi

Professor emer. Pertti J. Martikainen
University of Eastern Finland
Department of Environmental and Biological Sciences
P.O. Box 1627
70211 KUOPIO, FINLAND
email: pertti.martikainen@uef.fi

Reviewers: Professor Lars Kutzbach
University of Hamburg
Institute of Soil Science
Allende-Platz 2
20146 HAMBURG, GERMANY
email: lars.kutzbach@uni-hamburg.de

Assoc. Professor Christina Schädel
Northern Arizona University
Department of Biological Sciences
617 S. Beaver St.
86011, FLAGSTAFF, ARIZONA, USA
email: christina.schaedel@nau.edu

Opponent: Professor Steve Frolking
University of New Hampshire
Joint Appointment Depart. of Earth Sciences
Institute for the Study of Earth, Oceans, and Space
03824 DURHAM, NEW HAMPSHIRE, USA
email: steve.frolking@unh.edu

ABSTRACT

The Arctic region is warming, with temperatures rising faster than in the rest of the World. Under the current climate, Arctic soils act as a sink for carbon dioxide (CO_2) and a source of methane (CH_4). On-going warming and thawing of permafrost soils, however, will severely alter Arctic greenhouse gas (GHG) exchange. While the Arctic GHG balance is not well constrained even under the present climate, large uncertainties remain on how the biogeochemical cycling of Arctic ecosystems will react to a future climate.

The aim of this study is to shed light upon the effects of warming and simulated permafrost thaw on the GHG balance of subarctic tundra landscapes. These southern tundra regions, located in the marginal zone of permafrost distribution, experience rapid changes and will be one of the first Arctic ecosystems to react to climate warming. The data for this thesis was collected at two study sites, located in the Russian Arctic (67°03′ N, 62°55′ E) and in Finnish Lapland (68°89′ N, 21°05′ E). Simulated climate warming was achieved by *in situ* temperature manipulation on the dominant tundra surfaces in the study region (Russian Arctic): upland mineral tundra soils and permafrost peatlands. Sequential permafrost thaw was simulated in a climate-controlled chamber, using intact plant–soil systems (mesocosms) collected in a permafrost peatland (Finnish Lapland). Measurements of GHG fluxes were done by chamber techniques, and included not only CO_2 and CH_4, but also the strong GHG nitrous oxide (N_2O). To understand the regulatory parameters determining GHG exchange from various surfaces in the heterogeneous tundra landscape, flux measurements were complemented with detailed soil profile GHG measurements, as well as with vegetation analyses, and observations on environmental and soil physical-chemical parameters.

In situ warming increased emissions of all three GHGs from the dominant tundra surfaces, shifting the ecosystem from a growing season sink of -300 (peat soils) to -198 (mineral soils) g CO_2-eq m^{-2} into a net GHG source of up to 144 (peat soils) to 636 (mineral soils) g CO_2-eq m^{-2}. While CO_2 was the dominant GHG at the study site, CH_4 and N_2O emissions contributed to this shift from sink to source with warming. Methane emissions from these comparably dry tundra surfaces were small, but warming increased growing season CH_4 emissions from peat soils. A deeper active layer with simulated permafrost thaw on the other hand enhanced CH_4 uptake, with maximum uptake rates exceeding -10 mg CH_4 m^{-2} d^{-1} in vegetated permafrost peatland mesocosms. Additionally, warming increased N_2O emissions not only from bare peat surfaces which are known Arctic N_2O hot spots, but also from peat surfaces with vegetation cover. Downward leaching of water soluble compounds such as dissolved organic carbon was identified as a key process regulating GHG production at depth. Thawing of the upper permafrost layer revealed a previously unknown non-carbon feedback to the global climate: post-thaw N_2O emissions from bare peat surfaces increased five-fold (0.56 vs. 2.81 mg N_2O m^{-2} d^{-1}), with an increase in N_2O emissions

also from vegetated surfaces. This study identifies one fourth of the Arctic as an area with high potential for N_2O release, with soil nitrogen content, moisture and vegetation being the dominant regulators of the Arctic N_2O balance in a future climate. Permafrost thaw additionally increased old carbon release to the atmosphere, and revealed a high potential degradability of the exposed dissolved organic carbon pool in permafrost peatlands.
This study emphasizes the important role drier tundra surfaces, and permafrost peatlands in particular, will play in Arctic biogeochemistry as the climate warms, and highlights the vulnerability of these ecosystems to altered environmental conditions.

Universal Decimal Classification: 504.7, 551.345, 551.524, 551.588.7

CAB Thesaurus: greenhouse gases; climate change; environmental temperature; global warming; carbon dioxide; methane; nitrous oxide; permafrost; thawing; tundra; Arctic regions; peatlands; peat soils; nitrogen; moisture; vegetation

TIIVISTELMÄ (ABSTRACT IN FINNISH)

Arktinen alue lämpenee nopeammin kuin maapallomme muut alueet. Nykyisissä ilmasto-oloissa arktiset maat ovat hiilidioksidin (CO_2) nieluja ja metaanin (CH_4) lähteitä. Lämpeneminen ja ikiroudan sulaminen vaikuttavat kuitenkin merkittävästi näiden kasvihuonekaasujen vaihtoon arktisilla alueilla. Edes vallitsevissa oloissa arktisten alueiden kasvihuonekaasutasetta ei tunneta riittävän hyvin, ja hyvin suuria epävarmuuksia liittyy siihen, miten arktinen kasvihuonekaasutase tulee reagoimaan ilmastonmuutokseen.

Tämän tutkimuksen tavoitteena oli selvittää lämpenemisen ja simuloidun ikiroudan sulamisen vaikutuksia subarktisen tundran kasvihuonekaasutaseeseen. Nämä ikiroudan levinneisyysalueen etelärajalla sijaitsevat tundra-alueet ovat herkkiä ilmastonmuutoksen vaikutuksille. Tämän väitöskirjan aineisto kerättiin kahdelta Venäjän tundralla (67°03′ N, 62°55′ E) ja Suomen Lapissa (68°89′ N, 21°05′ E) sijaitsevalta tutkimusalueelta. Ilmastonmuutoksen vaikutuksia ikiroutasoiden ja tundran kivennäismaiden kaasunvaihtoon simuloitiin kenttäolosuhteissa venäläisellä tutkimusalueella tehdyssä lämmityskokeessa. Ikiroudan sulamista jäljiteltiin kontrolloiduissa laboratorio-olosuhteissa suoritetussa kokeessa, jossa käytettiin ikiroutasoilta Suomen Lapista kerättyjä kokonaisia turveprofiileja (mesokosmoksia) mukaan lukien paikalla luontaisesti esiintyvä kasvillisuus. Kasvihuonekaasuvoita mitattiin erilaisilla kammiomenetelmillä. Hiilidioksidi- ja metaanivuon lisäksi mitattiin myös voimakkaan kasvihuonekaasun, typpioksiduulin (N_2O) vuota. Tausta-aineistoksi kerättiin yksityiskohtaista tietoa kasvihuonekaasujen pitoisuuksista maaperäprofiilissa, kasvillisuus- ja ympäristömuuttujista sekä maan fysiko-kemiallisista ominaisuuksista.

Kentällä suoritettavassa lämmityskokeessa kaikkien kolmen kasvihuonekaasun vapautuminen lisääntyi tundralle tyypillisiltä kasvillisuuspinnoilta, minkä seurauksena nämä ekosysteemit muuttuivat kasvihuonekaasujen nieluista (turvemaat -300 g CO_2-eq m^{-2}, kivennäismaat -198 g CO_2-eq m^{-2}) kasvihuonekaasujen lähteiksi (turvemaat 144 g CO_2-eq m^{-2}, kivennäismaat 636 g CO_2-eq m^{-2}). Tämä muutos kasvihuonekaasujen nielusta lähteeksi johtui ennen kaikkea hiilidioksidipäästöjen lisääntymisestä, kun taas lisääntyneillä metaani- ja typpioksiduulipäästöillä oli vähäisempi vaikutus. Metaania vapautui vain vähän tutkimuksessa mukana olleilta melko kuivilta pinnoilta, mutta lämpeneminen lisäsi merkittävästi kasvukauden metaanipäästöjä turvemaista. Aktiivisen kerroksen syveneminen sulatuskokeessa taas lisäsi metaanin sidontaa varsinkin kasvipeitteisissä turvemaissa, joissa se ylitti usein -10 mg CH_4 m^{-2} d^{-1}. Lämpeneminen lisäsi typpioksiduulipäästöjä paljaista, kasvittomista turvemaista, jotka ovat voimakkaita typpioksiduulin lähteitä jo nykyisissä ilmasto-oloissa. Myös kasvipeitteisten turvemaiden typpioksiduulipäästö kasvoi sulamisen myötä. Vesiliukoisten yhdisteiden, kuten liukoisten orgaanisten hiiliyhdisteiden valunta maan pintakerroksista syvempiin maakerroksiin osoittautui merkittäväksi prosessiksi kasvihuonekaasujen tuoton

kannalta. Ikiroudansulatuskokeessa paljastui aiemmin tuntematon positiivinen palautevaikutus ilmaston lämpenemiseen: Ikiroudan sulamisen myötä paljaiden turvepintojen typpioksiduulipäästöt viisinkertaisiksi (0.56 mg N_2O m^{-2} d^{-1} ennen sulamista, 2.81 mg N_2O m^{-2} d^{-1} sulamisen jälkeen), ja myös kasvipeitteisten turvepintojen päästöt kasvoivat. Tämän tutkimuksen mukaan alueet, joilla on suuri potentiaali päästää ilmakehään typpioksiduulia, kattavat jopa neljänneksen arktisesta maa-alueesta. Maaperän typpipitoisuudella, maan kosteudella ja kasvipeitteellä on tärkeä rooli arktisten typpioksiduulipäästöjen säätelyssä tulevaisuuden muuttuvissa ilmasto-oloissa. Sulatuskokeessa havaittiin myös, että ikiroudan sulaminen lisäsi vanhan hiilen vapautumista ilmakehään ikiroutasoista. Sulamisen seurauksena maan huokosveteen vapautuneet liukoiset hiiliyhdisteet osoittautuivat helposti hajoaviksi.

Tämän tutkimuksen tulosten perusteella kuivat tundramaat, etenkin ikiroutasuot, ovat herkkiä ympäristöolosuhteissa tapahtuville muutoksille, ja niillä on siten suuri merkitys arktisten alueiden biogeokemian kannalta ilmaston lämmetessä.

Luokitus: 504.7, 551.345, 551.524, 551.588.7

Yleinen suomalainen asiasanasto: kasvihuonekaasut; ilmastonmuutokset; lämpeneminen; hiilidioksidi; metaani; dityppioksidi; ikirouta; sulaminen; tundra; arktinen alue; suot; turvemaat; typpi; kosteus; kasvillisuus

ACKNOWLEDGEMENTS

Almost six years ago to the day I received an email from my supervisor-to-be, inviting me to move to Finland for my PhD. Now, six years later, I am putting finishing touches to the ready PhD book.

Those six years have probably been the most challenging, but so far also the most adventurous and rewarding years of my life: filled with new experiences, lots of travel, excitement, sweat, tears, joy and friendship. The scientific aspect aside, these past few years have been inspiring and educational also on a personal level. I realized that it is possible to live under the simplest of conditions in the remotest corners of this world, and to feel at home there. I fell in love with the bright nights under the endless Arctic skies, being drawn to Russia's northernmost regions despite the legions of mosquitoes, harsh environment and often extreme living conditions. On top of everything, I was able to meet the most amazing people, get to know new cultures, and learn some Russian and Finnish. Hell, I even became a Finn.

Throughout this time, I was accompanied by my colleagues and friends, without whom it would not have been possible to be where I am today, and to whom I am deeply grateful. First of all, I would like to thank my supervisors Christina Biasi, Maija Marushchak, and Pertti Martikainen, for their enthusiasm and love for science, as well as for their support and trust in my work at all times. Further, I wish to express my thanks to Christina Schädel and Lars Kutzbach who acted as pre-examiners of this thesis, to Steve Frolking for agreeing to be the opponent, and to Jukka Pumpanen for being the custos during the public examination.

While I would like to thank all my co-authors and field team members for their contribution to this work, I specifically wish to thank Richard and Igor for their immense help and commitment during the summers of field work in Seida; and for keeping up the good spirits and working morale week after week, even under sometimes tough conditions.

A big thanks to my excellent colleagues here at UEF: I am proud to be part of the Biogeochemistry Research Group, and wish to thank all its members for the part they played in the completion of this thesis. Special thanks to the "Arctic science girls" Christina, Katka, as well as my tundra sisters Maija and Johanna: I hope to spend many hours doing science in your cheerful company in the future.

My work has been supported by various projects and funding sources which I acknowledge in the articles, but I am most grateful to the Emil Aaltonen Foundation, for supporting me during the final months of thesis writing.

My biggest thanks goes to my friends and family, who have stood by me during the highs and lows of my PhD time, and whose support I know I can always count on.

Kuopio, January 2018
Carolina Voigt

LIST OF ABBREVIATIONS

CO_2	carbon dioxide
CH_4	methane
N_2O	nitrous oxide
GHG	greenhouse gas
C	carbon
N	nitrogen
GWP	global warming potential
IPCC	Intergovernmental Panel on Climate Change
OTC	open-top chamber
SOM	soil organic matter
DOC	dissolved organic carbon
WFPS	water-filled pore space
NEE	net ecosystem exchange
ER	ecosystem respiration
GPP	gross primary production
NO_3^-	nitrate
NH_4^+	ammonium
N_2	dinitrogen

LIST OF ORIGINAL PUBLICATIONS

This dissertation is based on the following original publications:

I **Voigt C**, Lamprecht RE, Marushchak ME, Lind SE, Novakovskiy A, Aurela M, Martikainen PJ, Biasi C. (2017). Warming of Subarctic tundra increases emissions of all three important greenhouse gases – carbon dioxide, methane, and nitrous oxide. *Global Change Biology*, 23 (8): 3121-3138. doi: 10.1111/gcb.13563.

II Panneer Selvam B, Lapierre J-F, Guillemette F, **Voigt C**, Lamprecht RE, Biasi C, Christensen TR, Martikainen PJ, Berggren M. (2017). Degradation potentials of dissolved organic carbon (DOC) from thawed permafrost peat. *Scientific Reports*, 7: 45811. doi: 10.1038/srep45811.

III **Voigt C**, Mastepanov M, Lamprecht RE, Marushchak ME, Lindgren A, Dorodnikov M, Treat C, Oksanen T, Marushchak I, Jackowicz-Korczyński M, Lohila A, Christensen TR, Martikainen PJ, Biasi C. Ecosystem carbon response of Arctic peatlands to simulated permafrost thaw. *Manuscript*.

IV **Voigt C**, Marushchak ME, Lamprecht RE, Jackowicz-Korczyński M, Lindgren A, Mastepanov M, Granlund L, Christensen TR, Tahvanainen T, Martikainen PJ, Biasi C. (2017). Increased nitrous oxide emissions from Arctic peatlands after permafrost thaw. *Proceedings of the National Academy of Sciences of the United States of America*, 114 (24): 6238-6243. doi: 10.1073/pnas.1702902114.

AUTHOR'S CONTRIBUTION

I The author, Carolina Voigt, contributed to the design of the study. She had the main responsibility for the practical work, carried out the data analyses and wrote the first version of the manuscript, after which the co-authors contributed to the writing process.

II The author, Carolina Voigt, was responsible for the collection of peat mesocosms in the field, and the soil water collection from the mesocosms that were subsequently analyzed for DOC characteristics in this study. She further contributed to the writing of the manuscript.

III The author, Carolina Voigt, designed the study together with Maija Marushchak, Pertti Martikainen, Mikhail Mastepanov, Timo Oksanen and Christina Biasi. She carried the main responsibility for data collection and processing, and wrote the first version of the manuscript, after which Maija Marushchak, Claire Treat, and Mikhail Mastepanov contributed towards developing the manuscript.

IV The author, Carolina Voigt, designed the study together with Maija Marushchak, Richard Lamprecht, Pertti Martikainen, Christina Biasi, Torben Christensen, Mikhail Mastepanov and Marcin Jackowicz-Korczyński. She carried the main responsibility for developing the experimental set-up, data collection, and data analyses. She wrote the first version of the manuscript, after which Maija Marushchak, Christina Biasi and Pertti Martikainen, followed by other co-authors, contributed towards developing the manuscript.

CONTENTS

1 GENERAL INTRODUCTION

1.1 THE ARCTIC REGION

The Arctic is unique in terms of climate, flora, fauna, geography and biogeochemistry. Covering the Earth's northernmost region, the Arctic includes the Arctic Ocean, as well as the surrounding land areas of eight countries: Finland, Sweden, Norway, Denmark (Greenland), Iceland, Canada, the United States (Alaska), and Russia. Unlike other regions, the extent of the Arctic Region does not follow a clear definition, but is generally understood as the area above the Arctic circle (66.6°N), or defined by the extent of the treeline, as well as by temperature (average July temperature <10°C).

1.1.1 Zonation and permafrost distribution

Large areas of the Arctic are underlain by permafrost, defined as ground that remains frozen for at least two consecutive years (Grosse et al. 2011). The Northern circumpolar permafrost region covers an area of 17.8×10^6 km^2 (Hugelius et al. 2014). There, the permafrost region is divided into broad zones based on the proportion of the area that is underlain by permafrost (Brown et al. 2002; Heginbottom et al. 2012) (Figure 1): continuous permafrost (90–100%), discontinuous permafrost (50–90%), sporadic permafrost (10–50%), and isolated permafrost (0–10%).

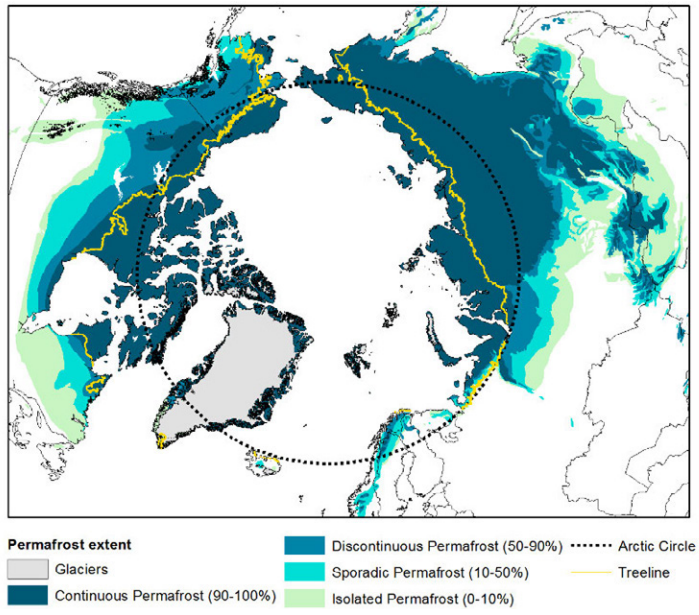

Figure 1. *Circum-Arctic map of permafrost distribution (modified after Brown et al. 2002).*

Permafrost thickness and temperature in the Arctic vary between region, altitude, and permafrost zone, with deep, cold permafrost found especially in continental regions of the High-Arctic (Heginbottom et al. 2012; Romanovsky et al. 2002). Comparably warm permafrost, with temperatures just below 0°C mainly occurs near the Southern boundary of permafrost distribution, in the discontinuous and sporadic permafrost zones (Vaughan et al. 2013), making these areas particularly vulnerable to climate warming (1.1.2). There, widespread thawing of permafrost is currently ongoing (Grosse et al. 2011; Romanovsky et al. 2010; Sannel & Kuhry 2011; Jones et al. 2016; Borge et al. 2017).

1.1.2 Recent climate change projections for the Arctic

Throughout this century, air temperatures are expected to rise, mainly due to an anthropogenically caused increase of heat trapping gases in the atmosphere. A pronounced warming trend is predicted particularly for the Arctic Region – a phenomenon known as Arctic amplification (Serreze et al. 2009; Overland et al. 2013) (Figure 2). Simulated mean annual warming in the Arctic is twice as high as the global mean warming (Kirtman et al. 2013). The strongest regional warming is predicted for the Arctic Ocean and Arctic land areas bordering on ocean waters with an observed sharp sea-ice decline (ACIA 2005; Vaughan et al. 2013) (Figure 2). There, the decline in sea ice and snow cover reduces the reflectance of incoming solar radiation (albedo), thereby further increasing the warming effect (Vaughan et al. 2013). Generally, winter is projected to display the highest temperature increase (Christensen et al. 2013; Koenigk et al. 2013; Bintanja & van der Linden 2013) (Table 1). Although regionally variable, precipitation in the Arctic is also projected to increase, with the largest changes occurring in autumn and winter (ACIA 2005; Vaughan et al. 2013; Christensen et al. 2013) (Table 1).

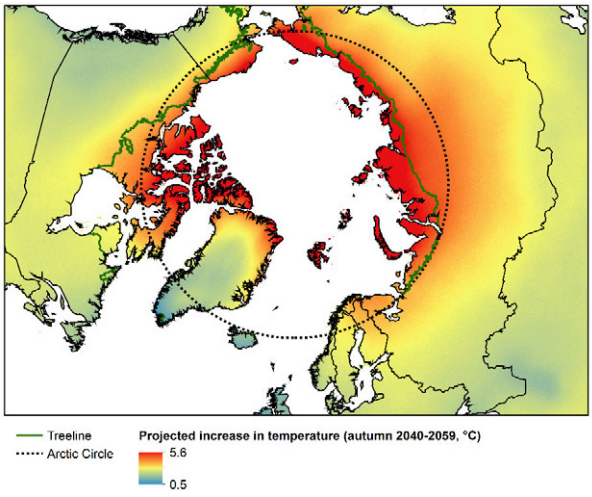

Figure 2. *Projected autumn temperature increase for the mid-21st century according to IPCC (modified after Hamilton 2011).*

Table 1. *Changes in temperature and precipitation as projected by the CMIP5 global models for Arctic land areas until the end of the 21st century (temperature change in the year 2100 compared to the 1986–2005 period), simulated by three different warming scenarios (data from Christensen et al. 2013).*

Season	Temperature (°C)			Precipitation (%)		
	Min	Median	Max	Min	Median	Max
RCP 2.6 scenario						
Winter (DJF)	-3.9	2.5	6.7	-11	12	36
Summer (JJA)	-1.1	1.0	4.4	-4	6	33
Annual	-2.9	1.9	5.6	-8	9	34
RCP 6.0 scenario						
Winter (DJF)	1.1	5.8	12.3	8	29	62
Summer (JJA)	1.1	2.8	6.8	4	14	42
Annual	1.0	4.5	9.1	5	20	50
RCP 8.5 scenario						
Winter (DJF)	5.3	9.6	16.8	27	47	93
Summer (JJA)	2.6	4.7	9.2	9	25	61
Annual	4.4	7.5	12.4	17	34	74

Even though the largest climate-related changes in the Arctic are predicted for the autumn and winter months (Christensen et al. 2013, Table 1), climate models also predict an increased number of weather extremes (ACIA 2005; Hartmann et al. 2013), such as heat waves and heavy rainfall events. Together with increased amounts of late-season precipitation (Christensen et al. 2013) and increased moisture input during spring snow melt, these weather extremes are thereby greatly affecting vegetation and nutrient dynamics during the biologically active summer season.

1.2 BIOGEOCHEMISTRY AND CLIMATIC RELEVANCE OF ARCTIC SOILS

Arctic ecosystems are an important player in the current climate debate, since they have the potential to both buffer and enhance climate warming by functioning as a sink or source for greenhouse gases (GHGs). This chapter discusses the role of Arctic soils in the global carbon (C) and nitrogen (N) cycle.

1.2.1 Carbon and nitrogen stocks in the Arctic

Arctic soils in the Northern circumpolar permafrost region are vast reservoirs of soil organic C, and are currently estimated to contain ~1307 Pg C in the upper 3m (Hugelius et al. 2014). This estimate is twice as high as the global amount of C stored in

vegetation (~450–650 Pg C), and also almost twice as high as the amount of C currently present in the atmosphere (~730–829 Tg C) (Schuur et al. 2008; Zimov et al. 2006b; Ciais et al. 2013). Stocks of N in Arctic soils are not as well constrained as C stocks, but with a conservative estimate of 67 Pg total N in the upper 3m (Harden et al. 2012) Arctic N stocks are also substantial. Large uncertainties are connected to both C and N stock estimates, mainly due to knowledge gaps on the extent of organic (e.g., peatlands) and cryoturbated soils in Northern latitudes (Tarnocai et al. 2009; Nieder & Benbi 2008), as well as on deep permafrost C and N stocks (Schuur et al. 2015).

Accumulated and preserved over thousands of years as frozen soil, litter, and peat, these long-term immobile C and N stocks could become available for transport and microbial decomposition as the permafrost thaws. Unlocked from their frozen state, these C and N forms are subject to active biogeochemical cycling following various pathways, e.g., plant uptake, leaching to surrounding aquatic systems, or release as GHGs (section 1.2.2).

Organic soils, such as peatlands, contain the highest amounts of C (and N) in the Arctic (Davidson et al. 2006; Hugelius et al. 2014): one third of the global soil C pool is stored in Northern peatlands (Gorham 1991), which often exhibit a several meter thick peat layer, and on-going C accumulation (Beilman et al. 2009; Olefeldt et al. 2012). Stocks of C and N in Arctic mineral soils are comparably small, and often highest in the surface soil, when the mineral soil is overlain by an organic layer. The largest areas of peatlands occur in the discontinuous and sporadic permafrost zones. Thus, the zone with the most sensitive, "warm" permafrost most prominently coincides with the occurrence of vast C and N stocks, making these areas particularly vulnerable to climate change.

1.2.2 Exchange of the greenhouse gases carbon dioxide (CO_2), methane (CH_4), and nitrous oxide (N_2O) in Arctic ecosystems

Due to the remote location and harsh climate conditions, measurements of GHG dynamics in polar regions are challenging. Due to the small number of data points, especially of year-round measurements including the winter season, our understanding of Arctic biogeochemistry, current as well as in a future warmer climate, remains to date woefully incomplete.

Besides water vapour and ozone, the increased concentration of the three GHGs carbon dioxide (CO_2), methane (CH_4), and nitrous oxide (N_2O) in the atmosphere is the main cause of climate warming due to radiative forcing (Hartmann et al. 2013; Myhre et al. 2013). Soils have the potential to either consume or release these gases via microbial, plant-related and physical processes and pathways. The conversion of even a fraction of the vast C and N pools currently locked in Arctic soils (section 1.2.1), and especially in the permafrost, to GHGs has the potential to alter our climate and amplify climate warming (Schuur et al. 2015; Schuur et al. 2008). Therefore, Arctic

CO_2 exchange is currently widely studied, since CO_2 acts as the dominant GHG in the majority of Arctic ecosystems (Schädel et al. 2016).
However, the release of strong non-CO_2 GHGs from Arctic soils, even if released at small rates, could locally outweigh CO_2 emissions. Hence, wetlands and lakes, which act as hot spots for CH_4 emissions (McGuire et al. 2010; Bartlett & Harriss 1993) are being studied extensively, as CH_4 is around 28 times more powerful in warming the climate than CO_2 based on a 100-yr horizon (Myhre et al. 2013). Permafrost thaw under anaerobic conditions is expected to release larger amounts of CH_4 than thawing under drier, aerobic conditions (Deng et al. 2014; Schuur et al. 2015; Schädel et al. 2016). Yet, recent studies using permafrost soil incubations indicate, that the total warming impact of CO_2 and CH_4 will be larger when thawing occurs under aerobic conditions, due to high CO_2 emissions (Schuur et al. 2015; Schädel et al. 2016; Lee et al. 2012; Elberling et al. 2013). Which proportion of permafrost thaw will thaw under aerobic versus anaerobic conditions, however, remains elusive, as moisture changes are challenging to predict (Schuur et al. 2015). Not well constrained either are the spatial variation and the time scale of permafrost C release occurring over the vast Arctic Region. The proportional contribution of old C versus young C derived from the surface soil to future C emissions poses a large question in Arctic climate change research: deep soil C often consists of recalcitrant substrates, resisting microbial decomposition (Christensen et al. 1999). Thus, fuelled by fresh substrates from litter input and root exudation, microbial activity and C respiration are often high in the surface soil, and decline with depth (Blodau et al. 2004). Therefore, the highest CO_2 emissions generally originate from the surface soil and the upper active layer (Hicks Pries et al. 2015; Heslop et al. 2017). Only a fraction of the old permafrost C pool might be available for rapid break-down (Moni et al. 2015; Dutta et al. 2006), while the remainder underlies a slow, more sustained C release occurring not abruptly but spread out over centuries (Schuur et al. 2015). Models indicate a potential C release of 37–174 Pg C from the permafrost region until 2100, whereas 59% of the C release is estimated to occur after 2100 (Schuur et al. 2015; Koven et al. 2011; Schneider von Deimling et al. 2012; Zhuang et al. 2006).
Most recently, studies have demonstrated that permafrost soils might not only be a source of gaseous C forms (CO_2 and CH_4), but could further emit the strong GHG N_2O (Repo et al. 2009; Marushchak et al. 2011; Elberling et al. 2010; Lamb et al. 2011). The release of N_2O from Artic soils – formerly believed to be insignificant due to low N turnover rates – might greatly affect the overall Arctic GHG balance, since N_2O is almost 300 times more powerful than CO_2 and around 10 times stronger than CH_4 in warming the climate (Myhre et al. 2013). So far, only a few studies report *in situ* N_2O fluxes from permafrost soils: recently, N_2O fluxes have been reported for high Arctic coastal lowlands (Lamb et al. 2011), polar deserts (Stewart et al. 2012), an Arctic transect across Canada (Paré & Bedard-Haughn 2012) as well as for maritime Antarctica (Zhu et al. 2014). Exceptionally high N_2O emissions have been found in permafrost

peatlands, especially when the vegetation cover is absent (Repo et al. 2009; Marushchak et al. 2011). These emission rates match those from tropical forest soils (Repo et al. 2009), the world's largest known terrestrial N_2O source among natural ecosystems (Ciais et al. 2013).

1.3 CLIMATE AND LANDSCAPE CONTROLS ON GREENHOUSE GAS EXCHANGE IN THE ARCTIC

The magnitude of CO_2, CH_4 and N_2O fluxes depends on a multitude of environmental controls, mainly associated with climate and substrate availability, the most important of which are elaborated in this chapter.

1.3.1 Temperature

Arctic land areas are predicted to warm by up to 5.6–12.4°C under different warming scenarios (median: 1.9–7.5°C; Table 1) (Christensen et al. 2013). In the Arctic, temperature is often the limiting factor for many biological processes. Hence, small changes in temperature have the potential to severely alter the regional GHG budget. As long as other environmental factors are not limiting, an increase in temperature accelerates microbial processes related to both, C and N cycling, as well as vegetation growth (chapter 1.3.4). Hence, decomposition and net C losses are expected to increase in these temperature sensitive, cold soils as a result of warming (Kirschbaum 1995). Warming generally causes an increase in respiration in tundra ecosystems (Grogan & Chapin 2000; Hobbie & Chapin III 1998; Rustad et al. 2001; Oberbauer et al. 2007; Dorrepaal et al. 2009; Fouché et al. 2014; Ravn et al. 2017), resulting in enhanced net C losses to the atmosphere (Jones et al. 1998; Rinnan et al. 2007; Biasi et al. 2008), as long as a warming-induced increase in plant CO_2 uptake does not outweigh respiratory losses (Oechel et al. 2000; Oechel et al. 1993). Studies indicate that especially winter warming will strongly increase respiration rates during the non-growing season, affecting the annual C balance (Natali et al. 2014; Natali et al. 2011). While air and soil temperatures are important drivers of the seasonal variability of N_2O emissions from hot spots (bare peat soils, Marushchak et al. 2011), the direct temperature effect on N_2O fluxes and underlying processes from Arctic soils remain uncertain. Warming generally accelerates N cycling processes, including nitrification and denitrification (Butterbach-Bahl et al. 2013). In previous studies, warming of Arctic soils has been shown to increase net N mineralization (Schaeffer et al. 2013; Rustad et al. 2001; Natali et al. 2012), soil N pools and N turnover rates (Biasi et al. 2008).

1.3.2 Soil moisture

Soil moisture regulates the oxygen status of the soil and is thus a main regulator of GHG production and consumption. Moisture conditions (aerobic vs. anaerobic) determine the form and amount of overall C release (Schädel et al. 2016; Schuur et al. 2015; Treat et al. 2014), and the production or consumption of N_2O (Butterbach-Bahl et al. 2013). The position of the water table level regulates CH_4 emissions and C accumulation rates in permafrost soils (Liblik et al. 1997) and northern peatlands (Daulat & Clymo 1998; Bridgham et al. 2008), with higher CH_4 and lower CO_2 emissions in water-saturated soils. Soil drying on the other hand enhances C decomposition, causing larger CO_2 losses to the atmosphere (Natali et al. 2015), especially during the non-growing season (Kwon et al. 2016). Drainage of previously wet tundra has additionally been shown to reduce plant CO_2 uptake by 25% (Kwon et al. 2016). Long-term drainage may also alter soil methanogenic and methanotrophic communities, leading to lower net CH_4 emissions (Kwon et al. 2017) if the methanotrophic activities increase, or the methanogenic activities decrease.

1.3.3 Permafrost thaw

In Arctic soils, the permafrost is overlain by a seasonally thawing active layer. The thickness of the active layer varies by region and soil type, and is mainly controlled by regional climate, ranging from just a few centimetres in the high Arctic to several metres in the discontinuous permafrost zone (Schuur et al. 2008). The seasonally thawing layer is the part of the soil system that actively participates in biogeochemical cycling, and influences the plant rooting depth, moisture conditions and the amount of available SOM exposed to above-freezing temperatures (Schuur et al. 2008). Permafrost thaw can occur either via a gradual deepening of the active layer (e.g., Åkerman & Johansson 2008), or abruptly, particularly at sites with ice-rich permafrost, or after disturbances (e.g., tundra fires, vegetation removal), resulting in thermokarst formation and surface inundation (Schuur et al. 2008; Grosse et al. 2011; Nauta et al. 2015; Schuur et al. 2015; Jones et al. 2015). Either way, permafrost thaw can result in the release of GHGs previously trapped in the soil during permafrost aggradation. Additionally, permafrost thaw reveals long-term immobile C and N stocks to microbial decomposition, and thus increases the availability of substrates for GHG production. The main regulators of the rate and magnitude of GHGs released from thawing permafrost are the quality of the exposed SOM (Walz et al. 2017; Treat et al. 2015; Pengerud et al. 2013), as well as temperature and moisture conditions (aerobic vs. anaerobic) at times of thaw (Wang & Roulet 2017; Schädel et al. 2016; Schuur et al. 2015).
Overall, models project large C losses from thawing permafrost (Koven et al. 2015; Zhuang et al. 2006; Schneider von Deimling et al. 2012), especially in southern tundra. In field studies, permafrost degradation has been shown to increase C emissions to

the atmosphere (e.g., Turetsky et al. 2002; Schuur et al. 2009); and laboratory-based incubations of permafrost sub-samples demonstrate substantial C production after thawing (Zimov et al. 2006a; Jones et al. 2017), especially under aerobic conditions (Elberling et al. 2013; Schädel et al. 2016; Schuur et al. 2015; Natali et al. 2015). Thawing of permafrost may additionally increase DOC concentrations and export (Olefeldt & Roulet 2012; Abbott et al. 2015; Drake et al. 2015; Frey & McClelland 2009), leading to off-site CO_2 emissions via photochemical and microbial degradation (Drake et al. 2015). In terms of the N cycle, high N mineralization rates have been found in thawed permafrost soil (Keuper et al. 2012), together with an increased mineral N pool (Keuper et al. 2012; Finger et al. 2016; Salmon et al. 2016). An enhanced mineral N pool theoretically favours N_2O production in soils (Butterbach-Bahl et al. 2013); and a high N_2O production potential has been reported for permafrost soils after drying and rewetting with N-rich meltwaters (Elberling et al. 2010).

1.3.4 Vegetation

A warming climate, a changed moisture regime and increase active layer depth and nutrient availability will affect vegetation growth and composition across the entire Arctic, with large consequences on Arctic GHG exchange.
In terms of CO_2 exchange, enhanced plant growth and longer growing seasons caused by a warmer climate will increase the net CO_2 uptake capacity of ecosystems. In fact, the majority of warming studies indicate that the stimulated CO_2 release via respiration is offset by the simultaneous increase in plant CO_2 uptake, mainly due to increased shrub growth, without majorly affecting the net C balance (e.g., Hobbie & Chapin III 1998; Oberbauer et al. 1998; Parmentier et al. 2011; Lu et al. 2013; Mauritz et al. 2017). However, growing evidence suggests that the growth response of vegetation to warming is not always able to buffer respiratory losses (Jones et al. 1998; Biasi et al. 2008; Xue et al. 2016), at least not in the short-term (Welker et al. 2004).
Also, with respect to CH_4 emissions from tundra, the vegetation composition plays a crucial role in regulating the amount of CH_4 emitted at the soil surface. Methane emissions occur via three main pathways (Lai 2009): diffusion, ebullition, and plant-mediated transport. In non-flooded or completely inundated soils, plant-mediated transport is the most effective way to transport CH_4 from the anaerobic zone, where CH_4 production occurs, to the surface. Thus, vegetation is not only important because it provides labile C compounds for methanogenesis, but gas transport through the aerenchyma tissue of vascular plants, acting as gas conduits, allows the CH_4 produced at depth to bypass the oxic layer of the soil column. It has been shown that in polygonal tundra as much as 70–90% of total CH_4 emissions occur through plant-mediated transport, while up to 99% of the CH_4 produced at depth are oxidized when vascular plants are absent (Knoblauch et al. 2015; Kutzbach et al. 2004). For this reason, the presence of vascular plants, especially graminoids and sedges, and the species composition control CH_4 emissions (Joabsson & Christensen 2001; Liblik et al.

1997; Marushchak et al. 2016; Knoblauch et al. 2015; Öquist & Svensson 2002), frequently overruling the effect of the water table level (Bellisario et al. 1999; Kutzbach et al. 2004).
Compared to C cycling in Arctic ecosystems, much less is known about how vegetation affects fluxes of N_2O. Since plants and microbes compete for N forms in these rather mineral N limited systems (Lohila et al. 2010), the absence of vegetation can increase the plant-available soil N pool (mineral N), leading to N_2O emissions from Arctic soils (Repo et al. 2009; Marushchak et al. 2011). Additionally, shading of vegetation and a reduced plant N uptake in boreal and cold climates has been shown to promote N_2O release to the atmosphere (Stewart et al. 2012; Shurpali et al. 2016; Regina et al. 1999).

1.4 CLIMATE MANIPULATION EXPERIMENTS IN ARCTIC REGIONS

Climate manipulation studies are an important means to simulate the impact of a future climate on biogeochemical cycles. Parameters that are usually manipulated are temperature, thaw depth, moisture, snow cover, nutrient and litter availability and input, and vegetation changes. At field-scale, manipulating a single of these parameters is tricky: soil warming often simultaneously affects soil moisture (Bokhorst et al. 2013; Marion et al. 1997), and higher soil moisture often increases the seasonal thaw depth (Christensen et al. 2004). These changes in temperature and moisture conditions not only affect GHG exchange directly, but also via changes in vegetation composition and growth (Kwon et al. 2016; Rustad et al. 2001; Arft et al. 1999; Elmendorf et al. 2012a). The effect of individual environmental parameters on GHG flux dynamics and other changes of the biome is hence often blurred by a mixed signal (Chapin et al. 1995). To distinguish between different environmental parameters, laboratory studies manipulating a single parameter, e.g., temperature, provide a good approach. Lab studies, however, do not necessarily mirror field conditions, as the conditions during incubation of often homogenized sub-samples, taken out of the context of the full plant–soil system, are highly artificial. Combining *in situ* field observations with detailed *ex situ* process studies provides the ideal tool to further our understanding on Arctic biogeochemical cycling.
As remote Arctic areas are difficult to access and, in many cases, lack main power sources, sophisticated set-ups and multi-year climate manipulation experiments are cost-intensive and challenging to maintain. An inexpensive and simple method to achieve air and near-surface soil warming is the use of open-top chambers (OTCs). This method induces air warming of about 1–3°C (Fouché et al. 2014; Marion et al. 1997), thus mimicking expected warming by the end of this century. Using OTCs, the effect of experimental air warming has been studied on various ecosystem compartments: GHG fluxes (Lamb et al. 2011; Natali et al. 2011; Biasi et al. 2008; Dorrepaal et

al. 2009; D'imperio et al. 2017), vegetation (Aerts et al. 2004; Arft et al. 1999; Hudson & Henry 2010; Hollister et al. 2005), litter and nutrient dynamics (Aerts et al. 2012), microbial community structure (Deslippe et al. 2012; Walker et al. 2008) combined with N pools (Weedon et al. 2012) and soil solution chemistry (Fouché et al. 2014). As warming by OTCs is generally restricted to air and the soil surface, heating wires, infrared lamps (Bokhorst et al. 2008), or snow fences (Natali et al. 2011) are commonly used to achieve deeper soil warming. Snow fences can be additionally used to simulate a deeper snow cover, enhanced moisture input during snow melt, and generally increase the thaw depth during the growing season (Salmon et al. 2016; Natali et al. 2011; Mauritz et al. 2017).

1.5 METHODS APPLIED IN THIS STUDY

The data for this thesis has been collected at two subarctic sites, located in the discontinuous permafrost zone in Russia and Finland (Figure 3). We used climate manipulation experiments to monitor GHG exchange, as well as a wide range of ancillary variables, as described in detail in this chapter.

1.5.1 Study sites

An in situ experimental warming study (chapter 2) has been established at the study site "Seida" (67°03′ N, 62°55′ E), which is located in Komi Republic, Eastern-European Russia. The site is situated in proximity to the Ural Mountains, about 10km west of the settlement Seida, and about 70km southwest of the nearest larger city, Vorkuta. The long-term mean (1977–2006) for air temperature at the site is -5.6°C, and annual precipitation amounts to 501mm (data from Vorkuta meteorological station, Marushchak et al. 2013). Due to its location just north of the tree line at the southern extent of permafrost distribution, the site is currently experiencing permafrost warming and thaw (Oberman & Mazhitova 2001; Romanovsky et al. 2010), making it ideal for assessing climate change impacts. The Seida site comprises a mosaic of different landform types, representing typical, heterogeneous tundra landscape: upland mineral soils cover the largest percentage of the area (57.9%, Marushchak et al. 2013), followed by large peat plateau areas (23.6%). These comparatively dry tundra soils are interspersed with wetlands (14.4%) and numerous small thermokarst lakes (1.1%). The dominant vegetation in the upland tundra areas (lichen-rich, dry shrub tundra) consists of *Betula nana* L., *Vaccinium uligunosum* L., *Salix* sp., *Empetrum nigrum* subsp. *hermaphroditum*, graminoids and mosses, whereas the peat plateau is dominated by bog vegetation (*Ledum decumbens*, *Rubus chmaemorus* L., *Vaccinium vitis-idaea* L., *Betula nana* L. and hummock mosses (*Sphagnum* sp). The upland tundra soils are mostly overlain by just a thin (2–9cm) organic layer on top of mineral soil, whereas peat plateaus in the area consist of a several meter thick peat layer. The peat plateau complex comprises fen peat deposits that were uplifted by frost heave ca. 2200 cal BP

(Routh et al. 2014), and overlaying peat bog deposits developed in more recent times following the permafrost uplift. Even though upland mineral soils cover a larger area in the region, these uplifted permafrost peat plateaus contain the largest proportion of C, which has accumulated in the peat layer (Hugelius et al. 2012; Hugelius et al. 2011). A distinctive feature of the Seida site are bare peat surfaces, which occur on top of the peat plateau (Figure 4). These bare peat surfaces can be sporadically covered by lichens, but vascular plants are absent, likely due to changing moisture conditions caused during the permafrost uplift (Zoltai & Tarnocai 1975), coupled with cryoturbation processes and wind abrasion (Kaverin et al. 2016). As a result, old, decomposed fen peat with an age of 5900 cal BP represents the surface layer (Ronkainen et al. 2015) of these bare peat surfaces, which are also known as "peat circles" (Repo et al. 2009; Marushchak et al. 2011).

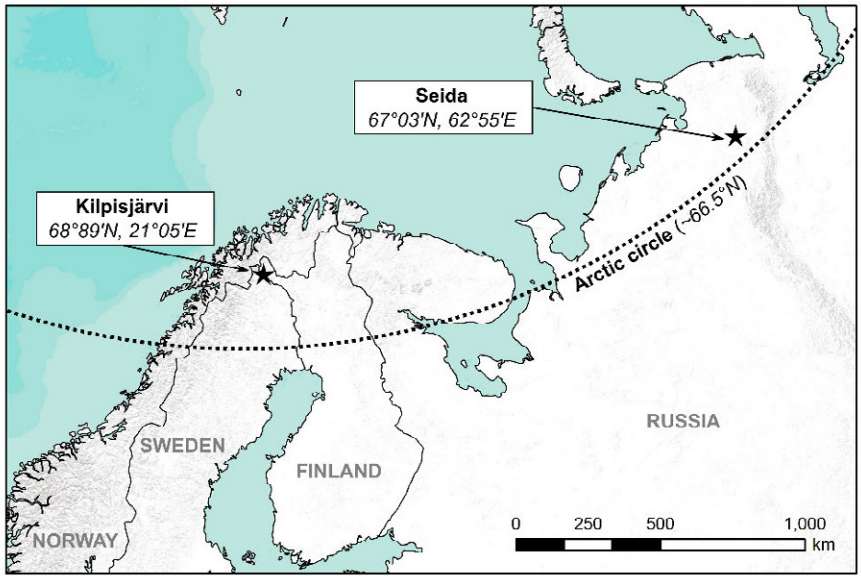

Figure 3. *The study sites "Kilpisjärvi" and "Seida" and their location in the Arctic.*

A permafrost thaw experiment (chapter 3, 4, and 5) was conducted using intact peat cores collected in a palsa mire near Kilpisjärvi Research Station (68°89', 21°05') in Finnish Lapland. The long-term mean (1981–2010) air temperature measured at Kilpisjärvi Station is -1.9°C, with a mean annual precipitation of 487mm (Pirinen et al. 2012). Palsa mires possess a permanently frozen core, and display a similar peat succession in their profile, as well as similar vegetation (dwarf shrubs and herbaceous plants, as well as mosses and lichens) as is found in peat plateaus (Zoltai & Tarnocai 1975). Similar to the peat plateau at the Seida site, the surface of the palsa examined in this study was dotted with bare peat surfaces (Figure 4). Palsas are often lacking vegetation in their initial stage of permafrost uplift, exposing bare peat at the

surface (Seppälä 2006; Seppälä 2003). The average thaw depth at the palsa is 60cm, and the palsa rises around 3m above the surrounding mire area (Kohout et al. 2014).

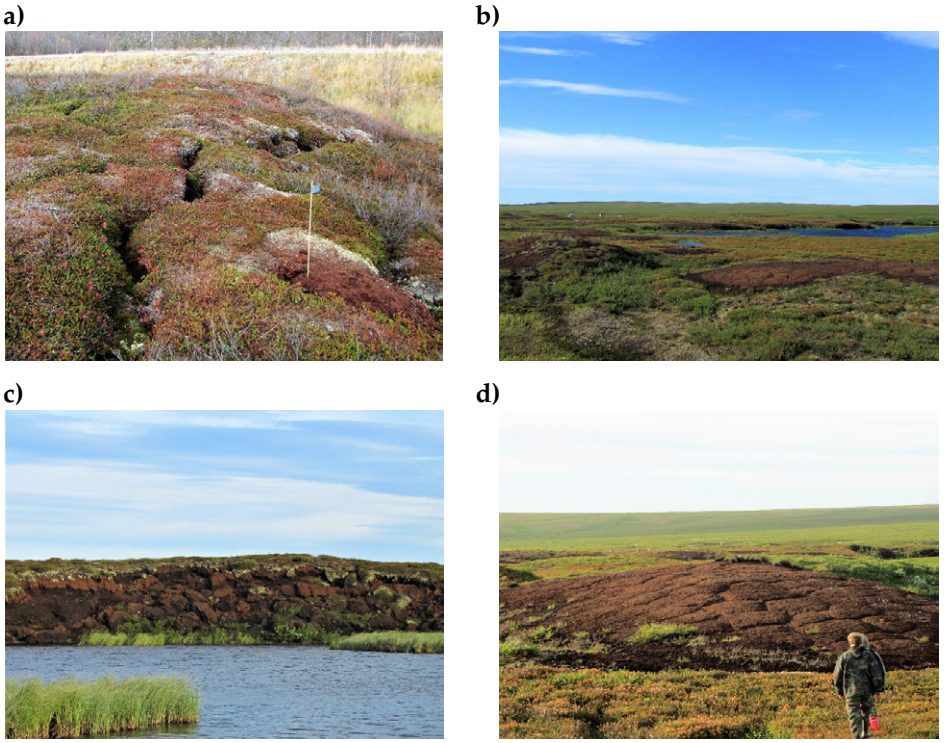

Figure 4. *The study sites: a) palsa surface at the sampling site near Kilpisjärvi, and b) Seida site, with upland tundra in the background, peat plateau with bare peat surfaces in the foreground; c) eroded wall of a peat plateau bordering on a thermokarst lake in Seida; d) bare peat surfaces in Seida.*

1.5.2 Simulated warming and permafrost thaw

Simulated *in situ* warming at the Seida site was achieved with open-top chambers (OTCs, Marion et al. 1997). Deployment of OTCs took place in the spring of 2012, and the OTCs were left in place for the snow-free seasons of 2012 and 2013, but removed over winter, in order to exclude the effect of snow accumulation within the OTCs. Each OTC-warmed plot was located next to a control plot, and OTCs were installed in five replicates on three surface types: upland mineral tundra, peat plateau, and bare peat. Details on OTC design, site set-up and achieved warming are elucidated in chapter 2.

Simulated permafrost thaw was realized in the laboratory, using large (10cm diameter, ~80cm length) and intact plant–soil systems (mesocosms). These peat mesocosms, collected near Kilpisjärvi (chapter 1.5.1), were frozen under mild freezing temperatures (-2 to -4°C) directly upon sampling and set-up in a climate controlled chamber, with adjustable humidity, temperature, and light regime. A specifically designed

saltwater bath within a glycol-circulated metal frame, cooled down to below zero temperatures, was used to keep the lower part of the peat profiles at mild freezing temperatures. Lowering the water level in the saltwater bath sequentially unfroze first the active layer part of the mesocosms, and finally the permafrost part, at intervals of 5–20 cm. The detailed technical set-up of this experiment is described in chapters 4 and 5.

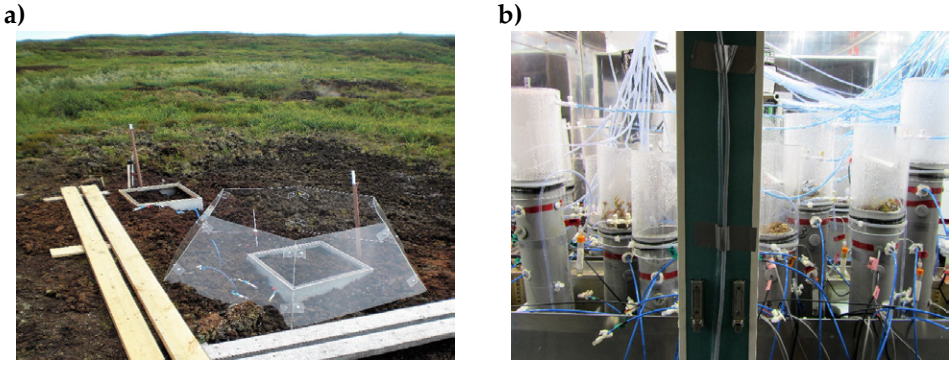

Figure 5. *Experimental manipulations: a) in situ field warming study with OTCs at the Seida site; b) mesocosm set-up in a climate chamber with palsa peat cores collected near Kilpisjärvi.*

1.5.3 Greenhouse gas flux measurements

This thesis focuses on the exchange of the major GHGs CO_2, CH_4 and N_2O. Flux measurements *in situ* (Seida) were conducted weekly during the snow-free season using the manual chamber technique (Hutchinson et al. 2000). Fluxes of CH_4 and N_2O were determined using static chambers combined with syringe sampling and subsequent gas analysis via gas chromatography, as described in detail in chapter 2. The flux of CO_2 was measured with a dynamic chamber system coupled with an infrared gas analyser (chapter 2). In the laboratory-based thawing experiment, all mesocosms were equipped with permanently installed transparent chambers. While N_2O samples were collected manually (chapter 5), the dynamics of CO_2 and CH_4 were monitored using a dynamic flow-through system and laser spectroscopy: this set-up provided continuous C exchange rates by comparing the GHG concentration in the headspace of each mesocosm to the ambient gas concentration of a reference line, as is described in detail in chapter 4.

1.5.4 Ancillary measurements of soil, climate, and vegetation parameters

To explain the observed changes in GHG fluxes achieved via experimental climate manipulation, a broad set of ancillary variables was measured, the methodology of which is described in the individual chapters of this thesis: soil profile concentrations of CO_2, CH_4 and N_2O (chapters 2, 4, and 5), soil nutrient profiles (chapters 2 and 5),

dissolved organic carbon (DOC) in the soils profile (chapters 2 and 4) as well as the degradability of pore water DOC (chapter 3), soil microbial respiration (chapter 2) and soil microbial biomass (chapters 4 and 5), soil physical and chemical properties (chapters 2, 4 and 5), vegetation composition and growth (chapter 2), and site meteorology (chapter 2).

1.6 AIMS OF THIS STUDY

The overarching aim of this thesis was to study the effect of experimentally induced climate change, namely warming and permafrost thaw, on GHG exchange in subarctic tundra landscapes, with a focus on permafrost peatlands. This thesis aims to not only quantify the aboveground GHG exchange, but to dig deeply into the reasons behind changed GHG dynamics as a result of climate manipulation. The observed changes in flux rates are linked to soil processes at depth in an attempt to identify the major controls on GHG exchange in warming tundra, and to increase mechanistic understanding of Arctic GHG biogeochemistry. Further, this thesis includes N_2O – a yet understudied Arctic GHG – in the assessment of climate change effects on GHG exchange in the permafrost region. For the first time, the direct effect of permafrost thaw on the full GHG balance is simulated under near-to-natural conditions.

Further, specific questions this thesis addresses are the following:

- Which tundra surface types are most vulnerable to warming – peat soils with their vast C and N stocks, or upland mineral soils, covering large areas in the tundra landscape?
- How does warming alter the regional GHG budget of a subarctic tundra site, considering the spatial coverage of individual surfaces within the landscape?
- How do soil processes at depth associated with warming and permafrost thaw affect the aboveground GHG release?
- Will organic C buried in permafrost become available for decomposition with climate change and, if yes, to which extent and in which form will it be released to the atmosphere (CO_2 or CH_4) or surronding aquatic systems (DOC)?
- Will the understudied, strong GHG N_2O be released from permafrost peatlands as a consequence of permafrost thaw?

6 GENERAL DISCUSSION

6.1 THE ROLE OF PERMAFROST PEATLANDS IN ARCTIC BIOGEOCHEMISTRY

This thesis shows the important role permafrost peatlands may play in a warming climate, not only in terms of the C balance, but also when considering their potential to increase the atmospheric N_2O load with warming (chapter 2) and permafrost thaw (chapter 5). While warming induces substantial CO_2 losses from upland mineral soils (chapter 2), permafrost peatlands can act as substantial sources of non-CO_2 GHGs in tundra. Further, the release of non-CO_2 GHGs increases as the climate warms (chapters 2, 4, 5).

Under the current climate, uplifted permafrost peatlands act as small sinks for CH_4, but may emit N_2O when the vegetation cover is disturbed (chapters 2 and 5). Reduced plant growth, resulting in a reduced plant N uptake, enhances the soil N pool available for microbial N_2O production (chapter 2). Thus, while peat surfaces without a vegetation cover are substantial sources of N_2O, vegetated peat surfaces may release N_2O if plant growth is hampered by warming (chapter 2), or additional N_2O is produced or released in the soil profile after permafrost thaw (chapter 5). However, the amount of N_2O released at the surface is regulated by the oxygen status of the peat column, governing N_2O production and consumption: a high water table leads to the reduction of N_2O to N_2, thus limiting N_2O release to the atmosphere, despite high N_2O concentrations at depth (chapter 5). Similarly, detailed soil profile measurements of CH_4 showed that CH_4 produced at depth might be oxidized during upwards diffusion through the aerobic peat profile, resulting in overall peatland CH_4 uptake (chapter 4). With mild (~1°C) air and surface soil warming, permafrost peatlands can turn into CH_4 sources, and increase their N_2O release (chapter 2). Soil warming causing permafrost to thaw further enhances N_2O release from permafrost peatlands (chapter 5). Together with warming-induced increases in CO_2 release (chapter 2), substrate availability from thawed permafrost (chapter 4), and the high decomposability of thawed, exported DOC (chapter 3), uplifted permafrost peatlands are likely to turn into larger GHG sources in the future.

The results of this thesis thus highlight the sensitivity of the vast peat C and N stocks to small changes in temperature. However, GHG release from permafrost peatlands is regulated by moisture conditions and the vegetation cover. Peat plateaus and palsas – the permafrost peatlands studied in this thesis – are unique in the sense that permafrost uplift causes aerobic conditions in the undecomposed peat profile, exposing the C and N pools to decomposition. Peat plateaus and palsas play an important role in Arctic peatland biogeochemistry, since their C balance is variable depending on the local vegetation cover, and due to lower CH_4 emissions compared to the

surrounding mire surfaces (Nykänen et al. 2003). While aerobic conditions promote GHG release from these ecosystems as the soils warm (chapter 2), peatland collapse after permafrost thaw can create wet conditions, which may limit CO_2 and N_2O emissions (chapter 4, chapter 5).

As long as the water table is high, pristine northern peatlands act as sinks for CO_2 (albeit with larger inter-annual variation) and sources of CH_4 (Blodau & Moore 2003; Lai 2009). While northern peatlands have had a net cooling effect on the climate for the past ~10000 years (Frolking & Roulet 2007), recent climate change has slowed down C accumulation, and is enhancing C losses to the atmosphere in many places (e.g., O'Donnell et al. 2012; Euskirchen et al. 2014; Jones et al. 2017). The future role of Northern peatlands in the global C cycle is thus highly uncertain (Moore et al. 1998; Limpens et al. 2008). The unique characteristics of permafrost peatlands with respect to location (Southern tundra), permafrost C (and N) pool (near to unlimited supply of C) and hydrology (water table fluctuations and high ice content in porous peat material of frozen peatlands) set peatlands apart from mineral soils, bestowing them with important climatic relevance.

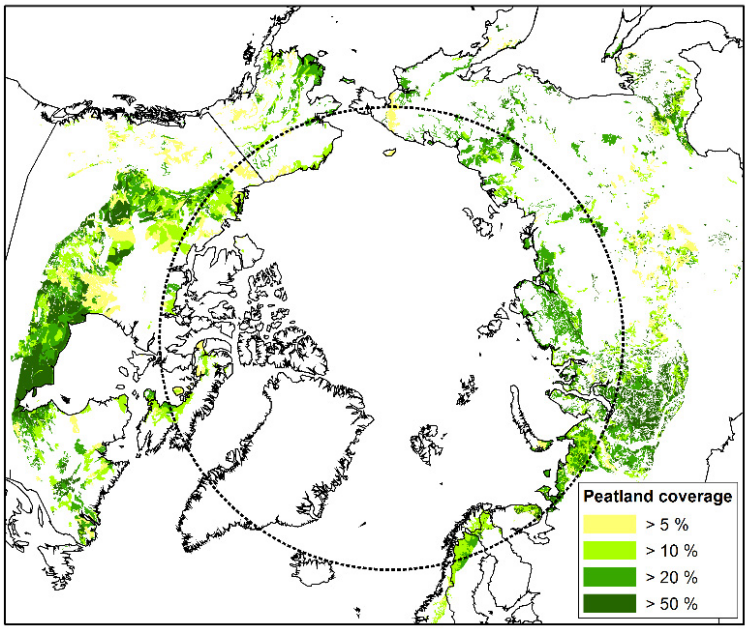

Figure 6. *Circum-Arctic map of peatland distribution. Peatland areas include soil classes histosols and histels (data from Hugelius et al. 2013).*

Adding to the sensitivity of permafrost peatlands, the C pool in these ecosystems is not protected from decomposition by adsorption to mineral soil, and thereby generally immediately accessible when permafrost thaws (Gentsch et al. 2015), and thus well connected to both atmosphere and aquatic systems (Frolking et al. 2009). Thus, not only is C lost via direct, on-site CO_2 or CH_4 emissions, but permafrost peatlands have been identified as origin of nutrients (Deshpande et al. 2016) and DOC leached

to aquatic systems, with increasing DOC losses from deep peat as the permafrost thaws (Frey & Smith 2005; Olefeldt & Roulet 2012). In fact, the DOC pool in permafrost peatlands displays a high potential degradability, both in the peat layer (chapter 3) as well as in recent vegetation-derived DOC (Wickland et al. 2007).
The results of this thesis have far-reaching implications for predictions on the future GHG balance of Arctic ecosystems, considering the extent of (permafrost) peatlands in the high latitudes: around 80% of the World's peatlands are located in cold-temperate climates of the Northern hemisphere (Limpens et al. 2008). Boreal and subarctic regions contain the largest peatland areas (~3.5×10^6 km^2), storing ~455 Pg C (Gorham 1991). In the Northern circumpolar permafrost region, peatlands cover more than 11% of the whole land area (Hugelius et al. 2013, chapter 5) (Figure 6). Still, permafrost peatlands – biogeochemical hot spots in the Arctic – remain understudied compared to other Arctic ecosystems (Sjöberg et al. 2015).

6.2 DRY ARCTIC TUNDRA – AN UNDERSTUDIED GREENHOUSE GAS SOURCE IN A WARMER WORLD?

The landform types studied in this thesis are comparatively dry tundra surfaces: upland mineral soils as well as uplifted permafrost peatlands. In the Subarctic, these dry tundra soils account for a large proportion of the landscape, covering regionally more than 80% of the area (Marushchak et al. 2013; D'imperio et al. 2017). However, dry tundra sites might be underrepresented in estimates of the current Arctic C balance, due to the site selection being biased towards high-Arctic wetland sites (Parmentier et al. 2017; Olefeldt et al. 2013).
Studies on the C balance at wet sites generally identify these sites as growing season sinks for CO_2 and sources of CH_4, resulting in an overall net C sink across ecosystem types, such as wet parts of palsa mires (Christensen et al. 2012), wet sedge and tussock tundra (Lafleur et al. 2012), and wet fens in permafrost peatlands (Heikkinen et al. 2002). Experimental warming studies at wet tundra sites often show only minor effects on the net C balance (Oberbauer et al. 1998; Hobbie & Chapin III 1998), or even lead to an increased net C uptake (Oberbauer et al. 2007) due to stimulated plant CO_2 uptake, also predicted by process-based model simulations (Hayes et al. 2014). Stimulated shrub growth in wet sedge tundra has also been shown to compensate for decreased C uptake by sphagnum mosses in response to an extreme summer, not affecting the net C balance (Zona et al. 2014). Additionally, wetting has been shown to counterbalance warming-induced C losses in high-Arctic tundra, thereby retaining the ecosystem's C sink function (Lupascu et al. 2014). Indirect effects of warming, such as better soil aeration due to drainage and a lowered water table, however, can

increase CO_2 emissions (Kwon et al. 2016), and turn these ecosystems into CO_2 sources (Oechel et al. 1993).

Dry and mesic tundra landscapes on the other hand may alternate between being a sink or source for CO_2 under current climate conditions (McGuire et al. 2012; Heikkinen et al. 2002; Marushchak et al. 2013; Zamolodchikov et al. 2000; Nykänen et al. 2003). The results of this thesis (chapter 2, chapter 4) confirm these findings: upland mineral soils varied between being net CO_2 sinks of -198±68 g CO_2 m^{-2} to small sources of 96±127 g CO_2 m^{-2} (chapter 2) throughout the snow-free period, and dry palsas continuously released CO_2 (chapters 4 and 6.1). Experimental warming at dry sites generally reduces the C sink strength or causes net C release to the atmosphere (chapter 2), by enhancing CO_2 emissions (Biasi et al. 2008; Oberbauer et al. 2007; Natali et al. 2011; Natali et al. 2014; Lund et al. 2012).

Our results further show that dry tundra surfaces have only a negligible role as CH_4 emitters under the current climate (chapter 2), and display CH_4 uptake (chapter 2, chapter 4). Dry tundra sites often consume atmospheric CH_4 (Flessa et al. 2008; Christensen & Cox 1995; Nykänen et al. 2003; Jørgensen et al. 2015; Bartlett & Harriss 1993; Malhotra & Roulet 2015; Lau et al. 2015; Van Huissteden et al. 2008), with increasing CH_4 uptake expected as the soils warm (Jørgensen et al. 2015; D'imperio et al. 2017; Curry 2009; Zhuang et al. 2013). The results of this thesis show that not only warmer soils, but also a deepening active layer associated with permafrost thaw, in fact, increases CH_4 uptake of palsas as long as conditions are dry, due to a high CH_4 oxidation potential (chapter 4), rather than promoting CH_4 release from permafrost. This is an important finding, considering that current models project increased CH_4 emissions from tundra when permafrost thaws and the landscape becomes wetter (Deng et al. 2014; Wilson et al. 2017; Koven et al. 2015; Anisimov 2007). Whether Arctic land areas will turn wetter or drier when permafrost thaws is, however, highly uncertain (Schuur et al. 2015) and will vary by region. In fact, mounting evidence suggests that permafrost degradation will lead to a reduction in wetland extent (Avis et al. 2011), by increasing drainage and run-off, causing surface drying (Liljedahl et al. 2016; Swindles et al. 2015; Malmer et al. 2005).

Enhanced surface drying, when occurring over large areas, is thus likely to affect the Arctic CH_4 sink, with potential repercussions on the global CH_4 budget. However, the CH_4 sink strength of Northern latitudes is not well constrained even under the present climate. This is surprising, considering the current discrepancy between global bottom-up estimates (upscaling of measured field fluxes) and top-down approaches (atmospheric observations) (Kirschke et al. 2013), indicating that CH_4 emis-

sions from northern wetlands are currently overestimated (Saunois et al. 2016). Recent studies show that CH_4 uptake by dry tundra soils can govern the regional CH_4 budget even if CH_4 emitting wetlands are present (Jørgensen et al. 2015; D'imperio et al. 2017). The results of this thesis (chapter 4) thus emphasize that CH_4 fluxes from dry tundra surfaces have to be considered when predicting the CH_4 budget of the Arctic, especially considering the potential of these dry surfaces to counterbalance CH_4 emissions from wetlands (D'imperio et al. 2017).

Importantly, this thesis shows that dry tundra surfaces, especially peatlands (chapter 6.1), are sources of the strong GHG N_2O, with increasing N_2O source strength in a warmer world (chapter 2, chapter 5). Accordingly, permafrost uplift, inducing dry conditions, poses a risk for N_2O emissions, especially in soils where the nutrient content is high. Dry tundra soils display high N mineralization and nitrification rates (Weintraub & Schimel 2003; Alves et al. 2013; Chapin 1996), producing mineral N available for N_2O production, and also disrupted plant growth may contribute towards enhancing the mineral N pool (chapter 2). Measurements of N_2O across the Arctic biome are still scarce (Table 2), but this thesis provides strong evidence that N_2O emissions from dry tundra surfaces are likely substantial, while emissions from wetter surfaces might be negligible (chapter 5).

Table 2. *Summary of N_2O emission rates measured from Arctic ecosystems.*

	Location	N_2O flux, mean	Experimental treatment				Reference
		[mg N_2O m^{-2} d^{-1}]	Warming	Permafrost thaw	N-addition	Drainage, rewetting, N-addition	
permafrost peatlands							
peat plateau, bare	67°03′ N 62°57′ E	8.11 to 10.30	-	-	-	-	(Marushchak et al. 2011)
peat plateau, vegetated	67°03′ N 62°57′ E	0.04 to 0.06	-	-	-	-	(Marushchak et al. 2011)
palsa, bare	69°35′ N 26°11′ E	2.60	-	-	-	-	(Marushchak et al. 2011)
palsa, vegetated	69°35′ N 26°11′ E	0.20	-	-	-	-	(Marushchak et al. 2011)
peat plateau, bare	67°03′ N 62°55′ E	0.16 to 0.75	0.56 to 0.68	-	-	-	this thesis (chapter 2)
peat plateau, vegetated	67°03′ N 62°55′ E	0.00 to 0.02	0.00 to 0.12	-	-	-	this thesis (chapter 2)
palsa, bare	68°89′ N 21°05′ E	0.56	-	2.81	-	-	this thesis (chapter 5)
palsa, vegetated	68°89′ N 21°05′ E	0.14	-	0.20	-	-	this thesis (chapter 5)
upland mineral tundra							
tundra heath	67°03′ N 62°57′ E	-0.01 to 0.01	-	-	-	-	(Marushchak et al. 2011)

dry shrub tundra	67°03′ N 62°55′ E	-0.02 to 0.02	0.01 to 0.04	-	-	-	this thesis (chapter 2)
Coastal areas and wetlands							
coastal lowland	78°53′ N 75°46′ W	2.62	-0.65	-	10.88	-	(Lamb et al. 2011)
Eriophorum wetland	74°30′ N 20°30′ W	0.40	-	3.8	-	34.0	(Elberling et al. 2010)
Lichen tundra, wetlands	64°50′ N 111°38′ W	0.61	-	-	-	-	(Paré & Bedard-Haughn 2012)
Lowland tundra	79°55′ N 11°56′ E	-0.11 to 0.10	-	-	0.19	-	(Chen et al. 2014)
Boreal fens							
aapa mire	67°59′ N 24°12′ E	0.00 to 0.46	-	-	-	-	(Lohila et al. 2010)
Polar deserts							
herb barren polar desert, raised beaches	77°07′ N 87°56′ W	0.19 to 0.38	-	-	-	-	(Stewart et al. 2012)
semi-polar desert	78°52′ N 75°54′ W	0.38 to 0.76	-	-	-	-	(Stewart et al. 2012)
herb barren polar desert, flood plain	82°36′ N 63°25′ W	-0.15 to 0.76	-	-	-	-	(Stewart et al. 2012)

6.3 PREDICTING THE GREENHOUSE GAS BALANCE OF THE ARCTIC IN A CHANGING CLIMATE

So far, this thesis has highlighted the role of dry tundra surfaces in Arctic biogeochemical cycling as the climate warms. How representative are these findings for the Arctic Region, and how do they improve our understanding of the future GHG balance of the Arctic over longer time scales? In order to project the results and draw conclusions over larger scales, two major aspects need to be considered: 1) the short-term vs. the long-term response of the Arctic to climate change; and 2) the small-scale heterogeneity of Arctic tundra governing the individual surface response.

6.3.1 Short-term and long-term response of Arctic tundra to climate change

The two-year warming experiment (chapter 2) and the <1 year permafrost thaw experiment (chapters 3, 4, and 5) that simulated permafrost thaw within the next 5–15 years, provide realistic, but short-term scenarios of the ecosystem response of subarctic tundra to warming and thaw. The results of this thesis demonstrate a strong and immediate response of various tundra surfaces to warming (chapter 2), with a clear increase in respiration, but also limited plant CO_2 uptake particularly on peat soils (chapter 2). The increase in CO_2 emissions in upland mineral tundra soils was driven by increased microbial respiration under higher temperatures (chapter 2). In

accordance with these results, tundra soils often show a strong initial increase in respiration to warming (Grogan & Chapin 2000; Rustad et al. 2001; Welker et al. 2004; Biasi et al. 2008), with a proportionally large response of surface soils (Hicks Pries et al. 2015). Nonetheless, over longer time scales, Arctic ecosystems have shown signs of adaptation. In many cases, long-term warming leads to shrub expansion (Welker et al. 2004; Sistla et al. 2013; Rinnan et al. 2009), buffering C losses and even reinstating a C sink after multi-year warming (Oechel et al. 2000).

Additionally, evidence suggests that plants and microbes operate on different time scales (Natali et al. 2011), meaning that aboveground vegetation might respond quicker to changes in environmental settings than the belowground microbial community (Deslippe et al. 2012; Lamb et al. 2011), or vice versa (Elmendorf et al. 2012a). In terms of CH_4 dynamics, slow microbial growth rates explain the lack of CH_4 production in anaerobic short-term incubations and mesocosm studies, where CH_4 production generally sets in with a considerable time lag (Treat et al. 2015; Schädel et al. 2016; Walz et al. 2017; Blodau & Moore 2003), and may remain low even after three years (Knoblauch et al. 2013). Hence, it is likely that with longer incubation time, simulated permafrost thaw in mesocosms under wet conditions (chapter 4) causes CH_4 emissions. Wet conditions after permafrost thaw, supporting a slowly growing methanogenic community, along with shifts towards fen-like vegetation (Prater et al. 2007; Hodgkins et al. 2014) likely lead to enhanced CH_4 production and release in the long-term (Turetsky et al. 2002). The common observation of a delayed CH_4 production after permafrost thaw also points towards a shortcoming of laboratory-based incubation studies: in the natural environment, thermokarst processes leading to input of methanogen communities from surrounding wetlands support CH_4 production immediately upon thaw.

Future vegetation changes are also likely to alter the Arctic N_2O budget, since disturbances in the vegetation cover and growth can promote N_2O release from peat soils (chapter 2). Considering the projected increase in extreme weather events leading to more frequent tundra fires and pest outbreaks, as well as the overall browning trend observed in the Arctic (Phoenix & Bjerke 2016), N_2O emissions might gain importance over longer time scales, especially in areas of active permafrost thaw (chapter 5) and thermokarst formation (Abbott & Jones 2015).

If considering not only a warming of the soil column, but the additional factor of enhanced substrate input from thawing permafrost (chapters 3, 4, and 5), the deep soil C (and N) pools are likely to provide an additional, long-lasting feedback to the climate via GHG release. While this thesis provides the first conclusive evidence on a permafrost-N feedback to climate change (chapter 5), a multitude of studies have ascertained substantial old C release from thawing permafrost landscapes (Schuur et al. 2009; Vogel et al. 2009; Turetsky et al. 2002; Dorrepaal et al. 2009). The results obtained in this thesis clearly show the contribution of permafrost C to CO_2 emissions, with an increasing radiocarbon age of the C respired after thawing the permafrost

(chapter 4). Permafrost C losses are expected to increase (Schuur et al. 2009), emphasizing the importance of this slowly degradable C pool at depth over longer time scales (Schädel et al. 2014; Bracho et al. 2016).
Observations and predictions on the long-term GHG response of Arctic ecosystems to climate change differ (Hollister et al. 2005), largely due to a multitude of indirect effects associated with climate warming, such as changes in moisture, vegetation, microbial community structure and functioning, substrate availability, and growing season length. Clearly, two factors largely determine the short- and long-term response of Arctic ecosystems to environmental change: first, the climatic location within the Arctic (high- vs. low-Arctic, coastal vs. inland); and second, the geomorphology, determining the topographic location, soil type and moisture regime.

6.3.2 Role of climatic location and small-scale heterogeneity in determining the ecosystem response of Arctic tundra

This study focused on southern tundra ecosystems in the discontinuous permafrost zone, where upland mineral and peat surfaces showed an immediate response to *in situ* warming (chapter 2): warming during the snow-free period of two consecutive years increased emissions of all three GHGs, increased microbial respiration and leaf area index (LAI) in mineral soils, but seemed to have an adverse effect on plant growth on peat soils (chapter 2). These changes associated to warming, observed right after initiation of the warming experiment, indicate the vulnerability of these low-Arctic ecosystems to environmental change: while high-Arctic ecosystems might be more resistant to short- and even longer-term changes, low-Arctic ecosystems, set in the marginal area of permafrost distribution, have already been subjected to gradual warming in the recent decades. With near-zero permafrost temperatures in these regions and on-going permafrost degradation, low-Arctic ecosystems might thus be far more susceptible to subtle temperature increase, and respond quickly to environmental change. While high-Arctic sites generally display a stronger response of vegetation to temperature (Henry & Molau 1997; Lamb et al. 2011; Hollister et al. 2005), shrub expansion is predicted mainly for low-Arctic regions (Myers-Smith et al. 2011; Elmendorf et al. 2012b; Arft et al. 1999), albeit with a strong regional variation. Within the low-Arctic, shrub expansion will be most pronounced in moist to wet areas, whereas cold regions might display stronger resistance to vegetation changes (Elmendorf et al. 2012b; Elmendorf et al. 2012a). Studies indicate that also microbial communities might show some initial resistance to environmental change in these high-Arctic ecosystems (Lamb et al. 2011).
Drastic landscape changes, affecting the GHG balance, occur increasingly in low-Arctic regions: permafrost degradation and thermokarst formation, as simulated in this study (chapters 3, 4 and 5), are accelerating across the Pan-Arctic (Kokelj & Jorgenson 2013), and especially pronounced in the Subarctic (Schuur et al. 2007; Schuur et al. 2009; Romanovsky et al. 2010; Sannel & Kuhry 2011; Hodgkins et al.

2014; Jones et al. 2017; Lara et al. 2016; Helbig et al. 2016; Sjöberg et al. 2015). Formation of thermokarst, and transition from frozen uplands and plateaus to thawed wetlands severely alters moisture conditions, locally leading to mire expansion (Malmer et al. 2005; Jackowicz-Korczyński et al. 2010) and formation of thaw ponds (Gorham 1991), enhancing CH_4 emissions (Johansson et al. 2006; Nauta et al. 2015; Natali et al. 2015; Wilson et al. 2017).

The patchiness of the mosaic-like tundra landscape, however, makes it difficult to predict future, and even current landscape-level GHG balances (Schneider von Deimling et al. 2012; Shaver et al. 2007; Sturtevant & Oechel 2013). Much of this uncertainty is linked to the still scarce observational site network across the vast Arctic landmasses (Sturtevant & Oechel 2013), but also to the nonlinear response (chapter 6.3.1) and small-scale heterogeneity of different soil and vegetation types to altered climatic conditions. Permafrost thaw in peatlands and other organic soils, for example, even though largely located in low-Arctic latitudes, might not progress as rapidly as in areas underlain by mineral soils (Hugelius et al. 2011): organic layers are a good insulator preserving the ice-core even during warm summers, due to the porous peat material (Oberman & Mazhitova 2001; Seppälä 2011). In addition, a thick vegetation cover can have an insulating effect and stabilize even warm permafrost, while moisture input via inflow of surface waters can destabilize even colder permafrost (Grosse et al. 2011). Thus, increases in annual precipitation (Table 1), as is predicted for the Arctic, (5-35% increase, ACIA 2005), will deepen the active layer and cause permafrost to thaw. Constraining the current extent of wetlands, lakes, uplands, peatlands, as well as areas covered by bare soil, should thus be considered a key priority to improve our understanding of Arctic GHG exchange.

6.3.3 Addressing uncertainties in future Arctic biogeochemical cycling

Not only the spatial heterogeneity of the Arctic region, but also diverse interactions and feedbacks on spatial and temporal scales (e.g., hydrology, topography, nutrient availability, vegetation, Grosse et al. 2016) need to be addressed to better predict climate-related changes in Arctic biogeochemical cycling. This study has highlighted that N_2O emissions from Arctic soils pose a large uncertainty in Arctic GHG budgets, since N_2O emissions are not currently considered to play a major role in Arctic GHG inventories. Yet, this thesis shows that N_2O emissions from the Arctic are likely substantial, and increase with warming (chapter 2) and permafrost thaw (chapter 5).

Not only this "non-carbon" permafrost–climate feedback, but also the permafrost–carbon feedback to our climate is not well constrained: Current permafrost–climate models identify the Arctic as a C sink due to enhanced plant productivity at higher temperatures (Koven et al. 2011; Qian et al. 2010). This C sink character is projected to level off within this century, turning these systems in net C sources to the atmosphere by 2100 (Koven et al. 2011; Qian et al. 2010; Abbott et al. 2016). However, con-

siderable uncertainties are connected with these model projections: small-scale hydrological effects and interactions between moisture changes and temperature are not well incorporated, and fundamental processes such as thermokarst erosion, interactions between the C and N cycle, leaching processes, and soil-plant interactions are lacking in these predictions (Koven et al. 2011; Schneider von Deimling et al. 2012; Koven et al. 2015; Abbott et al. 2016). The permafrost–C feedback has a substantial contribution to climate warming (Burke et al. 2017), and not accounting for the permafrost–C feedback significantly underestimates the warming scenarios currently presented in the IPCC report (Koven et al. 2011; Schaefer et al. 2014). However, constraining the permafrost–C feedback requires extensive studies on the temperature sensitivity and long-term decomposability of old C. Even though the permafrost C pool is often less labile than the surface C pool, deep soil C displays a high sensitivity to rising temperatures (Biasi et al. 2005; Dorrepaal et al. 2009; Fierer et al. 2005), implying that the long-term positive feedback of this slowly degrading C pool (Schädel et al. 2014) might be stronger than anticipated (chapter 4). The decomposition of this old C pool can further be accelerated by inputs of labile organic compounds derived from the surface soil and vegetation that are leached to deeper layers (Corbett et al. 2013). In fact, detailed time series of soil profile measurements of gases, DOC, nutrients, and microbial biomass obtained in connection with GHG flux measurements (chapters 2, 4 and 5) identified downward leaching as an important process promoting GHG production at depth. Thus, even without warming of deeper soil layers, plant–soil interaction greatly influence GHG production in the soil profile (chapter 2). This "priming" of old C at depth (Kuzyakov 2010; Wild et al. 2014; Wild et al. 2016), leading to a loss of the previously stable C (and N) pool (Walker et al. 2016), is not considered in Arctic soil C models (Ota et al. 2013; Koven et al. 2015).

Additionally, while models on the permafrost–C feedback attempt to include a gradual active layer deepening in current projections, the effects of abrupt thaw on GHG dynamics at the ecosystem level remain hard to predict (Koven et al. 2015; Koven et al. 2011; Schuur et al. 2015; Olefeldt et al. 2016; Burke et al. 2017). This study aimed at constraining this adverse response of the GHG balance to gradual versus abrupt permafrost thaw in subarctic peatlands (chapters 3, 4 and 5). While simulated peatland collapse only slightly lowered C emissions compared to the gradual active layer deepening scenario (chapter 4), increased wetness in the peat column affected transport and transformation pathways of gases: wet conditions suppressed N_2O emissions to the atmosphere after permafrost thaw, via complete denitrification and reduction of N_2O to N_2 (chapter 5), whereas limited out-diffusion of gases led to an accumulation of CO_2 in wet peat profiles (chapter 4). Together with an accumulation of DOC (chapter 4) with high potential degradability (chapter 3), this study indicates that lateral transport of labile C from thawing permafrost likely leads to off-site CO_2 emissions. The translocation of GHG emissions away from the thaw site, and the general coupling of the C and the hydrological cycle, are rarely considered (Vonk & Gustafsson 2013).

7 SUMMARY AND CONCLUSIONS

The key findings of this thesis are the following:

- **Warming of subarctic tundra increases overall GHG emissions to the atmosphere.** Mild air warming of ~1°C increased emissions not only of CO_2 and CH_4, but also of the strong GHG N_2O.
- **Permafrost thaw in subarctic peatlands increases CO_2 emissions to the atmosphere.** While surface soil and vegetation regulate active layer C fluxes, thawing of permafrost increases the proportion of old C in respired CO_2.
- **A deepening of the active layer in permafrost peatlands enhances CH_4 uptake.** Uplifted permafrost peatlands exhibit strong CH_4 oxidation in the peat profile, which is sustained even under high water table conditions, preventing CH_4 emissions to the atmosphere after permafrost thaw.
- **Permafrost thaw in subarctic peatlands increases N_2O emissions.** While Arctic N_2O emissions might be underestimated at present, permafrost thaw is likely to increase N_2O emissions, and areas with a high potential for N_2O release cover almost one fourth of the entire Arctic.
- **Enhanced GHG production due to warming is fuelled by leaching processes.** Even if the initial warming is limited to the air and surface soil, leaching of labile, surface soil-derived substrates enhanced GHG production at depth in the soil profile.
- **Soil processes at depth, and plant-soil interactions govern the amount of GHG emissions to the atmosphere.** Despite large GHG production potential from thawing permafrost, GHG production and emissions are decoupled, and the surface flux is regulated by soil biogeochemical processes during upwards diffusion of gases through the soil column.
- **Permafrost-derived DOC from peatlands shows a high degradation potential.** Leaching of DOC from the permafrost layer of Arctic peatlands to surrounding aquatic ecosystems may thus lead to offsite CO_2 production and emissions, which are not yet accounted for.
- **Vegetation and moisture regulate Arctic N_2O emissions.** Bare peat soils act as hot spots of N_2O in the Arctic, but reduced plant N uptake caused by higher temperatures, or excess N released from thawing permafrost, promotes N_2O emissions also from vegetated Arctic soils. Wet conditions suppress N_2O emissions.

BIBLIOGRAPHY

Abbott BW, Jones JB (2015) Permafrost collapse alters soil carbon stocks, respiration, CH_4, and N_2O in upland tundra. *Global Change Biology,* **21,** 4570-4587.

Abbott BW, Jones JB, Godsey SE, Larouche JR, Bowden WB (2015) Patterns and persistence of hydrologic carbon and nutrient export from collapsing upland permafrost. *Biogeosciences,* **12,** 3725-3740.

Abbott BW, Jones JB, Schuur EA *et al.* (2016) Biomass offsets little or none of permafrost carbon release from soils, streams, and wildfire: an expert assessment. *Environmental Research Letters,* **11,** 034014.

ACIA (2005) *Impacts of a Warming Arctic: Arctic Climate Impact Assessment.* Cambridge University Press, Cambridge, UK.

Aerts R, Callaghan TV, Dorrepaal E, van Logtestijn RSP, Cornelissen JHC (2012) Seasonal climate manipulations have only minor effects on litter decomposition rates and N dynamics but strong effects on litter P dynamics of sub-arctic bog species. *Oecologia,* **170,** 809-819.

Aerts R, Cornelissen JHC, Dorrepaal E, van Logtestijn RSP, Callaghan TV (2004) Effects of experimentally imposed climate scenarios on flowering phenology and flower production of subarctic bog species. *Global Change Biology,* **10,** 1599-1609.

Åkerman HJ, Johansson M (2008) Thawing permafrost and thicker active layers in sub-arctic Sweden. *Permafrost and Periglacial Processes,* **19,** 279-292.

Alves RJ, Wanek W, Zappe A, Richter A, Svenning MM, Schleper C, Urich T (2013) Nitrification rates in Arctic soils are associated with functionally distinct populations of ammonia-oxidizing archaea. *The ISME journal,* **7,** 1620-1631.

Anisimov O (2007) Potential feedback of thawing permafrost to the global climate system through methane emission. *Environmental Research Letters,* **2,** 045016.

Arft A, Walker M, Gurevitch Je *et al.* (1999) Responses of tundra plants to experimental warming: meta-analysis of the international tundra experiment. *Ecological Monographs,* **69,** 491-511.

Avis CA, Weaver AJ, Meissner KJ (2011) Reduction in areal extent of high-latitude wetlands in response to permafrost thaw. *Nature Geoscience,* **4,** 444-448.

Bartlett KB, Harriss RC (1993) Review and Assessment of Methane Emissions from Wetlands. *Chemosphere,* **26,** 261-320.

Beilman DW, MacDonald GM, Smith LC, Reimer PJ (2009) Carbon accumulation in peatlands of West Siberia over the last 2000 years. *Global Biogeochemical Cycles,* **23,** GB1012.

Bellisario LM, Bubier JL, Moore TR, Chanton JP (1999) Controls on CH_4 emissions from a northern peatland. *Global Biogeochemical Cycles,* **13,** 81-91.

Biasi C, Rusalimova O, Meyer H, Kaiser C, Wanek W, Barsukov P, Junger H, Richter A (2005) Temperature-dependent shift from labile to recalcitrant carbon sources of arctic heterotrophs. *Rapid Communications in Mass Spectrometry,* **19,** 1401-1408.

Biasi C, Meyer H, Rusalimova O *et al.* (2008) Initial effects of experimental warming on carbon exchange rates, plant growth and microbial dynamics of a lichen-rich dwarf shrub tundra in Siberia. *Plant and Soil,* **307,** 191-205.

Bintanja R, van der Linden EC (2013) The changing seasonal climate in the Arctic. *Scientific reports,* **3,** 1556.

Blodau C, Basiliko N, Moore TR (2004) Carbon turnover in peatland mesocosms exposed to different water table levels. *Biogeochemistry,* **67,** 331-351.

Blodau C, Moore TR (2003) Experimental response of peatland carbon dynamics to a water table fluctuation. *Aquatic Sciences,* **65,** 47-62.

Bokhorst S, Bjerke J, Bowles F, Melillo J, Callaghan T, Phoenix G (2008) Impacts of extreme winter warming in the sub-Arctic: growing season responses of dwarf shrub heathland. *Global Change Biology,* **14,** 2603-2612.

Bokhorst S, Huiskes A, Aerts R *et al.* (2013) Variable temperature effects of Open Top Chambers at polar and alpine sites explained by irradiance and snow depth. *Global Change Biology,* **19,** 64-74.

Borge AF, Westermann S, Solheim I, Etzelmüller B (2017) Strong degradation of palsas and peat plateaus in northern Norway during the last 60 years. *The Cryosphere,* **11,** 1-16.

Bracho R, Natali S, Pegoraro E *et al.* (2016) Temperature sensitivity of organic matter decomposition of permafrost-region soils during laboratory incubations. *Soil Biology and Biochemistry,* **97,** 1-14.

Bridgham SD, Pastor J, Dewey B, Weltzin JF, Updegraff K (2008) Rapid carbon response of peatlands to climate change. *Ecology,* **89,** 3041-3048.

Brown J, Ferrians Jr O, Heginbottom J, Melnikov E (2002) Circum-Arctic map of permafrost and ground-ice conditions. National Snow and Ice Data Center.

Burke EJ, Ekici A, Huang Y *et al.* (2017) Quantifying uncertainties of permafrost carbon–climate feedbacks. *Biogeosciences,* **14,** 3051.

Butterbach-Bahl K, Baggs EM, Dannenmann M, Kiese R, Zechmeister-Boltenstern S (2013) Nitrous oxide emissions from soils: how well do we understand the processes and their controls? *Philosophical Transactions of the Royal Society: Biological Sciences,* **368,** 20130122.

Chapin DM (1996) Nitrogen mineralization, nitrification, and denitrification in a high arctic lowland ecosystem, Devon Island, NWT, Canada. *Arctic and Alpine Research,* **28,** 85-92.

Chapin FS, Shaver GR, Giblin AE, Nadelhoffer KJ, Laundre JA (1995) Responses of Arctic Tundra to Experimental and Observed Changes in Climate. *Ecology,* **76,** 694-711.

Chen Q, Zhu R, Wang Q, Xu H (2014) Methane and nitrous oxide fluxes from four tundra ecotopes in Ny-Ålesund of the High Arctic. *Journal of Environmental Sciences,* **26,** 1403-1410.

Christensen JH, Krishna Kumar K, Aldrian E *et al.* (2013) Climate Phenomena and their Relevance for Future Regional Climate Change Supplementary Material. In: *Climate Change 2013: The Physical Science Basis. Contribution of Working Group I to the Fifth Assessment Report of the Intergovernmental Panel on Climate Change* (eds Stocker TF, Qin D, Plattner G-, et al), pp. 14SM-1-14SM-62. Cambridge University Press, Cambridge, UK.

Christensen TR, Jackowicz-Korczyński M, Aurela M, Crill P, Heliasz M, Mastepanov M, Friborg T (2012) Monitoring the multi-year carbon balance of a subarctic palsa mire with micrometeorological techniques. *Ambio,* **41,** 207-217.

Christensen TR, Johansson T, Åkerman HJ, Mastepanov M, Malmer N, Friborg T, Crill P, Svensson BH (2004) Thawing sub-arctic permafrost: Effects on vegetation and methane emissions. *Geophysical Research Letters,* **31,** L04501.

Christensen T, Cox P (1995) Response of Methane Emission from Arctic Tundra to Climatic-Change - Results from a Model Simulation. *Tellus Series B-Chemical and Physical Meteorology,* **47B,** 301-309.

Christensen T, Jonasson S, Callaghan T, Havstrom M (1999) On the potential CO_2 release from tundra soils in a changing climate. *Applied Soil Ecology,* **11,** 127-134.

Ciais P, Sabine C, Bala G *et al.* (2013) Carbon and other biogeochemical cycles. In: *Climate change 2013: the physical science basis. Contribution of Working Group I to the Fifth Assessment Report of the Intergovernmental Panel on Climate Change* (eds Stocker TF, Qin D, Plattner GK, et al), pp. 465-570. Cambridge University Press, Cambridge, United Kingdom and New York, NY, USA.

Corbett JE, Burdige DJ, Tfaily MM, Dial AR, Cooper WT, Glaser PH, Chanton JP (2013) Surface production fuels deep heterotrophic respiration in northern peatlands. *Global Biogeochemical Cycles,* **27,** 1163-1174.

Curry C (2009) The consumption of atmospheric methane by soil in a simulated future climate. *Biogeosciences,* **6,** 2355-2367.

Daulat WE, Clymo RS (1998) Effects of temperature and watertable on the efflux of methane from peatland surface cores. *Atmospheric Environment,* **32,** 3207-3218.

Davidson EA, Janssens IA, Luo YQ (2006) On the variability of respiration in terrestrial ecosystems: moving beyond Q_{10}. *Global Change Biology,* **12,** 154-164.

Deng J, Li C, Frolking S, Zhang Y, Backstrand K, Crill P (2014) Assessing effects of permafrost thaw on C fluxes based on multiyear modeling across a permafrost thaw gradient at Stordalen, Sweden. *Biogeosciences,* **11,** 4753-4770.

Deshpande BN, Crevecoeur S, Matveev A, Vincent WF (2016) Bacterial production in subarctic peatland lakes enriched by thawing permafrost. *Biogeosciences,* **13,** 4411-4427.

Deslippe JR, Hartmann M, Simard SW, Mohn WW (2012) Long-term warming alters the composition of Arctic soil microbial communities. *FEMS microbiology ecology,* **82,** 303-315.

D'imperio L, Nielsen CS, Westergaard-Nielsen A, Michelsen A, Elberling B (2017) Methane oxidation in contrasting soil types: responses to experimental warming with implication for landscape-integrated CH_4 budget. *Global Change Biology,* **23,** 966-976.

Dorrepaal E, Toet S, van Logtestijn RSP, Swart E, van de Weg MJ, Callaghan TV, Aerts R (2009) Carbon respiration from subsurface peat accelerated by climate warming in the subarctic. *Nature,* **460,** 616-620.

Drake TW, Wickland KP, Spencer RG, McKnight DM, Striegl RG (2015) Ancient low-molecular-weight organic acids in permafrost fuel rapid carbon dioxide production upon thaw. *Proceedings of the National Academy of Sciences of the United States of America,* **112,** 13946-13951.

Dutta K, Schuur E, Neff J, Zimov S (2006) Potential carbon release from permafrost soils of Northeastern Siberia. *Global Change Biology,* **12,** 2336-2351.

Elberling B, Christiansen HH, Hansen BU (2010) High nitrous oxide production from thawing permafrost. *Nature Geoscience,* **3,** 332-335.

Elberling B, Michelsen A, Schädel C, Schuur EA, Christiansen HH, Berg L, Tamstorf MP, Sigsgaard C (2013) Long-term CO_2 production following permafrost thaw. *Nature Climate Change,* **3,** 890-894.

Elmendorf SC, Henry GH, Hollister RD *et al.* (2012a) Global assessment of experimental climate warming on tundra vegetation: heterogeneity over space and time. *Ecology Letters,* **15,** 164-175.

Elmendorf SC, Henry GH, Hollister RD *et al.* (2012b) Plot-scale evidence of tundra vegetation change and links to recent summer warming. *Nature Climate Change,* **2,** 453-457.

Euskirchen ES, Edgar C, Turetsky M, Waldrop MP, Harden JW (2014) Differential response of carbon fluxes to climate in three peatland ecosystems that vary in the presence and stability of permafrost. *Journal of Geophysical Research: Biogeosciences,* **119,** 1576-1595.

Fierer N, Craine JM, McLauchlan K, Schimel JP (2005) Litter quality and the temperature sensitivity of decomposition. *Ecology,* **86,** 320-326.

Finger RA, Turetsky MR, Kielland K, Ruess RW, Mack MC, Euskirchen ES (2016) Effects of permafrost thaw on nitrogen availability and plant–soil interactions in a boreal Alaskan lowland. *Journal of Ecology,* **104,** 1542-1554.

Flessa H, Rodionov A, Guggenberger G *et al.* (2008) Landscape controls of CH_4 fluxes in a catchment of the forest tundra ecotone in northern Siberia. *Global Change Biology,* **14,** 2040-2056.

Fouché J, Keller C, Allard M, Ambrosi JP (2014) Increased CO_2 fluxes under warming tests and soil solution chemistry in Histic and Turbic Cryosols, Salluit, Nunavik, Canada. *Soil Biology and Biochemistry,* **68,** 185-199.

Frey KE, McClelland JW (2009) Impacts of permafrost degradation on arctic river biogeochemistry. *Hydrological Processes,* **23,** 169-182.

Frey KE, Smith LC (2005) Amplified carbon release from vast West Siberian peatlands by 2100. *Geophysical Research Letters,* **32,** L09401.

Frolking S, Roulet NT (2007) Holocene radiative forcing impact of northern peatland carbon accumulation and methane emissions. *Global Change Biology,* **13,** 1079-1088.

Frolking S, Roulet N, Lawrence D (2009) Issues related to incorporating northern peatlands into global climate models. In: *Carbon Cycling in Northern Peatlands* (eds Baird AJ, Belyea LR, Comas X, Reeve AS, Slater LD), pp. 19-35. American Geophysical Union, Washington, D. C., USA.

Gentsch N, Mikutta R, Shibistova O *et al.* (2015) Properties and bioavailability of particulate and mineral-associated organic matter in Arctic permafrost soils, Lower Kolyma Region, Russia. *European Journal of Soil Science,* **66,** 722-734.

Gorham E (1991) Northern peatlands: Role in the carbon cycle and probable responses to climatic warming. *Ecological Applications,* **1,** 182-195.

Grogan P, Chapin F (2000) Initial effects of experimental warming on above-and below-ground components of net ecosystem CO_2 exchange in arctic tundra. *Oecologia,* **125,** 512-520.

Grosse G, Goetz S, McGuire AD, Romanovsky VE, Schuur EA (2016) Changing permafrost in a warming world and feedbacks to the Earth system. *Environmental Research Letters,* **11,** 040201.

Grosse G, Romanovsky V, Jorgenson T, Walter Anthony K, Brown J, Overduin PP (2011) Vulnerability and feedbacks of permafrost to climate change. *Eos, Transactions American Geophysical Union,* **92,** 73-74.

Hamilton H (2011) Calculated change in seasonal temperature average (Fall: 2040-2059), under B1 emission scenario. Center for Applied Biodiversity Informatics, California Academy of Sciences.

Harden JW, Koven CD, Ping C *et al.* (2012) Field information links permafrost carbon to physical vulnerabilities of thawing. *Geophysical Research Letters,* **39,** L15704.

Hartmann DL, Tank AMK, Rusticucci M *et al.* (2013) Observations: atmosphere and surface. In: *Climate Change 2013 the Physical Science Basis: Working Group I Contribution to the Fifth Assessment Report of the Intergovernmental Panel on Climate Change* (eds Stocker TF, Qin D, Plattner GK, et al), pp. 159-254. Cambridge University Press, Cambridge, United Kingdom and New York, NY, USA.

Hayes DJ, Kicklighter DW, McGuire AD, Chen M, Zhuang Q, Yuan F, Melillo JM, Wullschleger SD (2014) The impacts of recent permafrost thaw on land-atmosphere greenhouse gas exchange. *Environmental Research Letters,* **9,** 045005.

Heginbottom JA, Brown J, Humlum O, Svensson H (2012) Permafrost and periglacial environments. *U.S. Geological Survey professional paper 1386-A-5,* A425-A496.

Heikkinen JE, Elsakov V, Martikainen PJ (2002) Carbon dioxide and methane dynamics and annual carbon balance in tundra wetland in NE Europe, Russia. *Global Biogeochemical Cycles,* **16,** 62-1-62-15.

Helbig M, Pappas C, Sonnentag O (2016) Permafrost thaw and wildfire: Equally important drivers of boreal tree cover changes in the Taiga Plains, Canada. *Geophysical Research Letters,* **43,** 1598-1606.

Henry G, Molau U (1997) Tundra plants and climate change: the International Tundra Experiment (ITEX). *Global Change Biology,* **3,** 1-9.

Heslop JK, Chandra S, Sobzcak WV, Davydov SP, Davydova AI, Spektor VV, Walter Anthony KM (2017) Variable respiration rates of incubated permafrost soil extracts from the Kolyma River lowlands, north-east Siberia. *Polar Research,* **36,** 1305157.

Hicks Pries CE, Logtestijn RS, Schuur EA, Natali SM, Cornelissen JH, Aerts R, Dorrepaal E (2015) Decadal warming causes a consistent and persistent shift from heterotrophic to autotrophic respiration in contrasting permafrost ecosystems. *Global Change Biology,* **21,** 4508-4519.

Hobbie SE, Chapin III FS (1998) The response of tundra plant biomass, aboveground production, nitrogen, and CO_2 flux to experimental warming. *Ecology,* **79,** 1526-1544.

Hodgkins SB, Tfaily MM, McCalley CK, Logan TA, Crill PM, Saleska SR, Rich VI, Chanton JP (2014) Changes in peat chemistry associated with permafrost thaw increase

greenhouse gas production. *Proceedings of the National Academy of Sciences of the United States of America,* **111,** 5819-5824.

Hollister RD, Webber PJ, Tweedie CE (2005) The response of Alaskan arctic tundra to experimental warming: Differences between short-and long-term responses. *Global Change Biology,* **11,** 525-536.

Hudson JMG, Henry GHR (2010) High Arctic plant community resists 15 years of experimental warming. *Journal of Ecology,* **98,** 1035-1041.

Hugelius G, Tarnocai C, Broll G, Canadell J, Kuhry P, Swanson D (2013) The Northern Circumpolar Soil Carbon Database: spatially distributed datasets of soil coverage and soil carbon storage in the northern permafrost regions. *Earth System Science Data,* **5,** 3-13.

Hugelius G, Strauss J, Zubrzycki S *et al.* (2014) Estimated stocks of circumpolar permafrost carbon with quantified uncertainty ranges and identified data gaps. *Biogeosciences,* **11,** 6573-6593.

Hugelius G, Routh J, Kuhry P, Crill P (2012) Mapping the degree of decomposition and thaw remobilization potential of soil organic matter in discontinuous permafrost terrain. *Journal of Geophysical Research: Biogeosciences,* **117,** G02030.

Hugelius G, Virtanen T, Kaverin D, Pastukhov A, Rivkin F, Marchenko S, Romanovsky V, Kuhry P (2011) High-resolution mapping of ecosystem carbon storage and potential effects of permafrost thaw in periglacial terrain, European Russian Arctic. *Journal of Geophysical Research: Biogeosciences,* **116,** G03024.

Hutchinson GL, Livingston GP, Healy RW, Striegl RG (2000) Chamber measurement of surface-atmosphere trace gas exchange: Numerical evaluation of dependence on soil, interfacial layer, and source/sink properties. *Journal of Geophysical Research-Atmospheres,* **105,** 8865-8875.

Jackowicz-Korczyński M, Christensen TR, Bäckstrand K, Crill P, Friborg T, Mastepanov M, Ström L (2010) Annual cycle of methane emission from a subarctic peatland. *Journal of Geophysical Research: Biogeosciences,* **115,** G02009.

Joabsson A, Christensen TR (2001) Methane emissions from wetlands and their relationship with vascular plants: an Arctic example. *Global Change Biology,* **7,** 919-932.

Johansson T, Malmer N, Crill PM, Friborg T, Akerman JH, Mastepanov M, Christensen TR (2006) Decadal vegetation changes in a northern peatland, greenhouse gas fluxes and net radiative forcing. *Global Change Biology,* **12,** 2352-2369.

Jones BM, Baughman CA, Romanovsky VE, Parsekian AD, Babcock EL, Jones MC, Grosse G, Berg EE (2016) Presence of rapidly degrading permafrost plateaus in south-central Alaska. *The Cryosphere,* **10,** 2673-2692.

Jones BM, Grosse G, Arp CD, Miller E, Liu L, Hayes DJ, Larsen CF (2015) Recent Arctic tundra fire initiates widespread thermokarst development. *Scientific reports,* **5,** 15865.

Jones M, Fahnestock J, Walker D, Walker M, Welker J (1998) Carbon dioxide fluxes in moist and dry arctic tundra during the snow-free season: responses to increases in summer temperature and winter snow accumulation. *Arctic and Alpine Research,* **30,** 373-380.

Jones MC, Harden J, O'donnell J, Manies K, Jorgenson T, Treat C, Ewing S (2017) Rapid carbon loss and slow recovery following permafrost thaw in boreal peatlands. *Global Change Biology,* **23,** 1109-1127.

Jørgensen CJ, Johansen KML, Westergaard-Nielsen A, Elberling B (2015) Net regional methane sink in High Arctic soils of northeast Greenland. *Nature Geoscience,* **8,** 20-23.

Kaverin D, Pastukhov A, Lapteva E, Biasi C, Marushchak M, Martikainen P (2016) Morphology and properties of the soils of permafrost peatlands in the southeast of the Bol'shezemel'skaya tundra. *Eurasian Soil Science,* **49,** 498-511.

Keuper F, Bodegom PM, Dorrepaal E, Weedon JT, Hal J, Logtestijn RS, Aerts R (2012) A frozen feast: thawing permafrost increases plant-available nitrogen in subarctic peatlands. *Global Change Biology,* **18,** 1998-2007.

Kirschbaum MU (1995) The temperature dependence of soil organic matter decomposition, and the effect of global warming on soil organic C storage. *Soil Biology and Biochemistry,* **27,** 753-760.

Kirschke S, Bousquet P, Ciais P *et al.* (2013) Three decades of global methane sources and sinks. *Nature geoscience,* **6,** 813-823.

Kirtman B, Power S, Adedoyin A *et al.* (2013) Near-term climate change: projections and predictability. In: *Climate Change 2013: The Physical Science Basis. Contribution of Working Group I to the Fifth Assessment Report of the Intergovernmental Panel on Climate Change* (eds Stocker TF, Qin D, Plattner GK, et al), pp. 953-1028. Cambridge University Press, Cambridge, United Kingdom and New York, NY, USA.

Knoblauch C, Beer C, Sosnin A, Wagner D, Pfeiffer E (2013) Predicting long-term carbon mineralization and trace gas production from thawing permafrost of Northeast Siberia. *Global Change Biology,* **19,** 1160-1172.

Knoblauch C, Spott O, Evgrafova S, Kutzbach L, Pfeiffer E (2015) Regulation of methane production, oxidation, and emission by vascular plants and bryophytes in ponds of the northeast Siberian polygonal tundra. *Journal of Geophysical Research: Biogeosciences,* **120,** 2525-2541.

Koenigk T, Brodeau L, Graversen RG, Karlsson J, Svensson G, Tjernström M, Willén U, Wyser K (2013) Arctic climate change in 21st century CMIP5 simulations with EC-Earth. *Climate Dynamics,* **40,** 2719-2743.

Kohout T, Bućko MS, Rasmus K, Leppäranta M, Matero I (2014) Non-Invasive Geophysical Investigation and Thermodynamic Analysis of a Palsa in Lapland, Northwest Finland. *Permafrost and Periglacial Processes,* **25,** 45-52.

Kokelj S, Jorgenson M (2013) Advances in thermokarst research. *Permafrost and Periglacial Processes,* **24,** 108-119.

Koven CD, Ringeval B, Friedlingstein P, Ciais P, Cadule P, Khvorostyanov D, Krinner G, Tarnocai C (2011) Permafrost carbon-climate feedbacks accelerate global warming. *Proceedings of the National Academy of Sciences of the United States of America,* **108,** 14769-14774.

Koven CD, Schuur EA, Schadel C *et al.* (2015) A simplified, data-constrained approach to estimate the permafrost carbon-climate feedback. *Philosophical transactions.Series A, Mathematical, physical, and engineering sciences,* **373,** 20140423.

Kutzbach L, Wagner D, Pfeiffer E (2004) Effect of microrelief and vegetation on methane emission from wet polygonal tundra, Lena Delta, Northern Siberia. *Biogeochemistry,* **69,** 341-362.

Kuzyakov Y (2010) Priming effects: interactions between living and dead organic matter. *Soil Biology and Biochemistry,* **42,** 1363-1371.

Kwon MJ, Beulig F, Ilie I *et al.* (2017) Plants, microorganisms, and soil temperatures contribute to a decrease in methane fluxes on a drained Arctic floodplain. *Global Change Biology,* **23,** 2396-2412.

Kwon MJ, Heimann M, Kolle O, Luus K, Schuur EA, Zimov N, Zimov SA, Göckede M (2016) Long-term drainage reduces CO_2 uptake and increases CO_2 emission on a Siberian floodplain due to shifts in vegetation community and soil thermal characteristics. *Biogeosciences,* **13,** 4219-4235.

Lafleur PM, Humphreys ER, St. Louis VL *et al.* (2012) Variation in peak growing season net ecosystem production across the Canadian Arctic. *Environmental science & technology,* **46,** 7971-7977.

Lai DYF (2009) Methane Dynamics in Northern Peatlands: A Review. *Pedosphere,* **19,** 409-421.

Lamb EG, Han S, Lanoil BD, Henry GHR, Brummell ME, Banerjee S, Siciliano SD (2011) A High Arctic soil ecosystem resists long-term environmental manipulations. *Global Change Biology,* **17,** 3187-3194.

Lara MJ, Genet H, McGuire AD *et al.* (2016) Thermokarst rates intensify due to climate change and forest fragmentation in an Alaskan boreal forest lowland. *Global Change Biology,* **22,** 816-829.

Lau MC, Stackhouse BT, Layton AC *et al.* (2015) An active atmospheric methane sink in high Arctic mineral cryosols. *The ISME journal,* **9,** 1880-1891.

Lee H, Schuur EA, Inglett KS, Lavoie M, Chanton JP (2012) The rate of permafrost carbon release under aerobic and anaerobic conditions and its potential effects on climate. *Global Change Biology,* **18,** 515-527.

Liblik LK, Moore TR, Bubier JL, S.D.Robinson (1997) Methane emissions from wetlands in the zone of discontinuous permafrost: Fort Simpson, Northwest Territories, Canada. *Global Biogeochemical Cycles,* **11,** 485-494.

Liljedahl AK, Boike J, Daanen RP *et al.* (2016) Pan-Arctic ice-wedge degradation in warming permafrost and its influence on tundra hydrology. *Nature Geoscience,* **9,** 312-319.

Limpens J, Berendse F, Blodau C *et al.* (2008) Peatlands and the carbon cycle: from local processes to global implications–a synthesis. *Biogeosciences,* **5,** 1475-1491.

Lohila A, Aurela M, Hatakka J, Pihlatie M, Minkkinen K, Penttilä T, Laurila T (2010) Responses of N_2O fluxes to temperature, water table and N deposition in a northern boreal fen. *European Journal of Soil Science,* **61,** 651-661.

Lu M, Zhou X, Yang Q *et al.* (2013) Responses of ecosystem carbon cycle to experimental warming: a meta-analysis. *Ecology,* **94,** 726-738.

Lund M, Falk JM, Friborg T, Mbufong HN, Sigsgaard C, Soegaard H, Tamstorf MP (2012) Trends in CO_2 exchange in a high Arctic tundra heath, 2000–2010. *Journal of Geophysical Research: Biogeosciences,* **117,** G02001.

Lupascu M, Welker J, Seibt U, Maseyk K, Xu X, Czimczik C (2014) High Arctic wetting reduces permafrost carbon feedbacks to climate warming. *Nature Climate Change,* **4,** 51-56.

Malhotra A, Roulet N (2015) Environmental correlates of peatland carbon fluxes in a thawing landscape: do transitional thaw stages matter? *Biogeosciences,* **12,** 3119-3130.

Malmer N, Johansson T, Olsrud M, Christensen TR (2005) Vegetation, climatic changes and net carbon sequestration in a North-Scandinavian subarctic mire over 30 years. *Global Change Biology,* **11,** 1895-1909.

Marion G, Henry G, Freckman D *et al.* (1997) Open-top designs for manipulating field temperature in high-latitude ecosystems. *Global Change Biology,* **3,** 20-32.

Marushchak M, Friborg T, Biasi C *et al.* (2016) Methane dynamics in the subarctic tundra: combining stable isotope analyses, plot-and ecosystem-scale flux measurements. *Biogeosciences,* **13,** 597-608.

Marushchak M, Kiepe I, Biasi C *et al.* (2013) Carbon dioxide balance of subarctic tundra from plot to regional scales. *Biogeosciences,* **10,** 437-452.

Marushchak ME, Pitkamaki A, Koponen H, Biasi C, Seppala M, Martikainen PJ (2011) Hot spots for nitrous oxide emissions found in different types of permafrost peatlands. *Global Change Biology,* **17,** 2601-2614.

Mauritz M, Bracho R, Celis G *et al.* (2017) Nonlinear CO_2 flux response to 7 years of experimentally induced permafrost thaw. *Global Change Biology,* **23,** 3646-3666.

McGuire AD, Hayes DJ, Kicklighter DW *et al.* (2010) An analysis of the carbon balance of the Arctic Basin from 1997 to 2006. *Tellus B,* **62,** 455-474.

McGuire A, Christensen T, Hayes D *et al.* (2012) An assessment of the carbon balance of Arctic tundra: comparisons among observations, process models, and atmospheric inversions. *Biogeosciences,* **9,** 3185-3204.

Moni C, Lerch TZ, de Zarruk KK, Strand LT, Forte C, Certini G, Rasse DP (2015) Temperature response of soil organic matter mineralisation in arctic soil profiles. *Soil Biology and Biochemistry,* **88,** 236-246.

Moore T, Roulet N, Waddington J (1998) Uncertainty in predicting the effect of climatic change on the carbon cycling of Canadian peatlands. *Climatic Change,* **40,** 229-245.

Myers-Smith IH, Forbes BC, Wilmking M *et al.* (2011) Shrub expansion in tundra ecosystems: dynamics, impacts and research priorities. *Environmental Research Letters,* **6,** 045509.

Myhre G, Shindell D, Bréon F *et al.* (2013) Anthropogenic and natural radiative forcing. In: *Climate Change 2013: The Physical Science Basis. Contribution of Working Group I to the Fifth Assessment Report of the Intergovernmental Panel on Climate Change* (eds Stocker TF, Qin D, Plattner GK, et al), pp. 659-740. Cambridge University Press, Cambridge, United Kingdom and New York, NY, USA.

Natali SM, Schuur EA, Rubin RL (2012) Increased plant productivity in Alaskan tundra as a result of experimental warming of soil and permafrost. *Journal of Ecology,* **100,** 488-498.

Natali SM, Schuur EA, Webb EE, Pries CEH, Crummer KG (2014) Permafrost degradation stimulates carbon loss from experimentally warmed tundra. *Ecology,* **95,** 602-608.

Natali SM, Schuur EAG, Mauritz M *et al.* (2015) Permafrost thaw and soil moisture driving CO_2 and CH_4 release from upland tundra. *Journal of Geophysical Research-Biogeosciences,* **120,** 525-537.

Natali SM, Schuur EAG, Trucco C, Pries CEH, Crummer KG, Lopez AFB (2011) Effects of experimental warming of air, soil and permafrost on carbon balance in Alaskan tundra. *Global Change Biology,* **17,** 1394-1407.

Nauta AL, Heijmans MMPD, Blok D *et al.* (2015) Permafrost collapse after shrub removal shifts tundra ecosystem to a methane source. *Nature Climate Change,* **5,** 67-70.

Nieder R, Benbi DK (2008) Carbon and nitrogen in the terrestrial environment. Springer Science & Business Media, Germany/Netherlands.

Nykänen H, Heikkinen JE, Pirinen L, Tiilikainen K, Martikainen PJ (2003) Annual CO_2 exchange and CH_4 fluxes on a subarctic palsa mire during climatically different years. *Global Biogeochemical Cycles,* **17,** 1018.

O'Donnell JA, Jorgenson MT, Harden JW, McGuire AD, Kanevskiy MZ, Wickland KP (2012) The effects of permafrost thaw on soil hydrologic, thermal, and carbon dynamics in an Alaskan peatland. *Ecosystems,* **15,** 213-229.

Oberbauer SF, Starr G, Pop EW (1998) Effects of extended growing season and soil warming on carbon dioxide and methane exchange of tussock tundra in Alaska. *Journal of Geophysical Research: Atmospheres (1984–2012),* **103,** 29075-29082.

Oberbauer SF, Tweedie CE, Welker JM *et al.* (2007) Tundra CO_2 fluxes in response to experimental warming across latitudinal and moisture gradients. *Ecological Monographs,* **77,** 221-238.

Oberman NG, Mazhitova GG (2001) Permafrost dynamics in the north-east of European Russia at the end of the 20th century. *Norsk Geografisk Tidsskrift - Norwegian Journal of Geography,* **55,** 241-244.

Oechel WC, Hastings SJ, Vourlitis G, Jenkins M, Riechers G, Grulke N (1993) Recent change of Arctic tundra ecosystems from a net carbon dioxide sink to a source. *Nature,* **361,** 520-523.

Oechel WC, Vourlitis GL, Hastings SJ, Zulueta RC, Hinzman L, Kane D (2000) Acclimation of ecosystem CO_2 exchange in the Alaskan Arctic in response to decadal climate warming. *Nature,* **406,** 978-981.

Olefeldt D, Roulet NT (2012) Effects of permafrost and hydrology on the composition and transport of dissolved organic carbon in a subarctic peatland complex. *Journal of Geophysical Research: Biogeosciences,* **117,** G01005.

Olefeldt D, Roulet NT, Bergeron O, Crill P, Bäckstrand K, Christensen TR (2012) Net carbon accumulation of a high-latitude permafrost palsa mire similar to permafrost-free peatlands. *Geophysical Research Letters,* **39,** L03501.

Olefeldt D, Turetsky MR, Crill PM, McGuire AD (2013) Environmental and physical controls on northern terrestrial methane emissions across permafrost zones. *Global Change Biology,* **19,** 589-603.

Olefeldt D, Goswami S, Grosse G *et al.* (2016) Circumpolar distribution and carbon storage of thermokarst landscapes. *Nature communications,* **7,** 13043.

Öquist M, Svensson B (2002) Vascular plants as regulators of methane emissions from a subarctic mire ecosystem. *Journal of Geophysical Research: Atmospheres,* **107,** 4580.

Ota M, Nagai H, Koarashi J (2013) Root and dissolved organic carbon controls on subsurface soil carbon dynamics: A model approach. *Journal of Geophysical Research: Biogeosciences,* **118,** 1646-1659.

Overland JE, Wang M, Walsh JE, Stroeve JC (2013) Future Arctic climate changes: Adaptation and mitigation time scales. *Earth's Future,* **2,** 68-74.

Paré MC, Bedard-Haughn A (2012) Landscape-scale N mineralization and greenhouse gas emissions in Canadian Cryosols. *Geoderma,* **189,** 469-479.

Parmentier F, Van Der Molen M, Van Huissteden J, Karsanaev S, Kononov A, Suzdalov D, Maximov T, Dolman A (2011) Longer growing seasons do not increase net carbon uptake in the northeastern Siberian tundra. *Journal of Geophysical Research: Biogeosciences (2005–2012),* **116,** G04013.

Parmentier FW, Christensen TR, Rysgaard S *et al.* (2017) A synthesis of the arctic terrestrial and marine carbon cycles under pressure from a dwindling cryosphere. *Ambio,* **46,** 53-69.

Pengerud A, Cécillon L, Johnsen LK, Rasse DP, Strand LT (2013) Permafrost distribution drives soil organic matter stability in a subarctic palsa peatland. *Ecosystems,* **16,** 934-947.

Phoenix GK, Bjerke JW (2016) Arctic browning: extreme events and trends reversing arctic greening. *Global Change Biology,* **22,** 2960-2962.

Pirinen P, Simola H, Aalto J, Kaukoranta J, Karlsson P, Ruuhela R (2012) Tilastoja suomen ilmastosta 1981–2010. *The Finnish Meteorological Institute,* 96 pp.

Prater JL, Chanton JP, Whiting GJ (2007) Variation in methane production pathways associated with permafrost decomposition in collapse scar bogs of Alberta, Canada. *Global Biogeochemical Cycles,* **21,** GB4004.

Qian H, Joseph R, Zeng N (2010) Enhanced terrestrial carbon uptake in the Northern High Latitudes in the 21st century from the Coupled Carbon Cycle Climate Model Intercomparison Project model projections. *Global Change Biology,* **16,** 641-656.

Ravn NR, Ambus P, Michelsen A (2017) Impact of decade-long warming, nutrient addition and shading on emission and carbon isotopic composition of CO_2 from two subarctic dwarf shrub heaths. *Soil Biology and Biochemistry,* **111,** 15-24.

Regina K, Silvola J, Martikainen PJ (1999) Short-term effects of changing water table on N_2O fluxes from peat monoliths from natural and drained boreal peatlands. *Global Change Biology,* **5,** 183-189.

Repo ME, Susiluoto S, Lind SE, Jokinen S, Elsakov V, Biasi C, Virtanen T, Martikainen PJ (2009) Large N_2O emissions from cryoturbated peat soil in tundra. *Nature Geoscience,* **2,** 189-192.

Rinnan R, Michelsen A, Bååth E, Jonasson S (2007) Mineralization and carbon turnover in subarctic heath soil as affected by warming and additional litter. *Soil Biology and Biochemistry,* **39,** 3014-3023.

Rinnan R, Stark S, Tolvanen A (2009) Responses of vegetation and soil microbial communities to warming and simulated herbivory in a subarctic heath. *Journal of Ecology,* **97,** 788-800.

Romanovsky V, Burgess M, Smith S, Yoshikawa K, Brown J (2002) Permafrost Temperature Records: Indicators of Climate Change. *EOS, Transactions, American Geophysical Union,* **83,** 589-600.

Romanovsky VE, Drozdov DS, Oberman NG *et al.* (2010) Thermal State of Permafrost in Russia. *Permafrost and Periglacial Processes,* **21,** 136-155.

Ronkainen T, Valiranta M, Mcclymont E, Biasi C, Salonen S, Fontana S, Tuittila E (2015) A combined biogeochemical and palaeobotanical approach to study permafrost environments and past dynamics. *Journal of Quaternary Science,* **30,** 189-200.

Routh J, Hugelius G, Kuhry P, Filley T, Tillman PK, Becher M, Crill P (2014) Multi-proxy study of soil organic matter dynamics in permafrost peat deposits reveal vulnerability to climate change in the European Russian Arctic. *Chemical Geology,* **368,** 104-117.

Rustad L, Campbell J, Marion G *et al.* (2001) A meta-analysis of the response of soil respiration, net nitrogen mineralization, and aboveground plant growth to experimental ecosystem warming. *Oecologia,* **126,** 543-562.

Salmon VG, Soucy P, Mauritz M, Celis G, Natali SM, Mack MC, Schuur EAG (2016) Nitrogen availability increases in a tundra ecosystem during five years of experimental permafrost thaw. *Global Change Biology,* **22,** 1927-1941.

Sannel ABK, Kuhry P (2011) Warming-induced destabilization of peat plateau/thermokarst lake complexes. *Journal of Geophysical Research: Biogeosciences,* **116,** G03035.

Saunois M, Bousquet P, Poulter B *et al.* (2016) The global methane budget 2000-2012. *Earth System Science Data,* **8,** 697-751.

Schädel C, Bader MK, Schuur EA *et al.* (2016) Potential carbon emissions dominated by carbon dioxide from thawed permafrost soils. *Nature Climate Change,* **6,** 950-953.

Schädel C, Schuur EA, Bracho R *et al.* (2014) Circumpolar assessment of permafrost C quality and its vulnerability over time using long-term incubation data. *Global Change Biology,* **20,** 641-652.

Schaefer K, Lantuit H, Romanovsky VE, Schuur EA, Witt R (2014) The impact of the permafrost carbon feedback on global climate. *Environmental Research Letters,* **9,** 085003.

Schaeffer SM, Sharp E, Schimel JP, Welker JM (2013) Soil–plant N processes in a High Arctic ecosystem, NW Greenland are altered by long-term experimental warming and higher rainfall. *Global Change Biology,* **19,** 3529-3539.

Schneider von Deimling T, Meinshausen M, Levermann A, Huber V, Frieler K, Lawrence D, Brovkin V (2012) Estimating the near-surface permafrost-carbon feedback on global warming. *Biogeosciences,* **9,** 649-665.

Schuur EA, Crummer KG, Vogel JG, Mack MC (2007) Plant species composition and productivity following permafrost thaw and thermokarst in Alaskan tundra. *Ecosystems,* **10,** 280-292.

Schuur EAG, McGuire AD, Schaedel C *et al.* (2015) Climate change and the permafrost carbon feedback. *Nature,* **520,** 171-179.

Schuur EAG, Bockheim J, Canadell JG *et al.* (2008) Vulnerability of permafrost carbon to climate change: Implications for the global carbon cycle. *Bioscience,* **58,** 701-714.

Schuur EAG, Vogel JG, Crummer KG, Lee H, Sickman JO, Osterkamp TE (2009) The effect of permafrost thaw on old carbon release and net carbon exchange from tundra. *Nature,* **459,** 556-559.

Seppälä M (2011) Synthesis of studies of palsa formation underlining the importance of local environmental and physical characteristics. *Quaternary Research,* **75,** 366-370.

Seppälä M (2006) Palsa mires in Finland. *The Finnish environment,* **23,** 155-162.

Seppälä M (2003) Surface abrasion of palsas by wind action in Finnish Lapland. *Geomorphology,* **52,** 141-148.

Serreze M, Barrett A, Stroeve J, Kindig D, Holland M (2009) The emergence of surface-based Arctic amplification. *The Cryosphere,* **3,** 11-19.

Shaver G, Street L, Rastetter E, Van Wijk M, Williams M (2007) Functional convergence in regulation of net CO2 flux in heterogeneous tundra landscapes in Alaska and Sweden. *Journal of Ecology,* **95,** 802-817.

Shurpali NJ, Rannik U, Jokinen S *et al.* (2016) Neglecting diurnal variations leads to uncertainties in terrestrial nitrous oxide emissions. *Scientific reports,* **6,** 25739.

Sistla SA, Moore JC, Simpson RT, Gough L, Shaver GR, Schimel JP (2013) Long-term warming restructures Arctic tundra without changing net soil carbon storage. *Nature,* **497,** 615-619.

Sjöberg Y, Marklund P, Pettersson R, Lyon SW (2015) Geophysical mapping of palsa peatland permafrost. *The Cryosphere,* **9,** 465-478.

Stewart KJ, Brummell ME, Farrell RE, Siciliano SD (2012) N2O flux from plant-soil systems in polar deserts switch between sources and sinks under different light conditions. *Soil Biology and Biochemistry,* **48,** 69-77.

Sturtevant CS, Oechel WC (2013) Spatial variation in landscape-level CO_2 and CH_4 fluxes from arctic coastal tundra: influence from vegetation, wetness, and the thaw lake cycle. *Global Change Biology,* **19,** 2853-2866.

Swindles GT, Morris PJ, Mullan D *et al.* (2015) The long-term fate of permafrost peatlands under rapid climate warming. *Scientific reports,* **5,** 17951.

Tarnocai C, Canadell J, Schuur E, Kuhry P, Mazhitova G, Zimov S (2009) Soil organic carbon pools in the northern circumpolar permafrost region. *Global Biogeochemical Cycles,* **23,** GB2023.

Treat CC, Natali SM, Ernakovich J *et al.* (2015) A pan-Arctic synthesis of CH_4 and CO_2 production from anoxic soil incubations. *Global Change Biology,* **21,** 2787-2803.

Treat CC, Wollheim WM, Varner RK, Grandy AS, Talbot J, Frolking S (2014) Temperature and peat type control CO_2 and CH_4 production in Alaskan permafrost peats. *Global Change Biology,* **20,** 2674-2686.

Turetsky M, Wieder R, Vitt D (2002) Boreal peatland C fluxes under varying permafrost regimes. *Soil Biology & Biochemistry,* **34,** 907-912.

Van Huissteden J, Maximov T, Kononov A, Dolman A (2008) Summer soil CH_4 emission and uptake in taiga forest near Yakutsk, Eastern Siberia. *Agricultural and Forest Meteorology,* **148,** 2006-2012.

Vaughan DG, Comiso JC, Allison I *et al.* (2013) Observations: Cryosphere. In: *Climate Change 2013: The Physical Science Basis. Contribution of Working Group I to the Fifth Assessment Report of the Intergovernmental Panel on Climate Change* (eds Stocker TF,

Qin D, Plattner GK, et al), pp. 317-382. Cambridge University Press, Cambridge, United Kingdom and New York, NY, USA.

Vogel J, Schuur EA, Trucco C, Lee H (2009) Response of CO_2 exchange in a tussock tundra ecosystem to permafrost thaw and thermokarst development. *Journal of Geophysical Research: Biogeosciences (2005–2012),* **114,** G04018.

Vonk JE, Gustafsson Ö (2013) Permafrost-carbon complexities. *Nature Geoscience,* **6,** 675-676.

Walker JK, Egger KN, Henry GH (2008) Long-term experimental warming alters nitrogen-cycling communities but site factors remain the primary drivers of community structure in high arctic tundra soils. *The ISME journal,* **2,** 982-995.

Walker TN, Garnett MH, Ward SE, Oakley S, Bardgett RD, Ostle NJ (2016) Vascular plants promote ancient peatland carbon loss with climate warming. *Global Change Biology,* **22,** 1880-1889.

Walz J, Knoblauch C, Böhme L, Pfeiffer E (2017) Regulation of soil organic matter decomposition in permafrost-affected Siberian tundra soils-Impact of oxygen availability, freezing and thawing, temperature, and labile organic matter. *Soil Biology and Biochemistry,* **110,** 34-43.

Wang Z, Roulet N (2017) Comparison of plant litter and peat decomposition changes with permafrost thaw in a subarctic peatland. *Plant and Soil,* **417,** 197-216.

Weedon JT, Kowalchuk GA, Aerts R, van Hal J, van Logtestijn R, Tas N, Roling WFM, van Bodegom PM (2012) Summer warming accelerates sub-arctic peatland nitrogen cycling without changing enzyme pools or microbial community structure. *Global Change Biology,* **18,** 138-150.

Weintraub MN, Schimel JP (2003) Interactions between carbon and nitrogen mineralization and soil organic matter chemistry in arctic tundra soils. *Ecosystems,* **6,** 0129-0143.

Welker JM, Fahnestock JT, Henry GH, O'Dea KW, Chimner RA (2004) CO_2 exchange in three Canadian High Arctic ecosystems: Response to long-term experimental warming. *Global Change Biology,* **10,** 1981-1995.

Wickland KP, Neff JC, Aiken GR (2007) Dissolved organic carbon in Alaskan boreal forest: Sources, chemical characteristics, and biodegradability. *Ecosystems,* **10,** 1323-1340.

Wild B, Schnecker J, Alves RJE *et al.* (2014) Input of easily available organic C and N stimulates microbial decomposition of soil organic matter in arctic permafrost soil. *Soil Biology and Biochemistry,* **75,** 143-151.

Wild B, Gentsch N, Capek P *et al.* (2016) Plant-derived compounds stimulate the decomposition of organic matter in arctic permafrost soils. *Scientific reports,* **6,** 25607.

Wilson R, Fitzhugh L, Whiting G, Frolking S, Harrison M, Dimova N, Burnett W, Chanton JP (2017) Greenhouse gas balance over thaw-freeze cycles in discontinuous zone permafrost. *Journal of Geophysical Research: Biogeosciences,* **122,** 387-404.

Xue K, Yuan MM, Shi ZJ *et al.* (2016) Tundra soil carbon is vulnerable to rapid microbial decomposition under climate warming. *Nature Climate Change,* **6,** 595-603.

Zamolodchikov D, Karelin D, Ivaschenko A (2000) Sensitivity of tundra carbon balance to ambient temperature. *Water, air, and soil pollution,* **119,** 157-169.

Zhu R, Ma D, Xu H (2014) Summertime N_2O, CH_4 and CO_2 exchanges from a tundra marsh and an upland tundra in maritime Antarctica. *Atmospheric Environment,* **83,** 269-281.

Zhuang Q, Chen M, Xu K *et al.* (2013) Response of global soil consumption of atmospheric methane to changes in atmospheric climate and nitrogen deposition. *Global Biogeochemical Cycles,* **27,** 650-663.

Zhuang Q, Melillo JM, Sarofim MC *et al.* (2006) CO_2 and CH_4 exchanges between land ecosystems and the atmosphere in northern high latitudes over the 21st century. *Geophysical Research Letters,* **33,** L17403.

Zimov SA, Davydov SP, Zimova GM, Davydova AI, Schuur EAG, Dutta K, Chapin,F.S.,,III (2006a) Permafrost carbon: Stock and decomposability of a globally significant carbon pool RID F-9371-2010. *Geophysical Research Letters,* **33,** L20502.

Zimov SA, Schuur EA, Chapin FSI (2006b) Permafrost and the global carbon budget. *Science,* **312,** 1612-1613.

Zoltai S, Tarnocai C (1975) Perennially frozen peatlands in the western Arctic and Subarctic of Canada. *Canadian Journal of Earth Sciences,* **12,** 28-43.

Zona D, Lipson DA, Richards JH, Phoenix GK, Liljedahl AK, Ueyama M, Sturtevant CS, Oechel WC (2014) Delayed responses of an Arctic ecosystem to an extreme summer: impacts on net ecosystem exchange and vegetation functioning. *Biogeosciences,* **11,** 5877-5888.

APPENDICES

APPENDIX 1:
SUPPLEMENTARY INFORMATION TO PUBLICATION I
Warming of Subarctic tundra increases emissions of all three important greenhouse gases – carbon dioxide, methane, and nitrous oxide.

APPENDIX 2:
SUPPLEMENTARY INFORMATION TO PUBLICATION II
Degradation potentials of dissolved organic carbon (DOC) from thawed permafrost peat.

APPENDIX 3:
SUPPLEMENTARY INFORMATION TO PUBLICATION III
Ecosystem carbon response of Arctic peatlands to simulated permafrost thaw.

APPENDIX 4:
SUPPLEMENTARY INFORMATION TO PUBLICATION IV
Increased nitrous oxide emissions from Arctic peatlands after permafrost thaw

APPENDIX 1:
SUPPLEMENTARY INFORMATION TO PUBLICATION I
Warming of Subarctic tundra increases emissions of all three important greenhouse gases – carbon dioxide, methane, and nitrous oxide.

Supplementary information to article "**Warming of subarctic tundra increases emissions of all three important greenhouse gases – carbon dioxide, methane, and nitrous oxide"**

Carolina Voigt, Richard E. Lamprecht, Maija E. Marushchak, Saara E. Lind, Alexander Novakovskiy, Mika Aurela, Pertti J. Martikainen, Christina Biasi

Supplementary methods

Experimental warming with OTCs and site selection

Temperature increase within OTCs is achieved by lowering wind speed and trapping heat radiation, potentially creating unwanted ecological effects such as shading, temperature extremes and altered soil moisture conditions (Marion *et al.*, 1997; Shaver *et al.*, 2000; Bokhorst *et al.*, 2013). Also, increases in deeper soil temperature within OTCs might be minor (Carlyle *et al.*, 2011). Snow fences (Natali *et al.*, 2011; Natali *et al.*, 2014; Salmon *et al.*, 2015) are efficient in warming also the soil, but they may delay summer warming and alter surface hydrology. They may also cause deeper thaw and surface subsidence (Natali *et al.*, 2011; Natali *et al.*, 2014; Salmon *et al.*, 2015), making it difficult to disentangle warming effects from effects of permafrost thaw. Active heating systems, such as heating cables and infra-red heaters (Bokhorst *et al.*, 2008) avoid changes in wind patterns and warm air and soil more evenly, but cause soil drying (Shaver *et al.*, 2000). Often passive heating systems such as OTCs thus provide the only possible heating system in remote arctic regions without permanent power supply, and side effects can be minimized when the OTC is adequately large (Marion *et al.*, 1997), as is the case in our study.

We established a warming experiment on three surface types (n = 5): Upland tundra and peat plateau including bare peat areas, which together cover more than 80 % of the area (Marushchak *et al.*, 2013). The replicates in upland tundra were placed along a transect and spaced approximately 10 m apart. The replicates in the peat plateau were installed 20–30 m apart, covering a distance of more than 100 m from the first to the last replicate, to account for the spatial variability within the peat plateau. The collars were installed within patches of bare peat, and the plot for the vegetated part of the peat plateau was selected in the vicinity of the bare peat. The selection of replicates took place by visual inspection of the plant community, and we chose replicates with similar vegetation, representative for the individual surface type. Each warmed plot was installed close (less than 3 m) to a control plot.

Environmental parameters

Two weather stations collected meteorological data directly at the Seida study site. Weather station I measured barometric pressure (S-BPA-CM10, Onset, Bourne, MA, USA) as well as air temperature (S-TMB-M002, Onset), photosynthetically active radiation (PAR; S-LIA-M003, Onset) and precipitation (S-RGA-M002,

Onset) by means of a HOBO Micro Station data logger (H21-002, Onset). Weather station II logged relative humidity as well as back up air temperature (Hygromer MP100A, Rotronic, Bassersdorf, Switzerland), backup PAR (LI-190 Quantum sensor, LI-COR, Lincoln, NE, USA), and precipitation (Young tipping bucket rain gauge, Campbell Scientific, Logan, UT, USA) to a Campbell data logger (CR10X , Campbell Scientific) with multiplexer (AM16/32, Campbell Scientific). Weather station I acted as the default weather station, while weather station II was used for additional meteorological parameters and to fill data gaps.

To obtain continuous plot-scale measurements of soil and air temperature, we used iButton loggers (1-Wire, Maxim Integrated, San Jose, CA, USA), installed at each plot in 5 cm and 15 cm depth in the soil as well as in 15 cm above the soil surface.

With each weekly gas sampling we manually took soil moisture measurements next to each flux plot in 0–6 cm depth, using a site-calibrated Thetaprobe (ML2x soil moisture sensor) connected to a HH2 moisture meter (Delta-T Devices, Cambridge, UK). From these volumetric water content values we calculated water-filled pore space (WFPS), using particle density and porosity values for the different soil types. Particle densities were derived from the ash content (Okruszko, 2003, referenced in Léon-Etienne and Ilnicki, 2003). Water table below the surface and depth of seasonal thaw were monitored once a week on the plot-scale following the method described in Marushchak et al. (2011).

Leaf area index (LAI, one-sided) on all the vegetated plots was measured weekly with a LAI-2200 optical plant canopy analyzer (LI-COR, Lincoln, NE, USA). The LAI-meter uses above and below canopy readings to calculate the light interception at five zenith angles. The data was recomputed with FV2200 software to exclude the outer zenith ring of data, due to the small plot area. In addition to that, we took vegetation photos once per week and determined the vegetation composition on the plots by use of the point frame method. The functional groups we used in order to determine long-term changes of warming on plant coverage were shrubs, graminoids, forbs, mosses and lichens.

Carbon dioxide exchange

Carbon dioxide fluxes were determined by use of a dynamic closed chamber technique (Heikkinen *et al.*, 2004). Net Ecosystem CO_2 Exchange (NEE) was measured with a transparent chamber (polyethylene, 2 mm), connected to an infrared gas analyzer (IRGA EGM-4, PP Systems, Amesbury, MA, USA). The chamber had a volume of 130 dm^3 and was equipped with a fan, as well as a HOBO Photosynthetic Light (PAR) Sensor (S-LIA-M003, Onset, Bourne, MA, USA), and two HOBO temperature sensors (S-TMB-M006), measuring temperature in- and outside the chamber. The sensors were connected to a HOBO Micro Station data logger (Onset, H21-002). . Fluxes were measured during daytime between 8:00 a.m. and 6:00 p.m and the order of measured plots was varied weekly, so results would not be biased by the time of measurement.

Nitrous oxide and methane fluxes

Nitrous oxide and methane fluxes were measured using static closed chambers (Repo *et al.*, 2009). We used an aluminum chamber with a volume of 76 dm^3, which was placed on permanently installed aluminum collars (60 cm x 60 cm) for the gas measurement. Each collar had a water-filled groove to guarantee the chamber was sealed towards the atmosphere. On the warmed plots the flux collar was placed in the center of the OTC, to keep disturbance of the OTC walls as small as possible. The flux chamber was equipped with a battery powered fan to mix the inside air during enclosure time, as well as a thermometer (Lollipop Thermometer, EC-LOLLITEMP) and an outlet tube (nylon, 4 mm) to generate pressure equilibrium within the chamber. A second nylon tube was connected to a three-way stopcock (STERITEX® 3W, CODAN Medical, Lensahn, Germany) and a syringe with Luer Lock Tip (Terumo®), with which the gas samples were taken. Fluxes were measured during daytime between 8:00 a.m. and 6:00 p.m and the order of measured plots was varied weekly, so results would not be biased by the time of measurement. We additionally took up to five ambient (i.e. atmospheric) air samples during the day and stored them in the same way as the regular gas samples.

Seasonal gas fluxes – carbon dioxide modelling

Response function for ER and GPP were created for each collar separately and data were split by years. Only if the number of data points per collar was too small to result in reliable regression, e.g. in case of exclusion of erroneous measurements, data were pooled for both summers.

The temperature-dependent ER was modelled using an Arrhenius type function as proposed by Lloyd and Taylor (1994):

$$ER = R_{ref} \times \left[E_0 \times \left(\frac{1}{T_{ref} - T_0} - \frac{1}{T - T_0}\right)\right]. \quad (1)$$

The term R_{ref} describes the respiration at the reference temperature [mg CO_2 m^{-2} h^{-1}], E_0 is the activation energy [K], T_{ref} is the reference temperature (283.15 K), T_0 the temperature constant for the start of biological processes (227.13 K) and T is the mean of measured soil temperature at 5 cm depth and air temperature 15 cm above the soil surface (outside the chamber). As temperature data we used data logged individually for each collar. As fluxes were measured over the course of four months with changing environmental conditions, a soil moisture term was included in case temperature alone did not suffice as explanatory variable. According to Bunnel et al. (1977), we included a saturation function into the existing respiration model

$$ER = R_{ref} \times \left[E_0 \times \left(\frac{1}{T_{ref} - T_0} - \frac{1}{T - T_0}\right)\right] \times \frac{M}{M_{1/2} + M}, \quad (2)$$

as well as a function with higher sensitivity of respiration towards low soil moisture contents during dry periods, as described in Reichstein et al. (2002):

$$ER = R_{ref} \times \left[E_0 \times \left(\frac{1}{T_{ref} - T_0} - \frac{1}{T - T_0}\right)\right] \times \frac{M - M_0}{(M_{1/2} - M_0) + (M - M_0)}, \quad (3)$$

where M is the measured volumetric water content [m^3/m^3], $M_{1/2}$ the water content at which half maximal respiration occurs and M_0 the residual water content, at which respiration is zero.
GPP was modelled by means of a Michaelis–Menten type equation (e.g, Beetz *et al.*, 2013):

$$GPP = \frac{GP_{max} \times \alpha \times PAR}{GP_{max} + \alpha \times PAR}, \quad (4)$$

with GP_{max} as the maximum limit of the C fixation rate when approaching infinite PAR [mg CO_2 m^{-2} h^{-1}], α the light use efficiency or initial slope of the curve [mg CO_2 m^{-2} h^{-1} / µmol m^{-2} s^{-1}] and PAR the photon flux density of the photosyntetically active radiation [µmol m^{-2} s^{-1}]. We used either
a) a linear soil moisture term (M + β, β = correction factor for soil moisture) or
b) a LAI term (LAI + δ, δ = correction factor for LAI)
as a multiplier, in case PAR alone did not yield sufficient explanation for GPP. For the vegetated sites the shoulder periods in spring and autumn (June and September), characterized by a rapid plant growth and senescence, respectively, were modelled separately.

Seasonal gas fluxes – methane and nitrous oxide

Fluxes of CH_4 and N_2O were interpolated linearly in order to obtain seasonal estimates. As our spring measurements occurred during a thaw peak, i.e. elevated fluxes of N_2O and CH_4 during spring thaw (Christensen & Tiedje, 1990; Buckeridge *et al.*, 2010), linear interpolation would have resulted in an overestimation of fluxes during the early growing season. As the spring peak is not expected to last for more than a few days, we assumed a 4-day spring peak in early June, based on the soil temperature in 5 cm depth, and an otherwise linear increase from a zero flux on 1 June towards the first flux measurement in early July (Repo *et al.*, 2009). The flux rates measured in early spring and late autumn in 2013 were used as a start and end point also for the 2012 data, as can be justified with similar weather conditions during those periods in both years.

References for supplementary methods

Beetz S, Liebersbach H, Glatzel S, Jurasinski G, Buczko U, Hoeper H (2013) Effects of land use intensity on the full greenhouse gas balance in an Atlantic peat bog. *Biogeosciences*, **10,** 1067-1082.

Bokhorst S, Bjerke J, Bowles F, Melillo J, Callaghan T, Phoenix G (2008) Impacts of extreme winter warming in the sub- Arctic: growing season responses of dwarf shrub heathland. *Global Change Biology,* **14,** 2603-2612.

Bokhorst S, Huiskes A, Aerts R *et al.* (2013) Variable temperature effects of Open Top Chambers at polar and alpine sites explained by irradiance and snow depth. *Global Change Biology,* **19,** 64-74.

Buckeridge KM, Cen Y, Layzell DB, Grogan P (2010) Soil biogeochemistry during the early spring in low arctic mesic tundra and the impacts of deepened snow and enhanced nitrogen availability. *Biogeochemistry,* **99,** 127-141.

Bunnell FL, Tait DEN, Flanagan PW, Vancleve K (1977) Microbial Respiration and Substrate Weight-Loss .1. General-Model of Influences of Abiotic Variables. *Soil Biology & Biochemistry,* **9,** 33-40.

Carlyle CN, Fraser LH, Turkington R (2011) Tracking soil temperature and moisture in a multi-factor climate experiment in temperate grassland: do climate manipulation methods produce their intended effects? *Ecosystems,* **14,** 489-502.

Christensen S, Tiedje JM (1990) Brief and vigorous N_2O production by soil at spring thaw. *Journal of Soil Science,* **41,** 1-4.

Heikkinen JE, Virtanen T, Huttunen JT, Elsakov V, Martikainen PJ (2004) Carbon balance in East European tundra. *Global Biogeochemical Cycles,* **18**, GB1023, DOI: 10.1029/2003GB002054.

Lloyd J, Taylor JA (1994) On the temperature-dependence of soil respiration. *Functional Ecology,* **8,** 315-323.

Marion G, Henry G, Freckman D *et al.* (1997) Open-top designs for manipulating field temperature in high-latitude ecosystems. *Global Change Biology,* **3,** 20-32.

Marushchak M, Kiepe I, Biasi C *et al.* (2013) Carbon dioxide balance of subarctic tundra from plot to regional scales. *Biogeosciences,* **10,** 437-452.

Marushchak ME, Pitkamaki A, Koponen H, Biasi C, Seppala M, Martikainen PJ (2011) Hot spots for nitrous oxide emissions found in different types of permafrost peatlands. *Global Change Biology,* **17,** 2601-2614.

Natali SM, Schuur EA, Webb EE, Pries CEH, Crummer KG (2014) Permafrost degradation stimulates carbon loss from experimentally warmed tundra. *Ecology,* **95,** 602-608.

Natali SM, Schuur EAG, Trucco C, Pries CEH, Crummer KG, Lopez AFB (2011) Effects of experimental warming of air, soil and permafrost on carbon balance in Alaskan tundra. *Global Change Biology,* **17,** 1394-1407.

Okruszko H (2003) Determination of specific gravity of hydrogenic soils on the basis of their mineral particles content. Wiadomosci Instytutu Melioracji i Uzytkow Zielonych, 10.1: 47–54 (in Polish with English summary). In: *Organic soils and peat materials for sustainable agriculture* (eds Léon-Etienne P, Ilnicki P), CRC Press LLC, Boca Raton.

Reichstein M, Tenhunen JD, Roupsard O, Ourcival JM, Rambal S, Dore S, Valentini R (2002) Ecosystem respiration in two Mediterranean evergreen Holm Oak forests: drought effects and decomposition dynamics. *Functional Ecology,* **16,** 27-39.

Repo ME, Susiluoto S, Lind SE, Jokinen S, Elsakov V, Biasi C, Virtanen T, Martikainen PJ (2009) Large N_2O emissions from cryoturbated peat soil in tundra. *Nature Geoscience,* **2,** 189-192.

Salmon VG, Soucy P, Mauritz M, Celis G, Natali SM, Mack MC, Schuur EA (2015) Nitrogen availability increases in a tundra ecosystem during five years of experimental permafrost thaw. *Global Change Biology,* **22**, 1927-1941.

Shaver G, Canadell J, Chapin F *et al.* (2000) Global warming and terrestrial ecosystems: A conceptual framework for analysis. *Bioscience,* **50,** 871-882.

Supplementary figures and tables

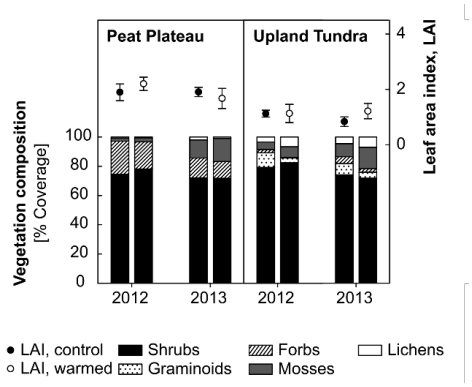

Fig. S1. Average vegetation abundance of functional plant groups of peat plateau and upland tundra (n = 5) and leaf area index (mean ± SE, n = 5). Vegetation composition was determined during the peak growing season (end of July until beginning of August) in all years and LAI is shown for the same week. The first bar represents the control plots and the second bar displays the warming treatment for each year.

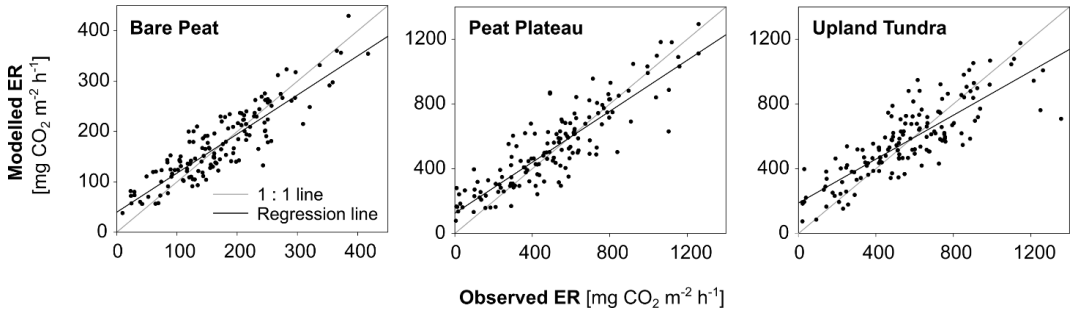

Fig. S2. Modelled vs. observed ecosystem respiration (ER) from the three surface types for the years 2012 and 2013. Only the data used in creating the response functions are shown.

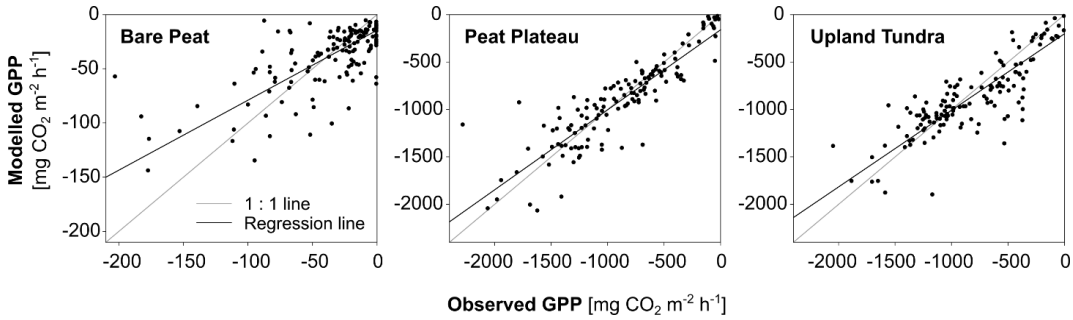

Fig. S3. Modelled vs. observed gross primary production (GPP) from the three surface types for the years 2012 and 2013. Only the data used in creating the response functions are shown.

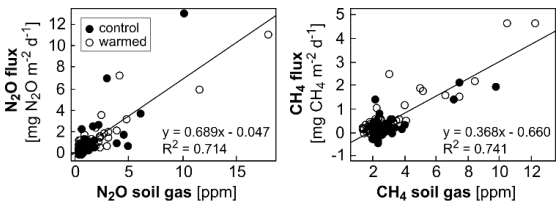

Fig. S4. Measured nitrous oxide (N_2O) and methane (CH_4) fluxes vs. N_2O and CH_4 gas concentrations in the soil profile in 15–30 cm and 30–45 cm depth, respectively, from bare peat.

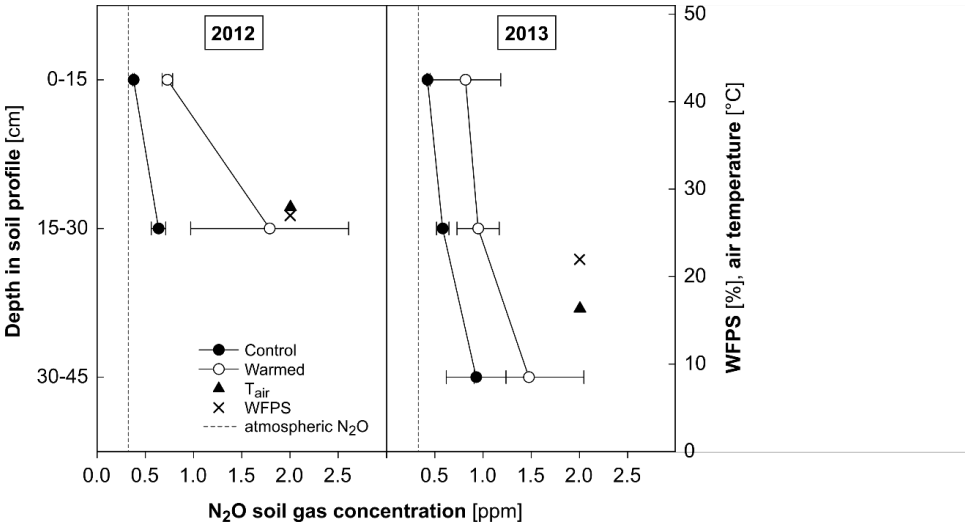

Fig. S5. Nitrous oxide (N_2O) concentration in the soil profile of bare peat surfaces during the last week of July, for control and warmed surfaces (mean ± SE, n = 5), as well as water-filled pore space (WFPS) and air temperature during time of measurement.

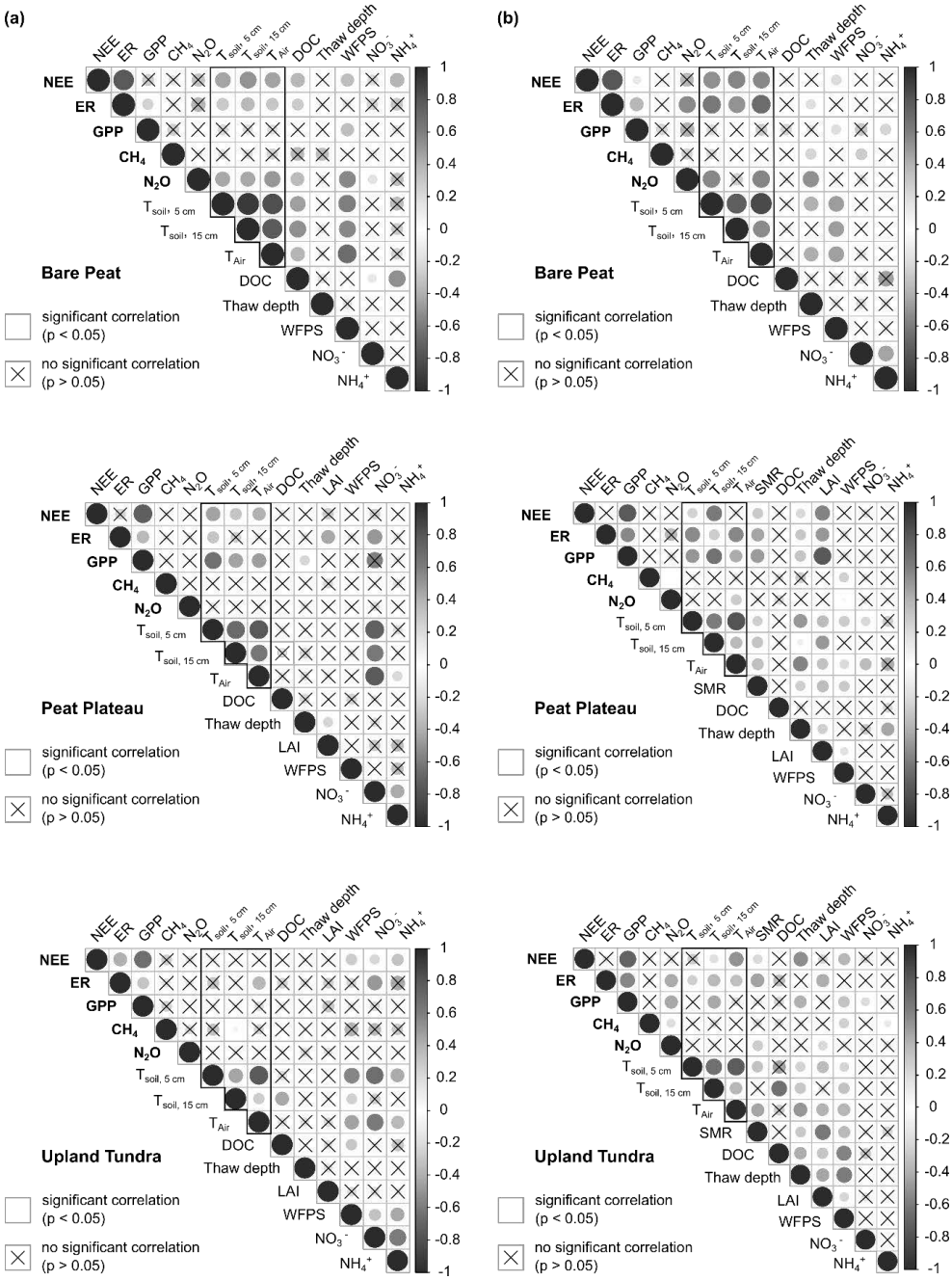

Fig. S6. Correlation matrices for the three components of the carbon dioxide flux (NEE, ER and GPP), methane (CH_4) and nitrous oxide (N_2O) for **(a)** summer 2012 and **(b)** summer 2013 at three different tundra surface types. The matrices include measurements taken during the peak growing season (July and August). The colours show Spearman's rank correlation coefficient and indicate a positive or negative correlation. The size of circles signifies the strength of the correlation. Non-significant correlations ($P > 0.05$) are marked.

Table S1. Meteorological conditions during the summer months of 2012 and 2013 at the Seida study site and comparison to long-term mean measured at Vorkuta station (67°48' N, 64°01' E, 172 m a.s.l., mean ± SD). PAR = photosynthetically active radiation, n. d. = not determined, thermic growing season = period of time when mean daily air temperature is continuously above 5 °C.

	2012		2013		1977–2006	
	Jul	Aug	Jul	Aug	Jul	Aug
Air temperature (°C)	14.7	9.4	18.2	11.7	13.0 ± 2.2	9.6 ± 2.0
Precipitation (mm)	32.6	34.4	14.1	52.5	55 ± 26	60 ± 30
PAR ($\mu molm^{-2}\ s^{-1}$)	368	230	466	271	n. d.	n. d.
thermic growing season length (d)	81		92			

Table S2. Carbon (C) and nitrogen (N) stored in vascular plants and the moss layer, as well as C:N ratio for peat plateau and upland tundra surfaces for control and warmed plots. Plant samples were taken in mid-July in both years. Data are means ± SE, n = 5. Asterisks indicate significant difference between control and warmed surfaces and $^{(+)}$ and $^{(-)}$ show whether the values from the warmed surfaces were significantly higher or lower, respectively. Level of significance: ***significant at $P \leq 0.001$, **significant at $P \leq 0.01$, *significant at $P \leq 0.05$.

Year	Treatment,	Vascular plants			Mosses and lichens		
	Surface type	C (%)	N (%)	C:N	C (%)	N (%)	C:N
	Control						
2012	Peat Plateau	49 ± 1	1.6 ± 0.2	33 ± 6	47 ± 0.4	1.0 ± 0.1	50 ± 5
	Upland Tundra	51 ± 1	1.0 ± 0.1	55 ± 5	48 ± 0.1	1.0 ± 0.1	50 ± 5
2013	Peat Plateau	49 ± 1	1.4 ± 0.4	45 ± 11	44 ± 0.2	0.9 ± 0.1	52 ± 7
	Upland Tundra	51 ± 1	1.2 ± 0.2	45 ± 6	45 ± 0.4	0.8 ± 0.1	58 ± 4
	Warmed						
2012	Peat Plateau	51 ± 1	1.3 ± 0.2	43 ± 7	47 ± 0.4	1.0 ± 0.1	48 ± 5
	Upland Tundra	51 ± 1	1.0 ± 0.1	50 ± 3	46 ± 0.5 $^{*(-)}$	1.0 ± 0.1	46 ± 3
2013	Peat Plateau	48 ± 1	1.5 ± 0.2	37 ± 8	45 ± 0.3	0.8 ± 0.1	61 ± 7
	Upland Tundra	49 ± 0.3	0.9 ± 0.1	59 ± 3	44 ± 0.3	0.9 ± 0.1	54 ± 5

Table S3. Soil characteristics at the three surface types from control and warmed plots, determined in mid-July 2013. Bulk density (BD), pH, soil organic matter content (SOM), carbon (C) and C:N ratio. Data are means ± SE, n = 5. The average depths for O, A and B horizon are 0–7 cm (O), 7–10 cm (A) and 10–20 cm (B). Asterisks indicate significant difference between control and warmed surfaces and $^{(+)}$ and $^{(-)}$ show whether the values from the warmed surfaces were significantly higher or lower, respectively. Level of significance: ***significant at $P \leq 0.001$, **significant at $P \leq 0.01$, *significant at $P \leq 0.05$.

Surface type Depth / horizon	BD (g cm^{-3})	pH	SOM (%)	C (%)	N (%)	C:N
Control						
Bare Peat						
0–5 cm	0.19 ± 0.01	4.0 ± 0.2	94 ± 1	50 ± 0.4	2.6 ± 0.1	19 ± 0.4
5–10 cm		4.0 ± 0.2	94 ± 0.4	50 ± 0.3	2.6 ± 0.2	20 ± 1
10–20 cm		4.1 ± 0.2	94 ± 0.4	50 ± 0.4	2.4 ± 0.2	21 ± 1
Peat Plateau						
0–5 cm	0.02 ± 0.01	3.8 ± 0.04	98 ± 0.2	48 ± 0.3	1.2 ± 0.1	40 ± 4
5–10 cm		3.7 ± 0.02	99 ± 0.3	47 ± 0.3	1.2 ± 0.1	40 ± 3
10–20 cm		3.6 ± 0.01	98 ± 0.4	47 ± 0.4	1.5 ± 0.1	32 ± 2
Upland Tundra						
O	0.06 ± 0.00	4.3 ± 0.1	93 ± 2	44 ± 3	1.5 ± 0.1	30 ± 2
A		4.7 ± 0.2	17 ± 4	11 ± 4	0.6 ± 0.2	19 ± 2
B		5.6 ± 0.1	12 ± 7	10 ± 9	0.4 ± 0.3	14 ± 3
Warmed						
Bare Peat						
0–5 cm		3.7 ± 0.2	94 ± 1	50 ± 0.2	2.7 ± 0.1	19 ± 1
5–10 cm		3.8 ± 0.2	95 ± 1	51 ± 0.3	2.5 ± 0.1	21 ± 1
10–20 cm		4.1 ± 0.2	95 ± 1	50 ± 0.3	2.4 ± 0.2	22 ± 1
Peat Plateau						
0–5 cm		3.9 ± 0.1	98 ± 0.2	48 ± 1	1.2 ± 0.1	42 ± 2
5–10 cm		3.7 ± 0.1	98 ± 1	48 ± 0.4	1.4 ± 0.2	38 ± 6
10–20 cm		3.6 ± 0.1	96 ± 1	48 ± 1	1.7 ± 0.3	31 ± 5
Upland Tundra						
O		4.2 ± 0.2	91 ± 4	46 ± 1	1.2 ± 0.1	39 ± 2**$^{(+)}$
A		4.4 ± 0.2	33 ± 4	24 ± 7	1.0 ± 0.2	22 ± 3
B		5.6 ± 0.1	6 ± 2	2 ± 1	0.2 ± 0.1	12 ± 1

Table S4. Amounts of extractable soil nutrients and organic carbon at the three surface types, determined in mid-July 2012 and 2013: Ammonium (NH_4^+), nitrate (NO_3^-), ratio of NH_4^+ to NO_3^- and dissolved organic carbon (DOC). Data are presented as means ± SE. The average depths for O, A and B horizon are 0–7 cm (O), 7–10 cm (A) and 10–20 cm (B).

Treatment Year	Surface type Depth	NH_4^+ concentration (mg NH_4^+–N kg^{-1} DW)	NO_3^- concentration (mg NO_3^-–N kg^{-1} DW)	NH_4^+ : NO_3^-	DOC concentration (mg C kg^{-1} DW)
Control					
2012	**Bare Peat**				
	0–5 cm	49 ± 17	118 ± 23	0.4	1400 ± 213
	5–10 cm	46 ± 16	41 ± 9	1.1	1228 ± 113
	10–20 cm	43 ± 13	47 ± 13	0.9	n. d.
	Peat plateau				
	0–5 cm	40 ± 9	0.8 ± 0.3	50	1790 ± 422
	5–10 cm	48 ± 10	0.5 ± 0.2	96	1283 ± 185
	10–20 cm	41 ± 10	0.7 ± 0.2	59	n. d.
	Upland tundra				
	O	30 ± 5	0.6 ± 0.1	50	1084 ± 88
	A	16 ± 5	0.2 ± 0.05	80	464 ± 119
	B	10 ± 3	0.6 ± 0.3	17	n. d.
2013	**Bare Peat**				
	0–5 cm	94 ± 37	419 ± 54	0.2	1340 ± 107
	5–10 cm	41 ± 15	176 ± 41	0.2	1215 ± 133
	10–20 cm	55 ± 27	86 ± 10	0.6	n. d.
	Peat plateau				
	0–5 cm	36 ± 8	3.2 ± 1.1	11	1350 ± 61
	5–10 cm	30 ± 7	2.3 ± 1.3	13	1057 ± 158
	10–20 cm	19 ± 2	1.2 ± 0.3	16	n. d.
	Upland tundra				
	O	37 ± 5	0.8 ± 0.2	46	1301 ± 6
	A	12 ± 8	0.3 ± 0.1	40	985 ± 728
	B	5 ± 2	1.3 ± 0.8	3.8	n. d.
Warmed					
2012	**Bare Peat**				
	0–5 cm	42 ± 8	157 ± 12	0.3	1130 ± 155
	5–10 cm	44 ± 9	61 ± 7	0.7	1186 ± 163
	10–20 cm	49 ± 5	38 ± 4	1.3	n. d.
	Peat plateau				
	0–5 cm	17 ± 5	1.1 ± 0.3	15	1325 ± 257
	5–10 cm	45 ± 10	0.5 ± 0.2	90	1284 ± 136
	10–20 cm	43 ± 13	1.8 ± 1.3	24	n. d.
	Upland tundra				
	O	23 ± 9	0.7 ± 0.3	33	1461 ± 643
	A	17 ± 3	0.1 ± 0.02	170	632 ± 202
	B	10 ± 2	1.4 ± 0.7	7	n. d.
2013	**Bare Peat**				
	0–5 cm	71 ± 24	308 ± 51	0.2	1462 ± 118
	5–10 cm	38 ± 15	148 ± 32	0.3	1150 ± 66
	10–20 cm	28 ± 6	78 ± 21	0.4	n. d.
	Peat plateau				
	0–5 cm	26 ± 7	1.3 ± 0.8	20	940 ± 220
	5–10 cm	22 ± 3	0.9 ± 0.2	24	699 ± 82
	10–20 cm	15 ± 2	0.6 ± 0.2	25	n. d.
	Upland tundra				
	O	28 ± 12	1.0 ± 0.3	28	940 ± 167
	A	13 ± 7	0.2 ± 0.1	65	297 ± 80
	B	3.3 ± 0.3	0.4 ± 0.2	8	n. d.

Table S5. Model parameters used to obtain half-hourly ecosystem respiration (ER) rates for the measured surface types (five replicates per surface type): E_0 = activation energy [K], R_{ref} = respiration at reference temperature 10°C [mg CO_2 m^{-2} h^{-1}], M = volumetric water content [m^3 m^{-3}], $M_{1/2}$ = water content at which half maximal respiration occurs, d.f. = degrees of freedom, Q_{10} = temperature sensitivity (0–10°C). For microsites marked with * data of 2012 and 2013 were pooled. Surfaces: bare peat (BP), peat plateau (PP) and upland tundra (UT). W = warmed.

	2012								2013							
Plot	E_0	R_{ref}	M	$M_{1/2}$	r^2	d.f.	equation	Q_{10}	E_0	R_{ref}	M	$M_{1/2}$	r^2	d.f.	equation	Q_{10}
BP1	460.0272	62.3758			0.92	5	1	5.96	184.0976	133.0798			0.63	10	1	2.04
BP2	161.0289	95.0923	0.1404	0.1393	0.47	23	3*	1.87	205.9768	91.6405			0.74	9	1	2.22
BP3	267.1362	63.7303			0.78	5	1	2.82	195.2991	108.2142			0.71	10	1	2.13
BP4	186.4266	81.2125			0.58	5	1	2.06	272.4605	82.4793			0.80	10	1	2.88
BP5	435.2173	60.8356			0.97	5	1	5.41	238.2826	86.0651			0.79	10	1	2.52
WBP1	199.3660	115.7218			0.91	5	1	2.17	179.4458	212.3477	0.1620		0.75	9	2	2.01
WBP2	152.7343	106.2205			0.36	5	1	1.81	166.8187	415.7548	0.3843		0.72	10	2	1.91
WBP3	107.6115	177.9821			0.70	5	1	1.52	212.4338	159.2171			0.92	10	1	2.28
WBP4	153.7164	115.3397			0.72	16	1*	1.82	154.2683	119.1320			0.76	10	1	1.82
WBP5	153.1604	101.3275	0.0095	0.0683	0.72	5	3	1.81	169.1683	135.7063			0.75	10	1	1.93
PP1	314.3766	412.8634	0.0863		0.84	5	2	3.39	225.6090	375.9442	0.0489		0.62	10	2	2.40
PP2	489.1669	158.1667			1.00	5	1	6.67	183.7248	385.1961	0.0044		0.84	11	2	2.04
PP3	236.0997	416.1311	0.0689		0.97	5	2	2.50	322.1316	494.1760	0.1654	0.1455	0.82	10	3	3.49
PP4	396.9859	240.3339	0.0724		0.77	5	2	4.66	302.5904	216.0782			0.81	10	1	3.23
PP5	403.0288	268.6359			0.64	5	1	4.77	175.6895	455.7634			0.32	17	1	1.98
WPP1	260.1372	192.2246			0.66	5	1	2.74	204.6444	325.6755	0.0077		0.44	9	2	2.21
WPP2	234.3251	264.6051	0.0611	0.0624	1.00	5	3	2.48	183.4749	470.5169	0.0257	0.0272	0.75	10	3	2.04
WPP3	382.7480	176.3388	0.1040	0.1306	0.78	5	3	4.41	224.5113	373.8642			0.83	10	1	2.39
WPP4	158.6887	466.8144	0.0842		0.61	16	2*	1.85	200.5827	305.6530	0.0282		0.64	14	2	2.18
WPP5	171.5271	565.1080			0.60	17	1*	1.95	133.2702	625.1948			0.53	17	1	1.68
UT1	328.4924	212.7990	0.1194	0.1350	0.61	6	3	3.58	170.8914	369.1550			0.58	9	1	1.94
UT2	316.5184	316.1443	0.0188		0.99	6	2	3.41	380.8453	256.4784	0.0103		0.68	10	2	4.38
UT3	212.1105	374.3126			0.72	5	1	2.28	465.2764	599.8396	0.0997		0.73	12	2	6.08
UT4	160.6648	545.5434			0.51	5	1	1.86	208.2865	462.9719			0.86	10	1	2.24
UT5	227.0280	457.2802			0.84	6	1	2.41	239.6976	378.2517	0.0196	0.0189	0.76	10	3	2.53
WUT1	171.3715	548.9251	0.0318		0.72	5	2	1.94	294.4595	348.5513			0.76	10	1	3.13
WUT2	183.6004	955.9802	0.0442		0.31	16	2	2.04	253.1938	602.8003	0.0286	0.0210	0.39	10	3	2.67
WUT3	195.7341	670.3684	0.0561	0.0550	0.24	5	3	2.14	285.5268	508.7835	0.0231	0.0175	0.69	10	3	3.03
WUT4	120.6919	486.7175	0.0358		0.85	5	2	1.60	234.6031	499.5025	0.0896		0.69	12	2	2.48
WUT5	152.7173	693.2727	0.0101		0.91	5	2	1.81	202.6701	300.4876			0.54	10	1	2.19

Table S6. Model parameters used to obtain half-hourly gross primary production (GPP) rates for the measured surface types (five replicates per surface type): α = light use efficiency [mg CO_2 m^{-2} h^{-1} / µmol m^{-2} s^{-1}], GP_{max} = maximum carbon fixation rate [mg CO_2 m^{-2} h^{-1}], β = correction factor for soil moisture, δ = correction factor for LAI, d.f. = degrees of freedom. For microsites marked with * data of 2012 and 2013 were pooled. Surfaces: bare peat (BP), peat plateau (PP) and upland tundra (UT). W = warmed.

	2012							2013							Shoulder periods (June and September)						
Plot	α	GP_{max}	β (VWC)	δ (LAI)	r^2	d.f.	equ.	α	GP_{max}	β (VWC)	δ (LAI)	r^2	d.f.	equ.	α	GP_{max}	β (VWC)	δ (LAI)	r^2	d.f.	equ.
BP1	-1.9409	-284.76	0.0405		0.85	5	4a	-1.1716	-1283.64	-0.1116		0.68	18	4a							
BP2	-0.0491	-348.43			0.87	6	4	-0.0414	-1196.52			0.37	14	4							
BP3	-0.0880	-2249.61			0.25	7	4	-0.1770	-77.37			0.18	16	4							
BP4	-0.0595	-123.53			0.29	18	4*	-0.0457	-488.61			0.32	16	4							
BP5	-0.0689	-19.97			0.09	9	4*	-0.0689	-19.97			0.09	9	4*							
WBP1	-0.2926	-1304.68	0.0343		0.98	5	4a	-0.0411	-187.94			0.53	15	4*							
WBP2	-0.0357	-124.91			0.63	5	4	-0.0300	-407.66			0.70	17	4*							
WBP3	-0.1498	-1079.17			0.79	6	4	-0.2831	-168.63			0.38	19	4							
WBP4	-0.0507	-130.23			0.74	5	4	-0.2699	-73.87	0.1843		0.18	22	4a*							
WBP5	-0.0851	-28.04			0.10	17	4*	-0.0851	-28.04			0.10	17	4							
PP1	-1.9034	-3260.45			0.86	6	4	-4.6330	-1585.73			0.81	20	4	-2.0844	-1739.76		-0.7606	0.99	7	4b
PP2	-2.0146	-2493.52			0.84	6	4	-3.6960	-951.80		0.1551	0.88	17	4b	-1.7796	-1204.38		-0.1000	0.43	7	4b
PP3	-3.9221	-2694.63			0.74	5	4	-6.4520	-2746.07			0.80	17	4	-1.3628	-1471.52		-0.4129	0.95	7	4b
PP4	-3.4723	-1235.84			0.57	21	4*	-3.6732	-1181.22			0.70	16	4	-2.7056	-826.25		-0.5040	0.90	6	4b
PP5	-3.3648	-1337.68			0.40	5	4	-6.3924	-1751.14			0.62	17	4	-1.0027	-911.01		-0.2644	1.00	6	4b
WPP1	-2.8928	-1010.38			0.55	6	4	-6.4501	-1257.45	0.7229		0.77	19	4a	-7.2311	-1619.32		-0.5417	0.95	6	4b
WPP2	-4.7995	-1213.10			0.52	17	4*	-2.4141	-904.51		0.3609	0.87	19	4b	-4.1809	-2587.58		-0.5311	0.99	6	4b
WPP3	-6.1337	-1582.37			0.15	5	4	-4.5285	-1709.23	0.9450		0.76	18	4a	-2.8232	-1306.03		-0.3219	0.98	5	4b
WPP4	-1.1318	-2345.30			0.81	6	4	-3.0125	-807.79			0.56	17	4	-3.6634	-800.70		-0.2934	0.89	6	4b
WPP5	-3.4041	-1063.27			0.33	5	4	-4.3590	-1955.51			0.68	17	4	-1.7376	-508.15		-0.0151	0.99	5	4b
UT1	-3.0609	-1550.94			0.96	6	4	-3.5618	-1622.13			0.64	13	4	-2.2486	-841.57		0.3574	0.63	7	4b
UT2	-4.6017	-2986.43	0.4855		0.72	9	4a	-7.7142	-2103.27	0.5244		0.80	13	4a	-4.5725	-3762.92		-0.1255	0.87	8	4b
UT3	-4.2480	-1453.12			0.95	7	4	-3.2640	-1461.79		0.1845	0.71	12	4b	-3.4520	-3361.95		-0.1252	0.93	7	4b
UT4	-5.4410	-1706.59			1.00	5	4	-5.0019	-2703.53			0.85	13	4	-5.9395	-3973.88		0.0251	0.76	6	4b
UT5	-3.5346	-1742.06			0.80	6	4	-6.2365	-1273.83			0.54	10	4	-3.8008	-3017.03		-0.2319	0.81	7	4b
WUT1	-3.9263	-1929.70			0.85	5	4	-4.1023	-2009.99			0.87	14	4	-3.2770	-1657.20		-0.0540	0.90	7	4b
WUT2	-1.7701	-1544.49			0.80	6	4	-2.8433	-1064.90			0.60	19	4*	-3.7951	-1730.01		-0.2865	0.68	8	4b
WUT3	-4.9381	-1229.87			0.69	6	4	-5.1741	-2012.32		-0.4224	0.58	13	4b	-4.7622	-1571.86		-0.2012	0.99	8	4b
WUT4	-3.6332	-1195.42			0.96	5	4	-3.7228	-1697.54			0.80	13	4	-3.2641	-1751.73		0.0068	0.88	7	4b
WUT5	-6.2624	-1448.00			0.82	6	4	-3.8604	-1886.38	0.7222		0.85	12	4a	-5.9075	-1139.21		-0.4133	0.92	6	4b

Table S7. *P*-values for Ecosystem respiration (ER), Net ecosystem exchange (NEE), methane (CH_4) flux and nitrous oxide (N_2O) flux. *P*-values are derived from Student's t-test or Welch's t-test and show differences between control and warming treatment. Significant differences ($P \leq 0.05$) are marked.

	2012 *P*-value	2013 *P*-value
CO_2 flux (ER)		
Bare Peat	**<0.001**	**0.004**
Peat Plateau	0.269	0.512
Upland Tundra	**0.005**	0.132
CO_2 flux (NEE)		
Bare Peat	**0.002**	**<0.001**
Peat Plateau	**0.002**	**<0.001**
Upland Tundra	**0.002**	0.055
CH_4 flux		
Bare Peat	**0.035**	**0.016**
Peat Plateau	**0.017**	**0.036**
Upland Tundra	0.787	0.162
N_2O flux		
Bare Peat	**0.002**	0.610
Peat Plateau	0.962	**0.038**
Upland Tundra	0.064	0.082

Table S8. *P*-values for soil profile concentrations of carbon dioxide (CO_2), methane (CH_4) and nitrous oxide (N_2O). *P*-values are derived from Student's t-test or Welch's t-test and show differences between control and warming treatment. Significant differences ($P \leq 0.05$) are marked.

Surface type, Depth	**CO_2 in the soil profile** 2012 *P*-value	2013 *P*-value	**CH_4 in the soil profile** 2012 *P*-value	2013 *P*-value	**N_2O in the soil profile** 2012 *P*-value	2013 *P*-value
Bare Peat						
0–15 cm	**0.006**	**0.004**	0.741	0.865	**0.003**	0.051
15–30 cm	**<0.001**	**0.009**	**0.038**	0.156	**0.039**	0.287
30–45 cm	n.d.	**<0.001**	n.d.	**0.015**	n.d.	**<0.001**
Peat Plateau						
0–15 cm	0.633	0.111	0.053	0.111	0.333	0.133
15–30 cm	0.133	0.241	**0.036**	0.502	0.845	0.238
30–45 cm	n.d.	n.d.	n.d.	n.d.	n.d.	n.d.
Upland Tundra						
0–15 cm	**0.003**	**0.006**	0.446	0.144	0.657	0.707
15–30 cm	0.103	0.952	0.226	0.454	0.163	0.183
30–45 cm	0.421	**<0.001**	0.489	**<0.001**	0.692	**0.010**

Table S9. *P*-values for dissolved organic carbon (DOC), nitrate (NO_3^-) and ammonium (NH_4^+) in soil pore water. *P*-values are derived from Student's t-test or Welch's t-test and show differences between control and warming treatment. Significant differences ($P \leq 0.05$) are marked.

Surface type, Depth	**DOC in soil pore water**		**NO_3^- in soil pore water**		**NH_4^+ in soil pore water**	
	2012 *P*-value	2013 *P*-value	2012 *P*-value	2013 *P*-value	2012 *P*-value	2013 *P*-value
Bare Peat						
0–5 cm	0.241	0.676	0.656	0.684	0.366	0.541
5–10 cm	0.361	0.257	0.077	0.484	0.387	0.544
10–20 cm	0.168	0.214	0.149	0.256	0.426	0.739
20–30 cm	n.d.	0.059	n.d.	0.764	n.d.	**0.032**
Peat Plaetau						
0–5 cm	0.128	0.537	0.893	0.992	0.703	0.635
5–10 cm	0.219	0.441	0.620	0.910	0.856	0.434
10–20 cm	**0.021**	**0.029**	0.336	0.379	0.528	0.862
20–30 cm	n.d.	**0.003**	n.d.	0.385	n.d.	0.588
Upland Tundra						
0–5 cm	0.691	0.690	0.287	0.299	0.061	0.596
5–10 cm	0.091	0.912	0.807	0.105	0.159	0.824
10–20 cm	0.519	0.954	0.574	0.108	0.270	0.489
20–30 cm	n.d.	0.758	n.d.	0.875	n.d.	0.993

Table S10. Linear mixed effects model estimates of fixed effects for the three surfaces bare peat, peat plateau and upland tundra, their standard error (SE), t-value, lower (2.5 %) and upper (97.5 %) confidence intervals and *P*-values for carbon dioxide (CO_2), methane (CH_4) and nitrous oxide (N_2O) fluxes. Warming = warming treatment, Tair = air temperature near the surface, Moisture = surface soil moisture. Level of significance: ***significant at $P \leq 0.001$, **significant at $P \leq 0.01$, *significant at $P \leq 0.05$.

Fixed effects	Estimate	SE	t-value	2.5 % CI	97.5 % CI	*P*-value	Signif.
CO_2 flux model (Ecosystem respiration)							
Bare Peat							
Intercept	135.42	26.72	5.07	83.67	188.17	<0.001	***
Warming	48.07	9.52	5.05	29.73	66.24	<0.001	***
Moisture	-347.28	75.79	-4.58	-479.67	-199.98	<0.001	***
Moisture × Tair	19.67	2.70	7.30	13.84	25.13	<0.001	***
Peat Plateau							
Intercept	511.39	81.84	6.25	338.89	670.13	<0.001	***
Warming	41.66	37.05	1.12	-28.53	122.37	0.263	
Moisture	-1289.74	419.31	-3.08	-2053.01	-448.32	0.003	**
Moisture × Tair	65.45	13.21	4.96	39.33	89.07	<0.001	***
Upland Tundra							
Intercept	545.43	50.65	10.77	441.48	646.73	<0.001	***
Warming	144.32	48.31	2.99	40.30	239.92	0.003	**
Moisture	-1070.26	513.52	-2.08	-2009.58	-100.84	0.041	*
Moisture × Tair	42.36	23.30	1.82	-4.98	87.24	0.084	
CH_4 flux model							
Bare Peat							
Intercept	0.088	0.208	0.425	-0.620	1.342	0.678	
Warming	0.287	0.070	4.083	0.222	0.912	<0.001	***
Moisture	0.873	0.515	1.697	-1.379	3.544	0.097	
Moisture × Tair	-0.036	0.020	-1.832	-0.182	0.014	0.071	
Peat Plateau							
Intercept	-0.122	0.081	-1.498	-0.250	0.064	0.160	
Warming	0.114	0.040	2.843	0.069	0.218	0.005	**
Moisture	0.374	0.416	0.900	-0.515	1.221	0.382	
Moisture × Tair	0.006	0.013	0.466	-0.022	0.032	0.642	
Upland Tundra							
Intercept	-0.130	0.097	-1.349	-0.242	0.160	0.239	
Warming	-0.146	0.069	-2.115	-0.265	0.115	0.036	*
Moisture	0.035	0.666	0.052	-2.054	1.237	0.959	
Moisture × Tair	0.024	0.034	0.716	-0.053	0.107	0.498	
N_2O flux model							
Bare Peat							
Intercept	0.411	0.146	2.813	-0.346	1.127	0.009	**
Warming	0.042	0.047	0.882	-0.215	0.311	0.380	
Moisture	-1.849	0.346	-5.339	-4.918	-0.960	<0.001	***
Moisture × Tair	0.071	0.013	5.336	0.087	0.236	<0.001	***
Peat Plateau							
Intercept	0.070	0.036	1.931	-0.004	0.142	0.075	
Warming	0.032	0.019	1.738	-0.004	0.069	0.085	
Moisture	-0.275	0.192	-1.434	-0.651	0.084	0.165	
Moisture × Tair	-0.003	0.006	-0.516	-0.015	0.008	0.607	
Upland Tundra							
Intercept	-0.001	0.011	-0.094	-0.022	0.022	0.933	
Warming	0.027	0.011	2.513	0.007	0.050	0.013	*
Moisture	-0.034	0.102	-0.330	-0.225	0.161	0.744	
Moisture × Tair	0.000	0.005	0.036	-0.009	0.011	0.973	

Table S11. Linear mixed effects model estimates of fixed effects, their standard error (SE), t-value, lower (2.5 %) and upper (97.5 %) confidence intervals and *P*-values for soil profile concentrations of carbon dioxide (CO_2) in three depths. T_{15cm} = soil temperature in 15 cm, DOC_{20cm} = concentration of dissolved organic carbon in soil pore water sampled in 10-20 cm depth, Rain = precipitation sum of 1 d, $Rain_{3d}$ = precipitation sum of 3 d. Level of significance: ***significant at $P \leq 0.001$, **significant at $P \leq 0.01$, *significant at $P \leq 0.05$.

Fixed effects	Estimate	SE	t-value	2.5 % CI	97.5 % CI	*P*-value	Signif.
CO_2 0–15 cm							
Intercept	6.459	0.064	100.880	6.333	6.595	<0.001	***
T_{15cm}	0.012	0.005	2.580	0.002	0.022	0.013	*
DOC_{20cm}	0.001	0.001	2.130	0.000	0.003	0.047	*
DOC_{20cm} × Rain	0.009	0.005	1.610	-0.002	0.019	0.110	
CO_2 15–30 cm							
Intercept	6.756	0.148	45.64	6.480	7.067	<0.001	***
Warming	0.104	0.038	2.737	0.029	0.172	0.006	**
DOC_{20cm}	0.003	0.001	2.575	0.001	0.005	0.010	*
DOC_{20cm} × Rain	0.016	0.008	1.863	-0.001	0.034	0.063	
CO_2 30–45 cm							
Intercept	6.986	0.184	37.990	6.626	7.350	<0.001	***
T_{15cm}	0.091	0.017	5.320	5.730	0.126	<0.001	***
DOC_{20cm}	-0.005	0.003	-1.850	-1.012	0.001	0.149	
DOC_{20cm} × $Rain_{3d}$	0.000	0.000	1.907	0.000	0.001	0.058	

APPENDIX 2:
SUPPLEMENTARY INFORMATION TO PUBLICATION II
Degradation potentials of dissolved organic carbon (DOC) from thawed permafrost peat.

Supplementary information for "Degradation potentials of dissolved organic carbon (DOC) from thawed permafrost peat"

Balathandayuthabani Panneer Selvam[1*], Jean-François Lapierre[2], Francois Guillemette[3], Carolina Voigt[4], Richard E. Lamprecht[4], Christina Biasi[4], Torben R. Christensen[1, 5], Pertti J. Martikainen[4], and Martin Berggren[1]

[1]Department of Physical Geography and Ecosystem Science, Lund University, Sweden.

[2]Département de sciences biologiques, Université de Montréal, Canada.

[3]Research Center for Watershed–Aquatic Ecosystem Interactions (RIVE), Department of Environmental Sciences, Université du Québec à Trois-Rivières, Trois-Rivières, Québec, Canada.

[4]Department of Environmental and Biological Sciences, University of Eastern Finland, Finland.

[5]Arctic Research Centre, Aarhus University, Denmark.

Supplementary Methods

Study site

A palsa is defined as peat which is lifted above the surrounding mire by permafrost[1]. The palsa in our study site rises ca. 3 m above the surrounding peat and it is at the starting stage of collapse and classified as a dome shaped and peat-cored palsa[2-4]. The ice content in the permafrost is likely high as peat cored palsas in northern Finland usually consist of peat that is perenially frozen and includes ice crystals in the peat pores and with segregated ice formation[5]. Palsas are a characteristic of the discontinuous permafrost zone[6] and most of the palsa mires in northern Finland are <1000 years old[7] or at most 2000-3000 years old in northernmost Finland[8]. The original peatland developed far earlier, ca. 8000-9000 years BP[8]. The peat on the surface is originating from Bryales mosses, lichens and Ericales shrubs with different origin at depth, e.g. consisting of Sphagnum, Carex and Eriophorum[2].

Intact peat profiles including living plants were collected at the end of September 2012 when annual thaw depth was at its maximum and the average active layer (AL) was 65 cm. Four cores from dry parts of the palsa mire were sampled, which are sparsely vegetated with dwarf shrubs such as *Empetrum hermaphroditum* and *Vaccinium vitis-idaea*, covered by brown mosses as well as lichen species commonly found on palsa surfaces[5,8-10]. Additionally, four cores were collected from natural bare peat surfaces (Figure S1). Batches of bare peat surfaces occur among the vegetated ones, mainly due to wind abrasion[11]. Coring was performed using a 80 cm long steel corer with exchangeable inner plastic tubes (diameter of 10 cm), which was hammered into the soil with a mechanical drill down to a depth of about 80 cm. Immediately after sampling, peat cores (containing about 65 cm of active layer and 15 cm of permafrost) were transported in mild freezing temperatures (-4°C ± 2) and subsequently stored at the same temperature from October 2012 to the end of March 2013.

In the beginning of March 2013, the impermeable sealed peat cores were incubated by setting them in an upright position in a water bath. The water bath was filled with salt water to keep the peat cores under frozen conditions, as the saltwater had a temperature of around -3/-4°C. There peat cores were not in physical contact with the salt water. This set-up was arranged in a climate chamber with an adjusted air temperature of 10°C. This study was part and made use of the set-up of a larger study that investigated the effect of sequential thawing on carbon and nitrogen cycling from subarctic peatlands. From an initially frozen state (-4°C), the cores were thawed in four-week steps, by lowering the salt-water level and thus increasingly exposing them to a constant air temperature of 10 °C. In the last experimental phase after 7 months the full core profile, including the permafrost part, were unfrozen (Figure S2). At that stage 20-40 ml of water were extracted via sampling outlets using a syringe with a Luer Lock Tip (Terumo®) from five depths. This experimental set-up was intended to simulate palsa collapse and to mimic the effect of an unusual warm and wet summer on biogeochemical cycles. Hence the water table level inside the cores was artificially raised and kept constant at 5-10 cm below the surface by adding milli-Q water.

In order to simulate the natural state and to make our study comparable to field conditions, the peat cores were kept under as close to natural conditions as possible during the treatment and transport and storage period.

Optical DOC characterization

Given the small number of samples, we quantified the fluorophores using a PARAFAC model that was developed for over 1300 boreal freshwater samples originating from lakes, rivers and wetlands with high terrestrial influence[12]. This model has been used to study the patterns in bio- and photo-degradation of DOC in a wide number of systems. Further, this model identified 6 fluorescence components that have been associated to detailed chemical characterization in a subset of boreal rivers using high resolution mass spectrometry[13]. In particular, components C1 to C5 were associated to a diverse set of humic-like substances and the component C6 was representative of freshly produced protein like substances[12]. The component C3 has been associated to high photochemical reactivity[12] but it was absent in most of our samples.

References

1 Seppälä, M. The term 'palsa'. *Z. Geomorphol.* **16**, 463 (1972).

2 Seppälä, M. in *Advances in periglacial geomorphology* (ed M.J. Clark) 247-278 (John Wiley, 1988).

3 Gurney, S. D. Aspects of the genesis, geomorphology and terminology of palsas: perennial cryogenic mounds. *Prog. Phys. Geogr.* **25**, 249-260, doi:10.1177/030913330102500205 (2001).

4 Hofgaard, A. Effects of climate change on the distribution and developments of palsa peatlands: background and suggestions for a national monitoring project. Report No. 952-11-2296-X, 33 (Norwegian Institute for Nature Research Project, Norway, 2003).

5 Seppälä, M. in *Finland - land of mires* (eds T Lindholm & R Heikkilä) 155-162 (Finnish Environment institute, 2006).

6 Seppälä, M. Introduction to the periglacial environment in Finland. *Bulletin of the Geological Society of Finland* **69**, 73-86 (1997).

7 Seppälä, M. Dating of palsas. *Geological Survey of Finland, Special Paper* **40**, 79-84 (2005).

8 Oksanen, P. Holocene development of the Vaisjeäggi palsa mire, Finnish Lapland. *Boreas* **35**, 81-95, doi:10.1080/03009480500359103 (2006).

9 Oksanen, P. O., Kuhry, P. & Alekseeva, R. N. Holocene development of the Rogovaya River peat plateau, European Russian Arctic. *Holocene* **11**, 25-40, doi:10.1191/095968301675477157 (2001).

10 Oksanen, P. O., Kuhry, P. & Alekseeva, R. N. Holocene Development and Permafrost History of the Usinsk Mire, Northeast European Russia. *Geogr. Phys. Quatern.* **57**, 169, doi:10.7202/011312ar (2003).

11 Marushchak, M. E. *et al.* Hot spots for nitrous oxide emissions found in different types of permafrost peatlands. *Global Change Biol.* **17**, 2601-2614, doi:10.1111/j.1365-2486.2011.02442.x (2011).

12 Lapierre, J. F. & del Giorgio, P. A. Partial coupling and differential regulation of biologically and photochemically labile dissolved organic carbon across boreal aquatic networks. *Biogeosciences* **11**, 5969-5985, doi:10.5194/bg-11-5969-2014 (2014).

13 Stubbins, A. *et al*. What's in an EEM? Molecular signatures associated with dissolved organic fluorescence in boreal Canada. *Environ. Sci. Technol.* **48**, 10598–10606, doi:10.1021/es502086e (2014).

Figure S1. Permafrost peat site where we collected samples. Four cores from dry and four cores from natural bare peat surfaces were collected.

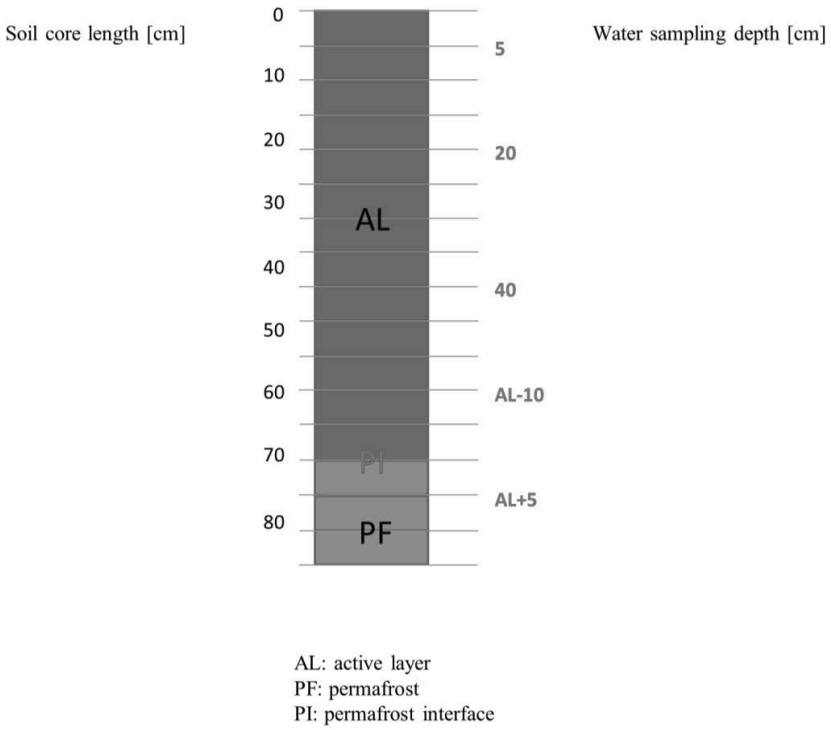

Figure S2. Soil core length and water sampling depth in the soil cores. The depths we used were 5cm, 20cm, 40cm, AL-10cm (active layer) and AL+5cm (permafrost) in accordance with the thawing steps used.

Table S1. General linear model was performed to test the influence of soil layers (active layer and permafrost) and vegetation (presence and absence) on DOC composition and degradation.

	Types of layers				Presence and absence of vegetation			
Variables	d.f.	MS	F	p	d.f.	MS	F	p
FI	1	0.08	14.54	.002*	1	0.00	0.03	.871
HIX	1	550.82	7.58	.017*	1	61.30	0.84	.376
FRESH	1	0.03	5.46	.038*	1	0.00	0.36	.561
BIX	1	0.02	4.75	.050	1	0.00	0.41	.535
a254/a365	1	2.00	18.54	.001*	1	0.35	3.28	.095
C1	1	198.53	12.67	.004*	1	59.75	3.81	.075
C2	1	1455.61	14.47	.003*	1	0.42	0.00	.950
C4	1	55.61	7.22	.020*	1	43.26	5.61	.035*
C5	1	0.20	0.02	.885	1	8.60	0.97	.345
C6	1	0.117	1.463	.25	1	0.15	1.87	.20
Sr	1	0.05	1.62	.228	1	0.03	0.90	.361
BP/DOC	1	0.00	2.55	.137	1	0.00	2.31	.155
BR/DOC	1	0.00	11.94	.005*	1	0.00	0.49	.498
BCC/DOC	1	0.00	8.22	.014*	1	0.00	2.27	.158
BGE	1	110.30	0.69	.421	1	162.50	1.02	.332
PD-E_w	1	0.00	8.02	.015*	1	0.00	2.27	.158

*significantly different ($p<0.05$)

Table S2. General linear model performed to test the influence of soil depth (active layer and permafrost) and vegetation (presence and absence) on $SUVA_{254}$. Results are shown for the complete data set and for a modified data set excluding an extreme $SUVA_{254}$ value of 8.90 L mg C^{-1} m^{-1}.

	Types of layers				Presence and absence of vegetation			
Variables	d.f.	MS	F	p	d.f.	MS	F	p
				By including the extreme $SUVA_{254}$				
$SUVA_{254}$	1	0.24	0.18	0.68	1	7.63	5.74	0.03
				By excluding the extreme $SUVA_{254}$				
$SUVA_{254}$	1	1.98	4.81	0.05	1	2.95	7.16	0.02

APPENDIX 3:
SUPPLEMENTARY INFORMATION TO PUBLICATION III
Ecosystem carbon response of Arctic peatlands to simulated permafrost thaw.

Supplementary Information

Ecosystem carbon response of Arctic peatlands to simulated permafrost thaw

Carolina Voigt, Mikhail Mastepanov, Richard E. Lamprecht, Maija E. Marushchak, Maxim Dorodnikov, Amelie Lindgren, Marcin Jackowicz-Korczyński, Timo Oksanen, Claire C. Treat, Annalea Lohila, Torben R. Christensen, Pertti J. Martikainen, Christina Biasi

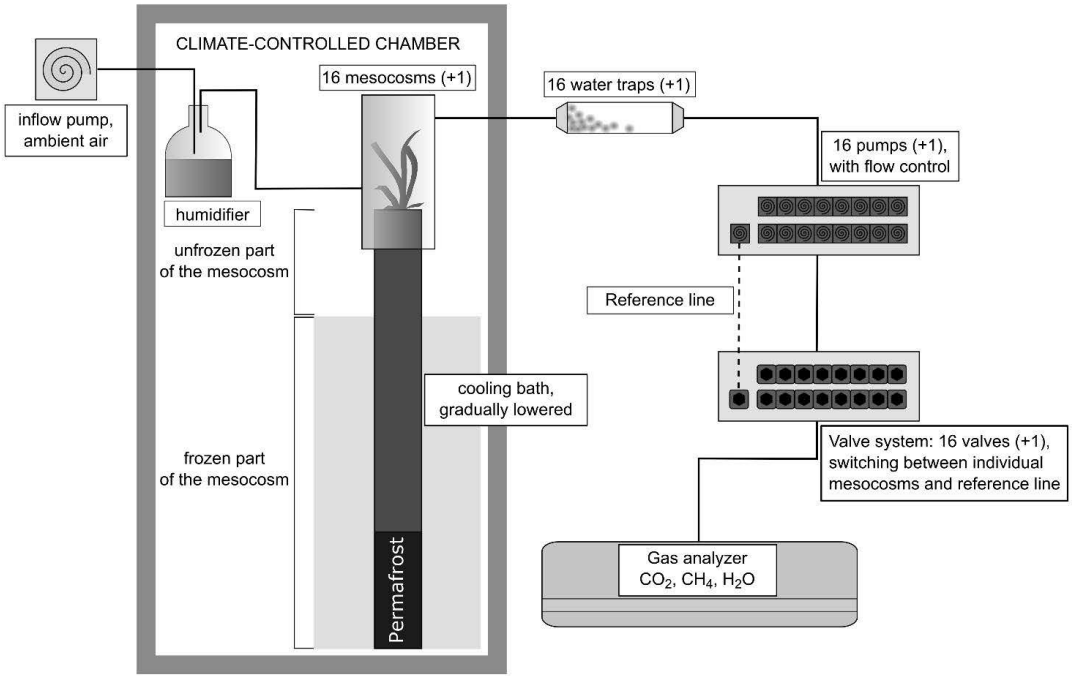

Fig. S1: Schematic design of experimental set-up.

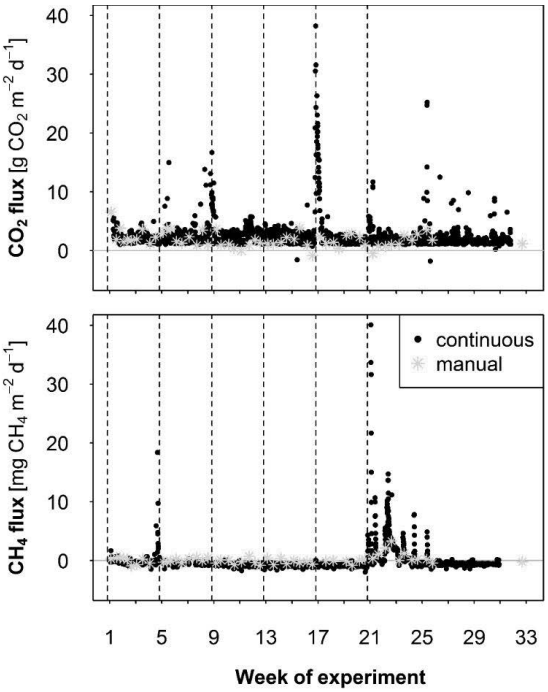

Fig. S2: Continuous flux observations of CO_2 and CH_4 measured via gas analyzer and flow through system compared to manual flux measurements via syringe sampling and closed chamber technique, followed by analysis with gas chromatograph. Fluxes are shown for individual replicates. CO_2: WV3, CH_4: DV4. Dashed lines indicate thawing steps. Week 1: Thawing down to ~20 cm, week 5: thawing down to ~40 cm, week 9: thawing down to 5 cm above the maximum seasonal thaw depth; week 13: thawing down to the maximum seasonal thaw depth; week 17: thawing down to 5 cm below the maximum seasonal thaw depth; week 21: thawing of the full core (15 cm below the maximum seasonal thaw depth).

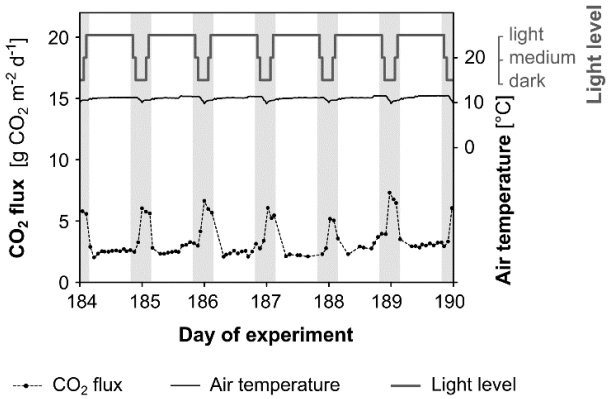

Fig. S3: Fluxes of CO_2 (net ecosystem exchange, NEE), as well as air temperature and light levels in the climate chamber during days 184-190 of the experiment (~week 27, two months after thawing the full core).

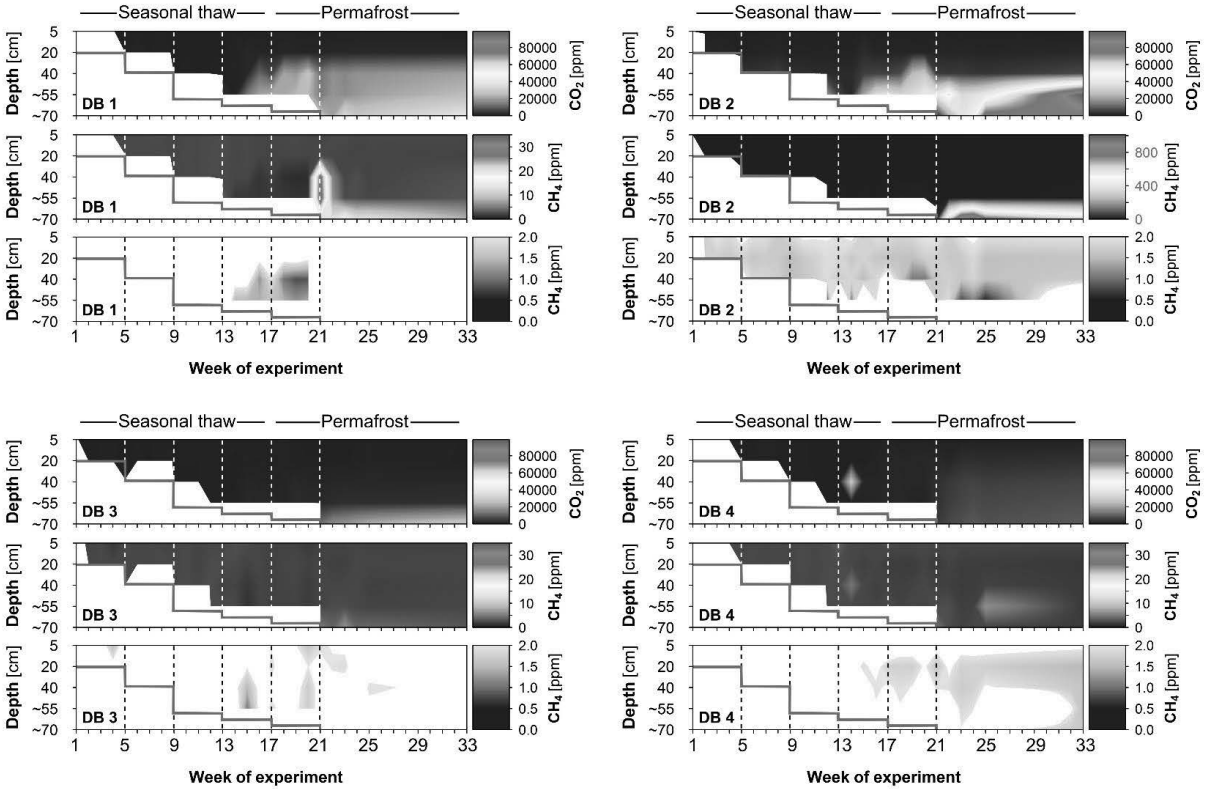

Fig. S4: Soil profile concentrations of carbon dioxide (CO_2), methane (CH_4), as well as below ambient (≤2 ppm) CH_4 in dry, bare mesocosms (DB). Gases can be either measured in the gas phase or dissolved in soil pore water, depending on wetness of mesocosm. Contour plots were created by linear interpolation between measurement points. The number of measurement time points was 26. White areas: no data available due to frozen soil conditions. Thick red line indicates thaw depths and dashed lines indicate thawing steps. Week 1: Thawing down to ~20 cm, week 5: thawing down to ~40 cm, week 9: thawing down to 5 cm above the maximum seasonal thaw depth; week 13: thawing down to the maximum seasonal thaw depth; week 17: thawing down to 5 cm below the maximum seasonal thaw depth; week 21: thawing of the full core (15 cm below the maximum seasonal thaw depth). Note deviating scaling of colour legends.

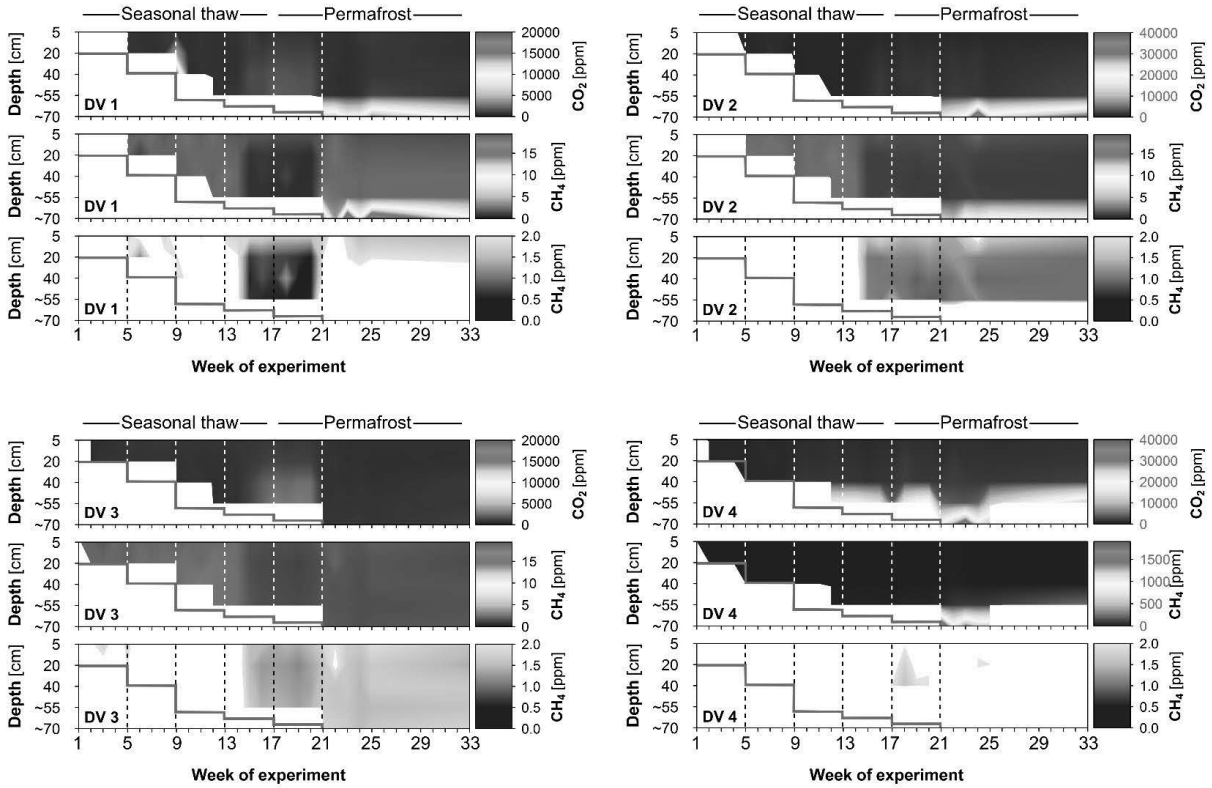

Fig. S5: Soil profile concentrations of carbon dioxide (CO_2), methane (CH_4), as well as below ambient (≤2 ppm) CH_4 in dry, vegetated mesocosms (DV). Gases can be either measured in the gas phase or dissolved in soil pore water, depending on wetness of mesocosm. Contour plots were created by linear interpolation between measurement points. The number of measurement time points was 26. White areas: no data available due to frozen soil conditions. Thick red line indicates thaw depths and dashed lines indicate thawing steps. Week 1: Thawing down to ~20 cm, week 5: thawing down to ~40 cm, week 9: thawing down to 5 cm above the maximum seasonal thaw depth; week 13: thawing down to the maximum seasonal thaw depth; week 17: thawing down to 5 cm below the maximum seasonal thaw depth; week 21: thawing of the full core (15 cm below the maximum seasonal thaw depth). Note deviating scaling of colour legends.

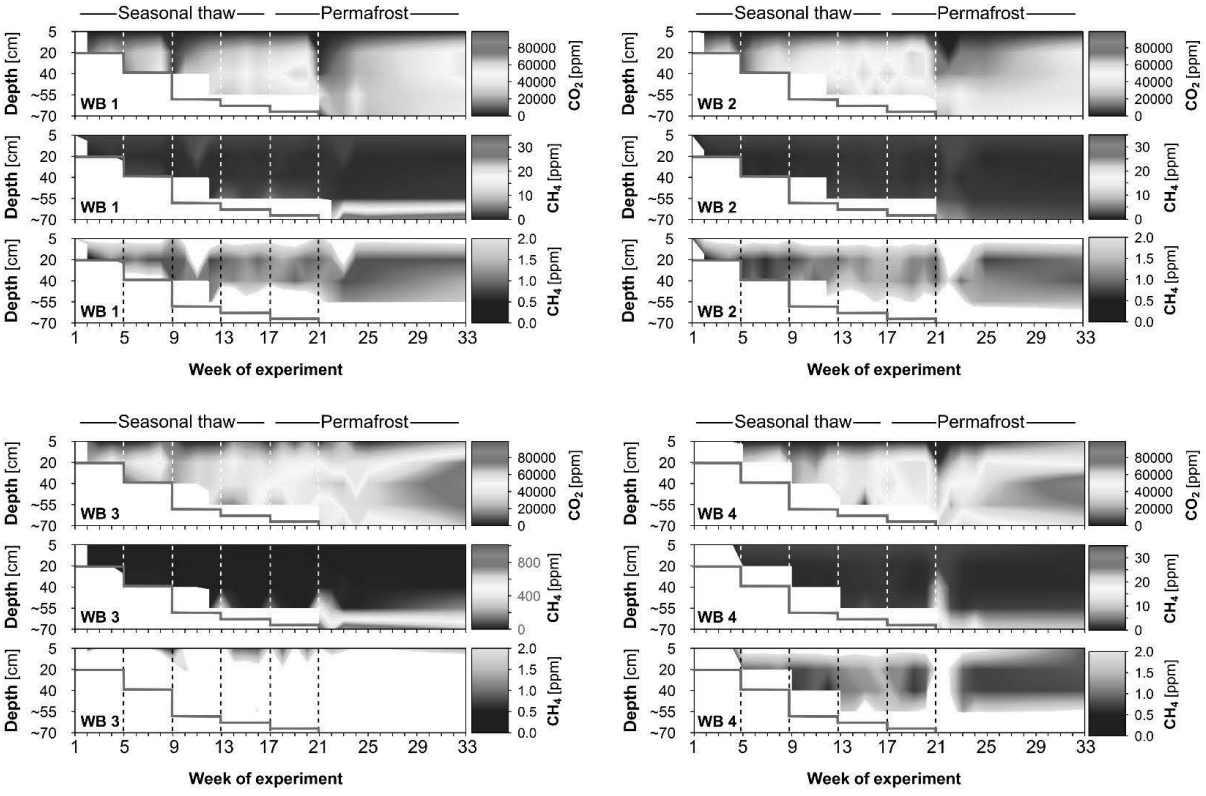

Fig. S6: Soil profile concentrations of carbon dioxide (CO_2), methane (CH_4), as well as below ambient (≤2 ppm) CH_4 in wet, bare mesocosms (WB). Gases can be either measured in the gas phase or dissolved in soil pore water, depending on wetness of mesocosm. Contour plots were created by linear interpolation between measurement points. The number of measurement time points was 26. White areas: no data available due to frozen soil conditions. Thick red line indicates thaw depths and dashed lines indicate thawing steps. Week 1: Thawing down to ~20 cm, week 5: thawing down to ~40 cm, week 9: thawing down to 5 cm above the maximum seasonal thaw depth; week 13: thawing down to the maximum seasonal thaw depth; week 17: thawing down to 5 cm below the maximum seasonal thaw depth; week 21: thawing of the full core (15 cm below the maximum seasonal thaw depth). Note deviating scaling of colour legends.

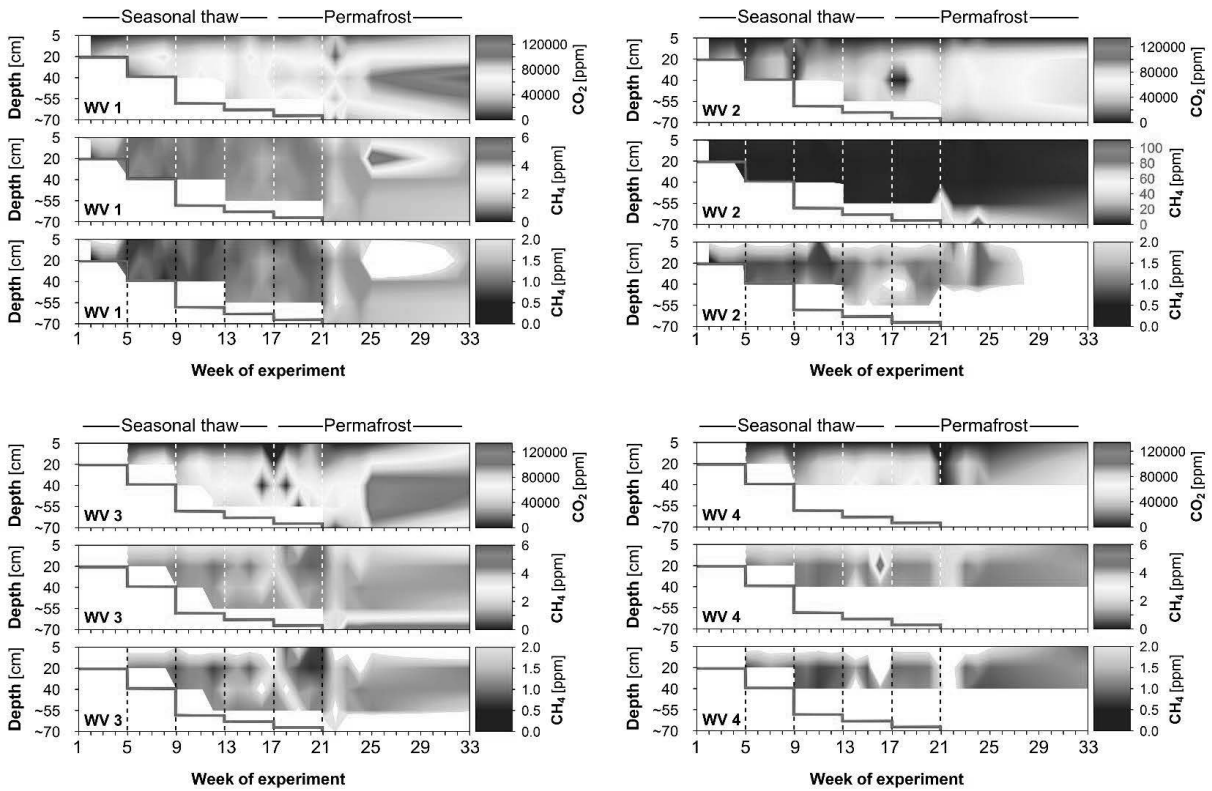

Fig. S7: Soil profile concentrations of carbon dioxide (CO_2), methane (CH_4), as well as below ambient (≤2 ppm) CH_4 in wet, vegetated mesocosms (WV). Gases can be either measured in the gas phase or dissolved in soil pore water, depending on wetness of mesocosm. Contour plots were created by linear interpolation between measurement points. The number of measurement time points was 26. White areas: no data available due to frozen soil conditions. Thick red line indicates thaw depths and dashed lines indicate thawing steps. Week 1: Thawing down to ~20 cm, week 5: thawing down to ~40 cm, week 9: thawing down to 5 cm above the maximum seasonal thaw depth; week 13: thawing down to the maximum seasonal thaw depth; week 17: thawing down to 5 cm below the maximum seasonal thaw depth; week 21: thawing of the full core (15 cm below the maximum seasonal thaw depth). Note deviating scaling of colour legends.

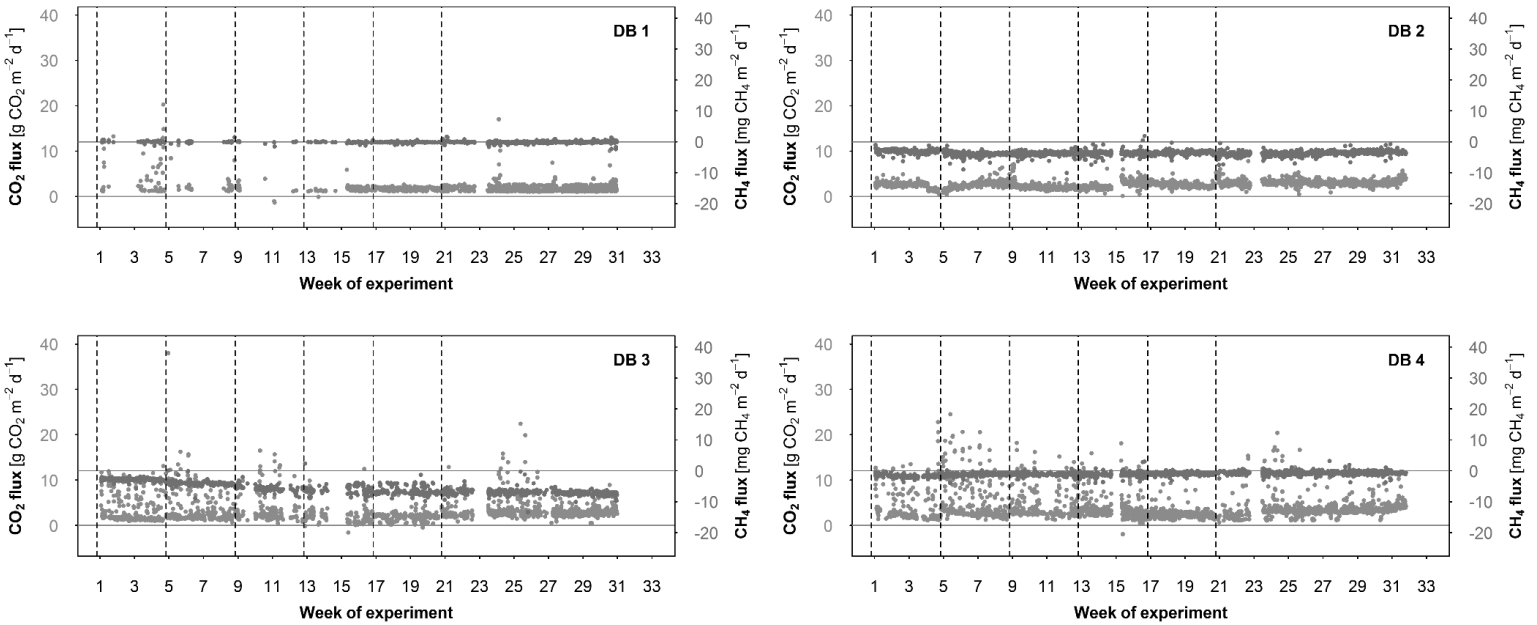

Fig. S8: Carbon dioxide (CO_2) and methane (CH_4) fluxes from the four replicates of dry, bare cores (DB). Dashed lines represent thawing steps. Week 0: Thawing down to 20 cm, week 4: thawing down to 40 cm, week 8: thawing down to 5 cm above the maximum seasonal thaw depth; week 12: thawing down to the maximum seasonal thaw depth; week 16: thawing down to 5 cm below the maximum seasonal thaw depth; week 20: thawing of the full core (15 cm below the maximum seasonal thaw depth).

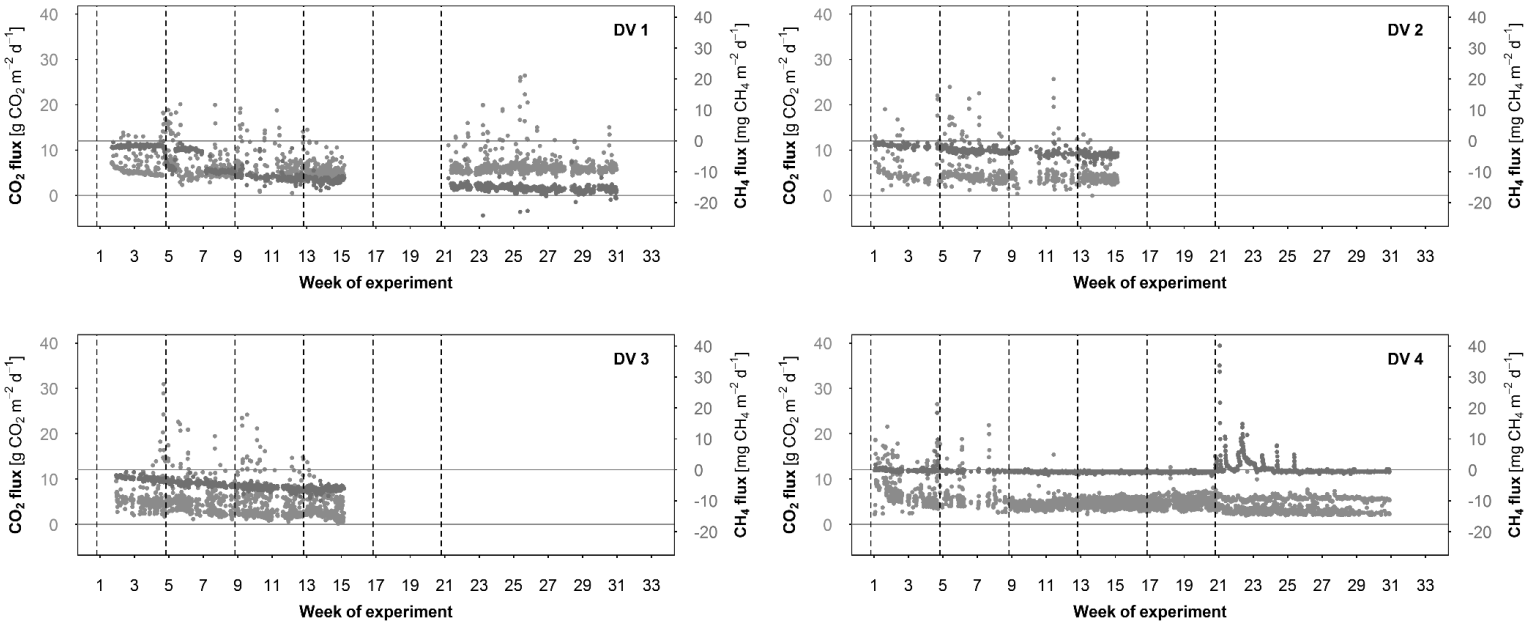

Fig. S9: Carbon dioxide (CO_2) and methane (CH_4) fluxes from the four replicates of dry, vegetated cores (DV). Dashed lines represent thawing steps. Week 0: Thawing down to 20 cm, week 4: thawing down to 40 cm, week 8: thawing down to 5 cm above the maximum seasonal thaw depth; week 12: thawing down to the maximum seasonal thaw depth; week 16: thawing down to 5 cm below the maximum seasonal thaw depth; week 20: thawing of the full core (15 cm below the maximum seasonal thaw depth).

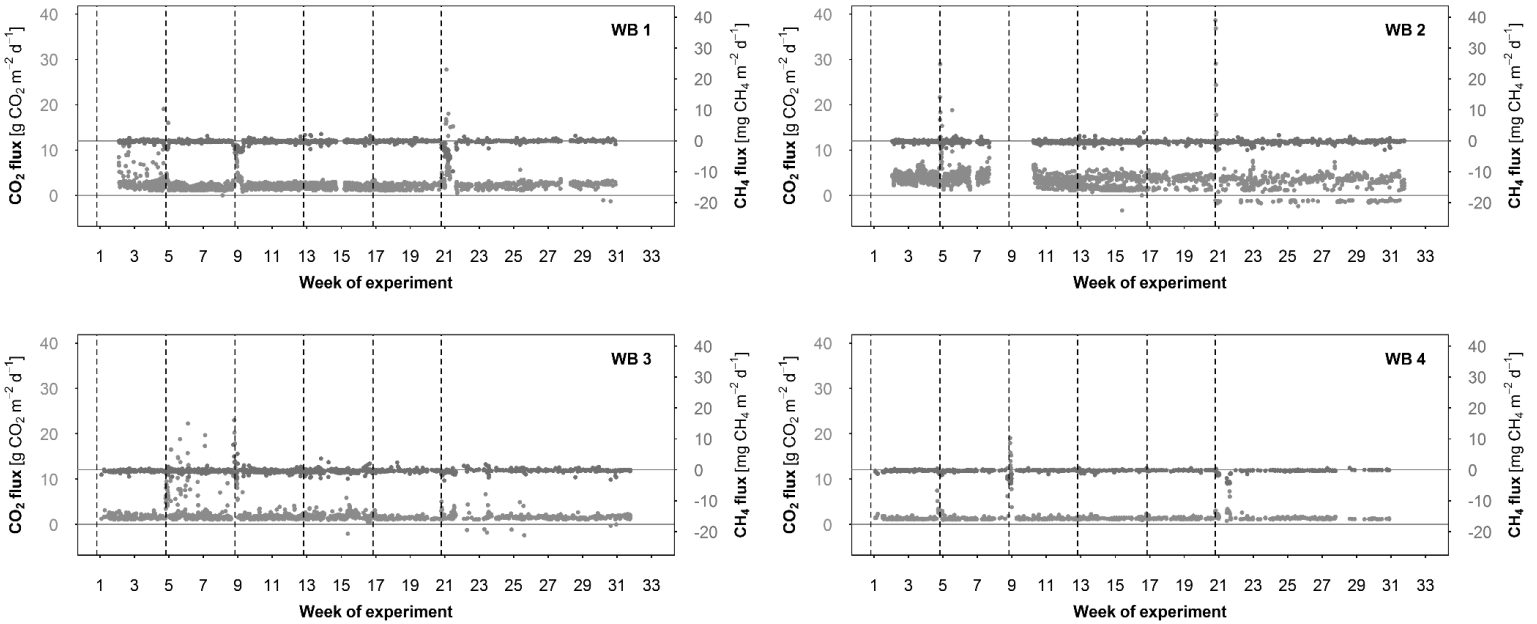

Fig. S10: Carbon dioxide (CO_2) and methane (CH_4) fluxes from the four replicates of wet, bare cores (WB). Dashed lines represent thawing steps. Week 0: Thawing down to 20 cm, week 4: thawing down to 40 cm, week 8: thawing down to 5 cm above the maximum seasonal thaw depth; week 12: thawing down to the maximum seasonal thaw depth; week 16: thawing down to 5 cm below the maximum seasonal thaw depth; week 20: thawing of the full core (15 cm below the maximum seasonal thaw depth).

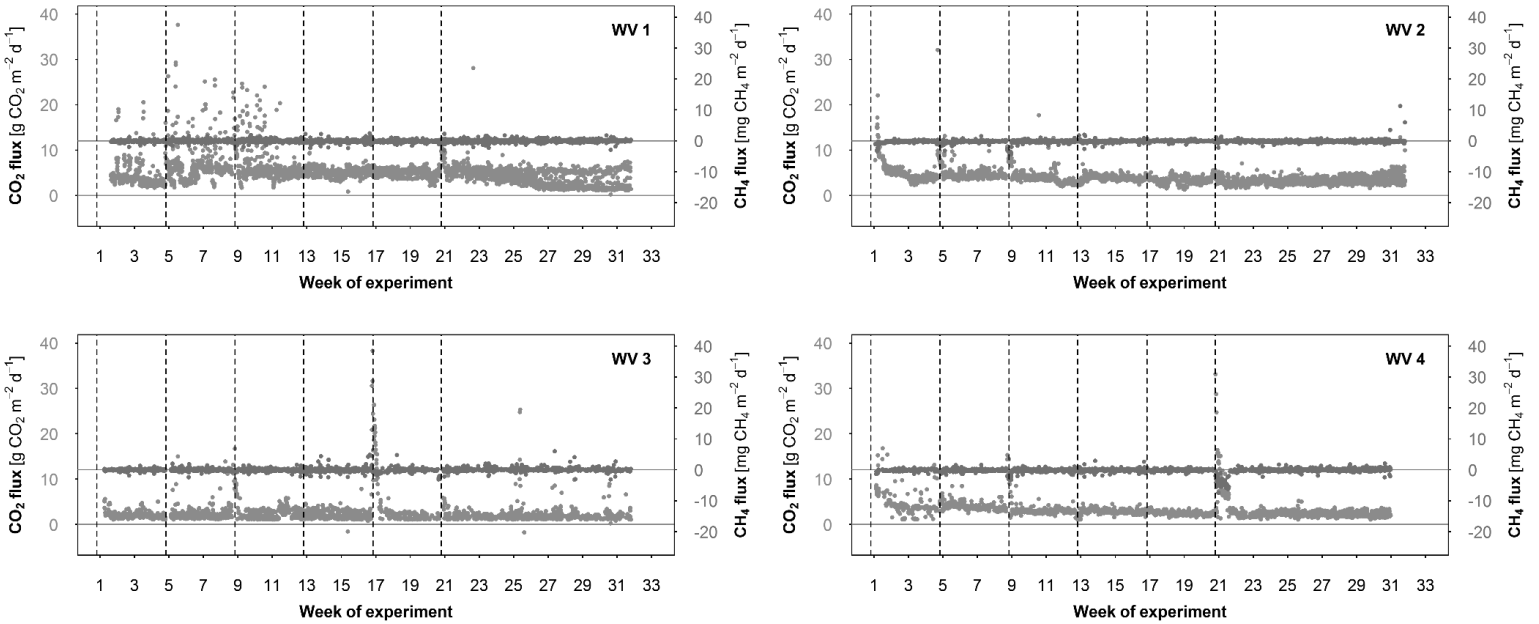

Fig. S11: Carbon dioxide (CO_2) and methane (CH_4) fluxes from the four replicates of wet, vegetated cores (WV). Dashed lines represent thawing steps. Week 0: Thawing down to 20 cm, week 4: thawing down to 40 cm, week 8: thawing down to 5 cm above the maximum seasonal thaw depth; week 12: thawing down to the maximum seasonal thaw depth; week 16: thawing down to 5 cm below the maximum seasonal thaw depth; week 20: thawing of the full core (15 cm below the maximum seasonal thaw depth).

Table S1. Carbon dioxide (CO_2) and methane (CH_4) fluxes from bare and vegetated mesocosms, dry and wet treatment. Fluxes are averaged over week 1–16 (sequential thawing of the active layer) and week 17–33 (sequential thawing of the permafrost part). In the wet mesocosms, statistics were calculated (a) with inclusion of thaw peaks related to thawing induced water table drop down, and (b) excluding the peaks in fluxes directly after thawing, when the water table was momentarily lowered. Asterisks indicate significant differences between week 1–16 and week 17–33, showing whether the values during thawing of the permafrost are significantly higher or lower compared to fluxes measured during thawing of the active layer. Levels of significance: ***significant at $P \leq 0.001$, **significant at $P \leq 0.01$, *significant at $P \leq 0.05$. *P*-values are derived from Welch's two-sample t-test.

Core type	Carbon dioxide fluxes					Methane fluxes				
	CO_2 flux, mean ± SD ($g\ CO_2\ m^{-2}\ d^{-1}$)	median	MIN	MAX	no. of data points	CH_4 flux, mean ± SD ($mg\ CH_4\ m^{-2}\ d^{-1}$)	median	MIN	MAX	no. of data points
					DRY					
Bare										
week 1–16	3.03 ± 2.57	2.36	-1.94	37.99	4140	-2.92 ± 1.61	-3.05	-10.14	2.98	4133
week 17–33	2.78 ± 1.48 *** (P < 0.001)	2.67	-0.47	22.39	4989	-2.94 ± 2.59 (P = 0.565)	-3.11	-13.40	3.13	4933
Vegetated										
week 1–16	5.32 ± 3.33	4.63	-0.07	93.89	4325	-4.06 ± 3.79	-3.25	-16.08	18.39	4323
week 17–33	4.92 ± 2.12 *** (P < 0.001)	5.10	1.92	26.42	2329	-6.09 ± 7.88 *** (P < 0.001)	-0.78	-24.18	40.13	2330
					WET					
Bare										
week 1–16 (a)	2.50 ± 2.02	1.84	-3.34	28.96	4472	-0.42 ± 0.58	-0.34	-4.40	8.09	4464
week 1–16 (b)	2.32 ± 1.56	1.80	-3.34	22.22	4161	-0.36 ± 0.41	-0.33	-3.66	3.57	4168
week 17–33 (a)	2.27 ± 2.50 *** (P = 0.001)	1.83	-2.41	38.56	1528	-0.49 ± 0.95 ** (P = 0.006)	-0.25	-9.89	2.38	1532
week 17–33 (b)	2.08 ± 1.47 *** (P < 0.001)	1.81	-2.41	15.17	1314	-0.31 ± 0.57 ** (P = 0.006)	-0.22	-4.45	2.38	1302
Vegetated										
week 1–16 (a)	4.04 ± 2.52	3.67	-1.57	37.58	6553	-0.16 ± 0.45	-0.14	-4.36	4.85	6545
week 1–16 (b)	3.93 ± 2.36	3.64	-1.57	37.58	6234	-0.13 ± 0.36	-0.13	-3.36	4.85	6206
week 17–33 (a)	3.39 ± 3.88 *** (P < 0.001)	2.86	-1.79	224.79	5586	-0.15 ± 0.64 (P = 0.312)	-0.11	-7.47	11.15	5590
week 17–33 (b)	3.12 ± 1.48 *** (P < 0.001)	2.78	-1.79	28.02	5268	-0.10 ± 0.42 *** (P < 0.001)	-0.10	-3.16	11.15	5230

Table S2. Soil profile concentrations of carbon dioxide (CO_2) in 5 depths (below surface) along the soil profile of bare and vegetated cores, dry and wet treatment (mean ± SE). Concentrations are averaged over week 1–16 (sequential thawing down to the maximum seasonal thaw depth) and week 17–33 (sequential thawing of the permafrost part). Asterisks indicate significant differences between week 1–16 and week 17–33, showing whether the values during thawing of the permafrost are significantly higher or lower compared to concentrations measured during thawing of the active layer. Levels of significance: ***significant at $P \leq 0.001$, **significant at $P \leq 0.01$, *significant at $P \leq 0.05$. Exact *P*-values are listed in Table S4.

Core type	5 cm		20 cm		40 cm		~55 cm (AL-10 cm)		~70 cm (AL+5 cm)	
	CO_2 (ppm, mean ± SE)	**n**	**CO_2** (ppm, mean ± SE)	**n**	**CO_2** (ppm, mean ± SE)	**n**	**CO_2** (ppm, mean ± SE)	**n**	**CO_2** (ppm, mean ± SE)	**n**
	DRY									
Bare										
week 1–16	606 ± 63	63	780 ± 46	54	2660 ± 790	37	7021 ± 2408	18	n. d.	0
week 17–33	626 ± 19	40	1319 ± 100 ***	40	8070 ± 1314***	40	18349 ± 3197**	39	25480 ± 4181 n. d.	24
Vegetated										
week 1–16	722 ± 20	64	837 ± 72	54	1385 ± 426	36	5025 ± 1603	20	n. d.	0
week 17–33	825 ± 32**	40	1080 ± 55**	40	1451 ± 93	40	4069 ± 993	39	16025 ± 2650 n. d.	21
	WET									
Bare										
week 1–16	1947 ± 445	62	32263 ± 1536	57	34802 ± 1918	44	32138 ± 2906	19	n. d.	0
week 17–33	3713 ± 1109	39	36252 ± 3003	37	45221 ± 3063**	40	44574 ± 2130***	39	39951 ± 2967 n. d.	23
Vegetated										
week 1–16	4572 ± 871	63	43535 ± 2383	53	46472 ± 2870	40	46953 ± 3186	13	n. d.	0
week 17–33	9729 ± 2159*	38	48506 ± 3142	39	61751 ± 4796**	40	64018 ± 3915**	29	40427 ± 5159 n. d.	22

Table S3. Soil profile concentrations of methane (CH_4) in 5 depths (below surface) along the soil profile of bare and vegetated cores, dry and wet treatment (mean ± SE). Concentrations are averaged over week 1–16 (sequential thawing down to the maximum seasonal thaw depth) and week 17–33 (sequential thawing of the permafrost part). Asterisks indicate significant differences between week 1–16 and week 17–33, showing whether the values during thawing of the permafrost are significantly higher or lower compared to concentrations measured during thawing of the active layer. Levels of significance: ***significant at $P \leq 0.001$, **significant at $P \leq 0.01$, *significant at $P \leq 0.05$. Exact *P*-values are listed in Table S5.

	5 cm		20 cm		40 cm		~55 cm (AL-10 cm)		~70 cm (AL+5 cm)	
Core type	**CH_4** (ppm, mean ± SE)	**n**	**CH_4** (ppm, mean ± SE)	**n**	**CH_4** (ppm, mean ± SE)	**n**	**CH_4** (ppm, mean ± SE)	**n**	**CH_4** (ppm, mean ± SE)	**n**
	DRY									
Bare										
week 1–16	2.23 ± 0.03	64	2.15 ± 0.04	54	2.14 ± 0.09	37	2.20 ± 0.21	19	n. d.	0
week 17–33	2.13 ± 0.03*	40	1.93 ± 0.04***	40	2.61 ± 0.66	40	3.46 ± 0.76	39	172.82 ± 69.06 $^{n.d.}$	24
Vegetated										
week 1–16	2.14 ± 0.03	64	2.08 ± 0.06	54	2.09 ± 0.08	36	4.49 ± 1.12	20	n. d.	0
week 17–33	1.84 ± 0.09**	40	1.71 ± 0.17*	40	2.00 ± 0.37	40	18.91 ± 7.05*	39	306.83 ± 124.32 $^{n.d.}$	22
	WET									
Bare										
week 1–16	2.14 ± 0.07	62	1.91 ± 0.27	57	3.08 ± 0.60	44	23.28 ± 17.85	19	n. d.	0
week 17–33	2.10 ± 0.07	40	1.83 ± 0.23	36	3.21 ± 0.69	40	30.08 ± 14.15	38	208.35 ± 78.40 $^{n.d.}$	20
Vegetated										
week 1–16	2.28 ± 0.33	63	1.01 ± 0.09	54	1.16 ± 0.07	40	1.41 ± 0.11	13	n. d.	0
week 17–33	1.88 ± 0.11	40	1.43 ± 0.14*	40	1.38 ± 0.08*	40	4.51 ± 2.33	30	22.66 ± 6.33 $^{n.d.}$	22

Table S4. *P*-values for carbon dioxide (CO_2) concentration of the mesocosms. *P*-values are given for 5 depths (below surface) along the soil profile of bare and vegetated cores, dry and wet treatment: *P*-values are derived from Welch's two-sample t-test and show differences between the active layer and the permafrost part of the core. Measured values for CO_2 soil profile concentrations are shown in Table S2.

	5 cm	20 cm	40 cm	~55 cm (AL-10 cm)	~70 cm (AL+5 cm)
Core type	CO_2 *P*-value	CO_2 *P*-value	CO_2 *P*-value	CO_2 *P*-value	CO_2 *P*-value
DB	0.402	***<0.001***	***0.001***	***0.007***	n. d.
DV	***0.009***	***0.009***	0.882	0.615	n. d.
WB	0.146	0.242	***0.005***	***0.001***	n. d.
WV	***0.031***	0.211	***0.008***	***0.002***	n. d.

Table S5. *P*-values for methane (CH_4) concentration of the mesocosms. *P*-values are given for 5 depths (below surface) along the soil profile of bare and vegetated cores, dry and wet treatment: *P*-values are derived from Welch's two-sample t-test and show differences between the active layer and the permafrost part of the core. Measured values for CH_4 soil profile concentrations are shown in Supplementary Table S3.

	5 cm	20 cm	40 cm	~55 cm (AL-10 cm)	~70 cm (AL+5 cm)
Core type	CH_4 *P*-value	CH_4 *P*-value	CH_4 *P*-value	CH_4 *P*-value	CH_4 *P*-value
DB	***0.038***	***<0.001***	0.488	0.117	n. d.
DV	***0.003***	***0.044***	0.824	***0.050***	n. d.
WB	0.749	0.825	0.886	0.767	n. d.
WV	0.247	***0.017***	***0.041***	0.194	n. d.

Table S6. Differences among pairs (veg vs. bare and wet vs. dry), lower and upper 95% confidence intervals and adjusted *P*-values, obtained from ANOVA coupled with Tukey's HSD posthoc test. The influence of the parameters vegetation type and moisture were tested for the cumulative fluxes of CO_2, CH_4, N_2O, as well as on the full GHG balance. Levels of significance: ***significant at $P \leq 0.001$, **significant at $P \leq 0.01$, *significant at $P \leq 0.05$, ˣmarginally significant at $P \leq 0.1$.

Parameters	diff	lower	upper	*P*-value	Signif.
CO_2 flux					
Type (veg/bare)	266.27	7.04	525.49	0.045	*
Moisture (wet/dry)	-116.12	-375.35	143.11	0.351	
CH_4 flux					
Type (veg/bare)	-2.72	-19.85	14.41	0.737	
Moisture (wet/dry)	17.16	0.03	34.29	0.050	*
N_2O flux					
Type (veg/bare)	-1.10	-2.17	-0.04	0.043	*
Moisture (wet/dry)	-0.95	-2.01	0.11	0.076	ˣ
GHG flux					
Type (veg/bare)	222.91	-31.70	477.53	0.081	ˣ
Moisture (wet/dry)	-137.74	-392.35	116.88	0.264	

Table S7. *P*-values for dissolved nitrogen (DN), dissolved organic carbon (DOC), microbial biomass N (MBN) and microbial biomass C (MBC). Statistical differences for soil C and N pools are shown for the active layer vs. permafrost layer (all replicates, as well as separated by treatment), for dry vs. wet, and for bare vs. vegetated. This table is supplementary to Fig. X). *P*-values are derived from Student's t-test.

	DN	DOC	MBN	MBC
	P-value	*P*-value	*P*-value	*P*-value
Depth				
Active layer : permafrost	***<0.001***	***<0.001***	0.484	0.260
DB	***0.042***	0.289	0.617	0.761
DV	***0.004***	***0.005***	0.309	***0.028***
WB	0.129	***0.004***	0.921	0.361
WV	***0.008***	***0.010***	0.840	0.732
Treatment				
Dry : wet	0.275	0.578	0.839	0.729
Type				
Bare : vegetated	0.350	0.364	***0.003***	***0.006***

APPENDIX 4:
SUPPLEMENTARY INFORMATION TO PUBLICATION IV
Increased nitrous oxide emissions from Arctic peatlands after permafrost thaw

SI Appendix

"Increased nitrous oxide emissions from Arctic peatlands after permafrost thaw"

SI Text

Study site. Peat mesocosms for this study were collected from a palsa mire (68°89'N, 21°05E) located in the discontinuous permafrost zone, near the settlement Kilpisjärvi, in Finnish Lapland. Palsas and peat plateaus, permafrost peatlands uplifted by frost heave, are a common feature in the Arctic, occurring especially in the discontinuous and sporadic permafrost zones (1–3). There, thick peat deposits with good insulating properties are able to preserve a permanently frozen core (4). A locally thin or missing snow cover, together with low temperatures and relatively low precipitation – key factors for palsa formation – allow for the frost to penetrate deep into the peat (4). With time, growth of the frozen core gradually lifts the palsa above the surface of the surrounding mire complex, and above the water table of the surrounding wetlands (5). The resulting dry conditions as well as exposure of the palsa surface to wind abrasion cause a shift in vegetation composition (5), and often result in palsas completely lacking vegetation, exposing bare peat at the surface (6, 7). The uplifting process also creates a typical sequence of the peat profile, consisting of sedge (fen) peat on the base of the peatland, overlain by sphagnum moss (bog) peat (5).

Underlain by discontinuous permafrost, the palsa selected for this study is a large (~300 m x 80 m), peat-cored palsa with an average thaw depth of 60 cm, rising around 3 m above the surrounding mire complex (8). The palsa is characterized as a mature palsa in its early collapsing stage (8), featuring collapsed parts and cracks on the palsa surface. The vegetation cover on the palsa surface is dominated by dwarf-shrubs and herbaceous plants, such as *Betula nana* L., *Rubus chamaemorus* L., as well as by *Empetrum nigrum* subsp. *hermaphroditum*, *Vaccinium vitis-idaea* L. and lichens, whereas the wetter areas are characterized by the growth of mosses (*Dicranum* spp., *Polytrichum* spp., *Pleurozium* spp.). Patches of bare peat, naturally free of vascular plants and only sporadically covered by lichens, are scattered among the vegetated areas. The long-term mean temperature (1981–2010) in our study region is -1.9°C (range: -6.0–2.2°C), and the mean annual precipitation amounts to 487 mm (9).

Sampling and transport of peat mesocoms. The collection of 16 mesocosms took place with following coring system: A steel corer (~1 m length) with removable steel-cap was hammered into the soil using a pneumatic drill (Fig. S2). The soil cores were collected within plastic tubes (polypropylene, diameter = 10 cm, Fig. S3), which were inserted into the steel corer before drilling. The peat mesocosms were kept within the plastic shells throughout the experiment to minimize the disturbances on the outer monolith walls. A chain connected to a pulley and tripod was used to retrieve the peat cores. The sampling took place at maximum seasonal thaw depth at the end of September 2012. Before sampling we determined the thaw depth next to each coring plot by means of a metal stick. The coring was stopped at 15 cm below the measured thaw depth, collecting, on average, 65 cm of active layer peat and the upper 15 cm of permafrost.

The plastic shells with the intact peat profiles were closed from both ends and frozen immediately upon sampling. Great care was taken to keep the cores frozen at gentle minus temperatures (-5 °C minimum) at all times during the transport and the 5 months pre-incubation period (= artificial winter), until the start of the experiment in March 2013.

Climate chamber set-up and replication. The cores were set up in a climate-controlled chamber (BDR16 Reach-in plant growth chamber, CONVIRON, Winnipeg, Canada), providing constant humidity and air temperature (+10 °C), and the possibility to regulate the light level. We chose a diurnal light rhythm, resembling natural

conditions during the snow-free period at our study site, with 18 h of full light, 4 h of darkness, and an additional hour at reduced light before and after the simulated nighttime. Small amounts of distilled water were added weekly to the soil surface, to prevent the surface soil from drying out and to compensate for water loss during sampling.

To simulate thawing by sequentially unfreezing the mesocosms, we installed them in two replicate saltwater baths (dimensions: 145 cm x 60 cm x 25.5 cm, total volume of 221.85 L per bath), placed inside the climate chamber. The double metal walls of the baths were circulated with glycol, acting as a cooling agent, and sealed towards the atmosphere. Each bath was filled with saltwater (salt concentration: 7.66 %) and equipped with two pumps to ensure equal temperature distribution of -3 to -4 °C in the saltwater. To prevent saltwater from entering the soil cores, the plastic tubes containing the soil were carefully closed at the bottom end with PVC plugs sealed with silicon and a plastic bag reaching above the saltwater level. Cores were placed in a Styrofoam grid and weighted down at the bottom to keep them in position. Water tightness, optimal salt concentration and maintaining of a constant saltwater temperature were tested thoroughly before subjecting the soil cores to thawing.

Sequential thawing and sensor set-up in the mesocosms. Sequential thawing was achieved by lowering the water level of the saltwater baths. We unfroze the peat mesocosms from top to bottom by six thawing steps (Fig. S4, Table S1). We used step-wise thawing to distinguish between emissions derived from the active layer and the permafrost, but also from smaller increments of the peat column. The four-week duration of each thawing step ensured sufficient time for the post-thaw peak to settle, before continuing to thaw the next layer, allowing us to assess the production potential of individual soil layers.

Installation of temperature sensors and sampling probes for pore water and gas took place successively after each thawing step. Installation holes were drilled into the still frozen soil immediately after initiation of thawing to minimize disturbances of the soil matrix. The sensors and sampling probes were installed through butyl rubber septa, providing a gas- and watertight seal.

Nitrous oxide fluxes. Flux chambers were equipped with two three-way-valves (STERITEX® 3W, CODAN Medical, Lensahn, Germany) for the gas sampling. Nitrous oxide (N_2O) samples were taken manually 2–3 times per week from each mesocosm, using a static closed chamber method (10). We acknowledge that we may have missed some of the short-term emission peaks, meaning that our fluxes are conservative estimates. We took four gas samples within a 30 min enclosure interval with a 35 mL syringe with Luer Lock Tip (Terumo®). The sampled volume was replace with N_2 to maintain a constant pressure within the chamber. Samples were transferred to pre-evacuated screw-cap vials with pierceable rubber septum (Labco Exetainer®, Labco, UK) and analyzed for N_2O concentrations via gas chromatography (GC) as described earlier (11). The fluxes were calculated from the concentration change in the chamber over time. The general requirement for the acceptance of fluxes was an $r^2 \geq 0.85$ for the fit of the regression lines. As not to result in an overestimation of flux rates, low fluxes were included regardless of their r^2 value, with ±0.15 mg N_2O m^{-2} day^{-1} determined as a threshold for low fluxes, based on the RSME. Cumulative sums of gas fluxes were determined per each thawing step, lasting four weeks (28 days), by interpolating linearly between measurement points.

Soil profile concentration of nitrous oxide. Soil gas was sampled weekly from soil gas collectors made of a perforated plastic tube (nylon, diameter = 8 mm) wrapped in a fine nylon net and connected to a longer nylon tube (diameter = 4 mm) equipped with three-way valve (STERITEX® 3W, CODAN Medical, Lensahn, Germany). As a number of soil gas collectors were installed below the water table, we applied two different methods to determine soil profile concentrations of N_2O: Above the water table level 15 mL of gas was sampled,

transferred into pre-evacuated vials as described in above, and diluted with N_2 in order to achieve overpressure in the vials required for GC analysis (11). For samples taken below the water table level, we determined the amount of N_2O dissolved in the soil pore water by applying a headspace method: We sampled 7 mL of pore water with a syringe, added a headspace of 28 mL of N_2 (1:4 ratio), and equilibrated the gases within the water and headspace by vigorously shaking the syringe for 1 min. After transferring the headspace into pre-evacuated vials, N_2O concentrations were determined via gas chromatography (11). Leftover water was returned to the individual cores at the same depth it was taken from. High concentration samples were diluted to fit the measurement range during GC analysis.

The amount of gas dissolved in water was derived from the concentration measured in the equilibrated headspace gas. The temperature dependent solubility k_H of the individual gases was calculated based on Henry's law, with coefficients taken from literature (12):

$$k_H = k_H^\theta \times \exp\left(\frac{-\Delta_{soln}H}{R} \times \left(\frac{1}{T} - \frac{1}{T^\theta}\right)\right),$$

where k_H^θ the Henry's law constant at standard temperature [0.0250 mol atm^{-1}], $\frac{-\Delta_{soln}H}{R}$ the temperature coefficient [2600 K], T the soil temperature at the depth where the sample was taken and T^ϑ the standard temperature [298.15 K].

Soil temperature profiles, required for calculation of the soil gas profile based on Henry's law, were recorded continuously in one core of each treatment by means of PT-100 temperature probes connected to a data logger (CR5000) with multiplexer (AM16/32, Campbell Scientific, Logan, UT, USA). Temperature sensors were installed in five depths along the soil profile, using the same depths as the soil gas collectors.

Nutrient profile in soil pore water. The Rhizon tubes were extended using semi-rigid PE tubing (OD = 3.2, ID = 1.0 mm) when needed. Pre-evacuated 12 mL screw-cap vials (Labco Exetainer®, Labco, UK) were connected to the Rhizon tubes every second week and left in place for four days before the water samples were transferred to 15 mL PP vials (Sarstedt, Nuembrecht, Germany) and frozen until further analysis.

Amounts of nitrate (NO_3^-) and ammonium (NH_4^+) in the pore water were determined spectrophotometrically (13, 14), using modified methods requiring a smaller sample volume (18). After achieving the colour reaction, samples were analyzed with a Wallac 1420 VICTOR microplate reader (Perkin Elmer, Turku, Finland), using 544 nm and 650 nm wavelengths for NO_3^- and NH_4^+, respectively.

Soil analyses. After completion of the incubation experiment, we conducted detailed analyses of the soil physical-chemical properties of each peat core. Therefore, the cores were refrozen at -4 °C, facilitating subsequent cutting with an automated precision saw. We obtained 2–3 cm thick soil slices from each core in 5 depths: 5 cm, 20 cm and 40 cm below the soil surface, 10 cm above the maximum seasonal thaw depth (~55 cm) and 5 cm below the maximum seasonal thaw depth (~70 cm). Soil organic matter content (SOM), total C and N content, C to N ratio, bulk density, pH, water-filled pore space (WFPS) and amounts of extractable NO_3^- and NH_4^+ were determined as described in earlier studies (11, 15). We determined microbial biomass N by applying a chloroform fumigation extraction method: after fumigation in chloroform atmosphere for 24 h, fumigated and non-fumigated samples were extracted with 0.5M K_2SO_4. Samples were analyzed with a TN analyzer (LiquicTOC II; Elementar, Hanau, Germany), and the microbial biomass determined by correcting for incomplete extraction of microbial N (K_{EN} = 0.54) (16).

Hyperspectral imaging of peat profiles. Two additional cores (one bare, one vegetated) were collected along with the 16 cores used in the mesocosm experiment. These cores were kept frozen under natural conditions and not subjected to sequential thawing, representing natural, unaltered peat structure and chemistry. To

gain an insight into the spatial variability of the peat profile, we took images with two pushbroom hyperspectral cameras covering the visible to near infrared (VNIR, 400–1000 nm, bandwidth: 3.5 nm FWHM; ImSpector V10, Spectral Imaging Ltd, Oulu, Finland) and shortwave infrared (SWIR, 1000–2500 nm, bandwidth: 12 nm FWHM; LVDS-100, Spectral Imaging Ltd, Oulu, Finland). For the imaging, the cores were cut vertically into half in a frozen state, and images were taken after unfreezing the cores at +4°C. The peat profiles were illuminated with eight 35 W tungsten halogen lamps, in a 45/0 geometry. Hyperspectral images are three dimensional data cubes, where, for each spatial pixel, a reflectance value is calculated. The reflectance value was derived by first subtracting a dark image and then dividing the result by a reference white image, acquired from a Spectralon® reference plate.
Image processing and principal component analysis (PCA) for the SWIR data were done using Evince software (Predictera AB, Umeå, Sweden), using the three main principal components as channels for the false colour images (PC1 = Red, PC2 = Green, PC3 = Blue). For the PCA, data were mean centered and background subtracted. Pixel-wise PCA for hyperspectral data cubes is an unsupervised method for detecting the main components of variance within the sample (17). The first three components of the PCA explained 99.5% of the variety within the data.

Statistical analyses and spatial upscaling. Statistical analyses were performed in R version 3.2.2 (18) and included visual inspection of variables and creation of density plots, Q-Q plots and histograms, as well as assessment for normality and variance homogeneity prior to statistical tests. To test for differences of soil characteristics and extractable nutrients between the active layer and the permafrost, data were averaged for the active layer (including 4 sampling depths) and the permafrost (including 1–2 sampling depths). For N_2O fluxes and soil profile concentrations of N_2O, data were split by sampling time, separating between time points before (week 1–16) and after (week 17–33) thawing reached the permafrost layer. Differences between active layer and permafrost were determined by means of two-sample Student's t-test and Welch's two-sample t-test, depending on whether data were near-normal or not normally distributed. If not otherwise specified, values are reported with their respective standard error (SE), with n = 4. To determine the influence of soil gas concentration and production at depth in describing the aboveground N_2O emissions from dry, bare mesocosms, we applied linear-mixed-effects models (package *lme4* (19)). The N_2O concentration in the active layer, its interaction with the N_2O concentration in the permafrost layer, as well as the interaction between permafrost NH_4^+ and N_2O concentration were included as fixed effects. The mesocosm replicate no. was included as a random effect in the model, to account for repeated measurements of the same mesocosm. We applied a top-down approach to select the final model structure (20), starting out with a beyond-optimum model including all variables and possible interactions. Variables were gradually dropped by means of their variance inflation factors (VIF), as described in our previous study (11). The best model fit was selected by means of the Akaike's Information Criterion (AIC). Model validation was performed by inspecting residuals and the final model was fit using restricted maximum likelihood (REML) estimation.
We used a GIS-based approach to identify areas vulnerable for N_2O emissions with permafrost thaw. For this purpose, we used the circum-Arctic map of permafrost and ground ice conditions (21) as base map for the circumpolar zonation of permafrost distribution (continuous, discontinuous, sporadic, isolated). We used the coverage of peatlands (histosols and histels) (22, 23) within the circumpolar permafrost region and the most recent knowledge on the distribution of landscape vulnerable for thermokarst (24). The areas with high peatland coverage (>15%) and high (30–60%) and very high (60–100%) coverage of thermokarst were pointed out as the most probable hot-spots of Arctic N_2O emissions. Mapping was done in ArcGIS version 10.0.

SI Figures and tables

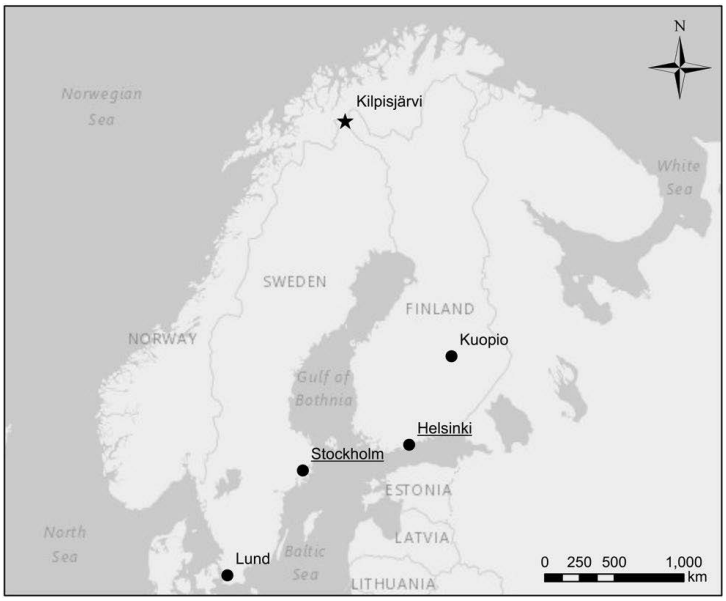

Fig. S1. Overview map of the sampling site Peera Palsa near Kilpisjärvi (68°89'N, 21°05'E). Peat cores were frozen immediately upon sampling, and transported from Kilpisjärvi (Finland) to Lund (Sweden), to be set up in a climate controlled chamber. During the transport, cores were kept in natural freezing temperatures (~ -3 to -4°C) by means of a custom-made temperature control system attached to a freezer. The freezer was kept running continuously during the 3-day car ride to Lund, powered by a generator pulled on a trailer. Final gas, soil, and water sample analyses took place in Kuopio (Finland).

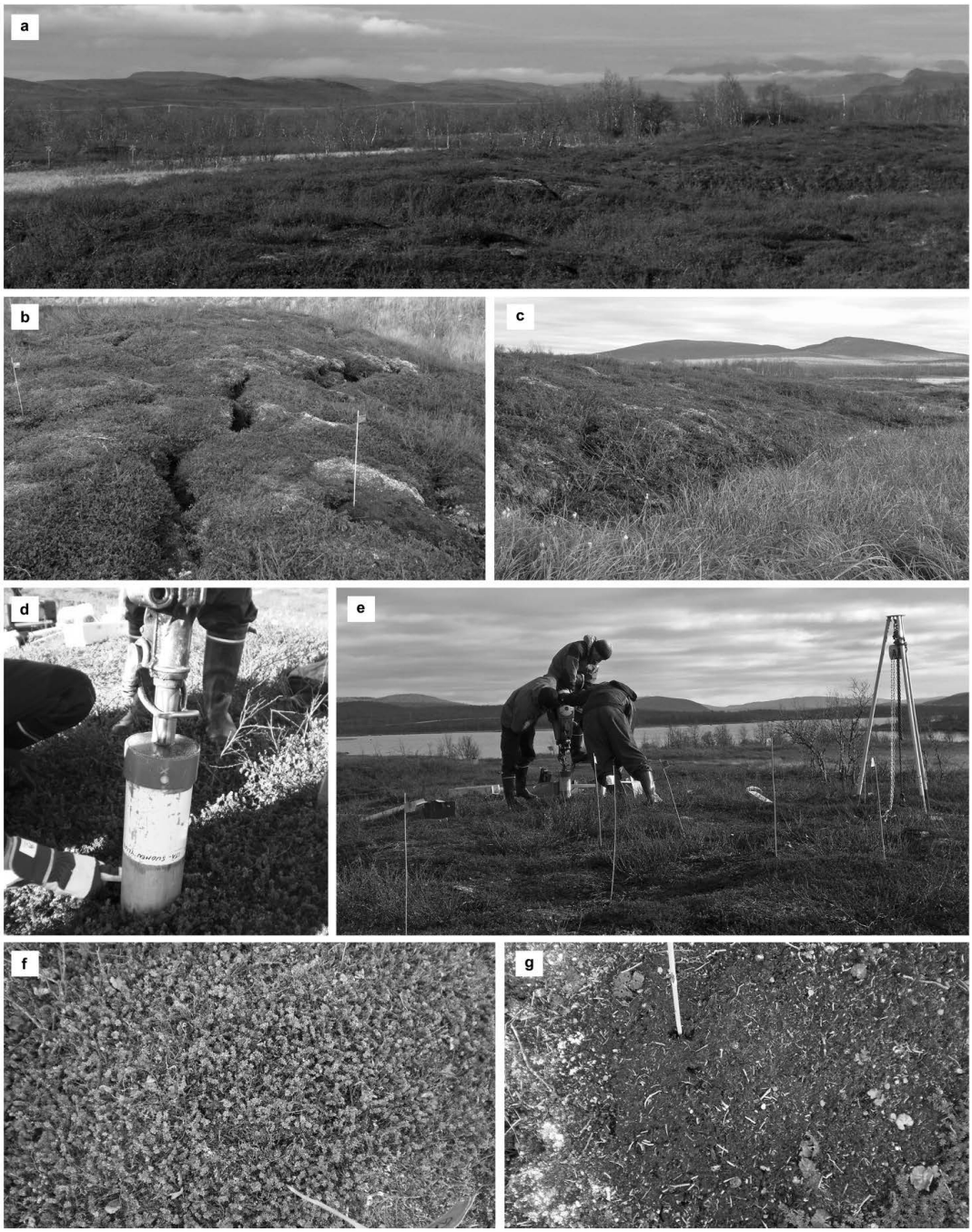

Fig. S2. Sampling site and sampling of mesocosms. a–c: Sampling location Peera Palsa (68°89'N, 21°05'E), overview of palsa surface and surrounding mire area, **d**: sampling of cores by means of steel corer, hammered into the soil using a pneumatic drill with gas powered engine. The soil cores were collected within individual plastic tubes (diameter 10 cm) that were inserted into the steel corer before drilling **e**: core sampling and lifting system, consisting of a chain connected to a pulley and tripod, **f**: vegetated palsa surface, **g**: bare palsa surface.

Fig. S3. Set-up of mesocosms in the climate chamber. a: Aluminum baths with glycol-circulated frames, filled with saltwater solution at a temperature of -4°C, keeping the submerged parts of the cores constantly frozen, **b**: cores were kept in plastic tube (here: with schematic drawing of thaw depths) and sealed from the bottom using plastic caps, **c**: cores set up in saltwater baths (here: with already lowered saltwater table for deeper thaw) in the climate chamber, with installed chambers for flux measurements, as well as soil gas collectors, pore water samplers, and soil moisture and temperature sensors.

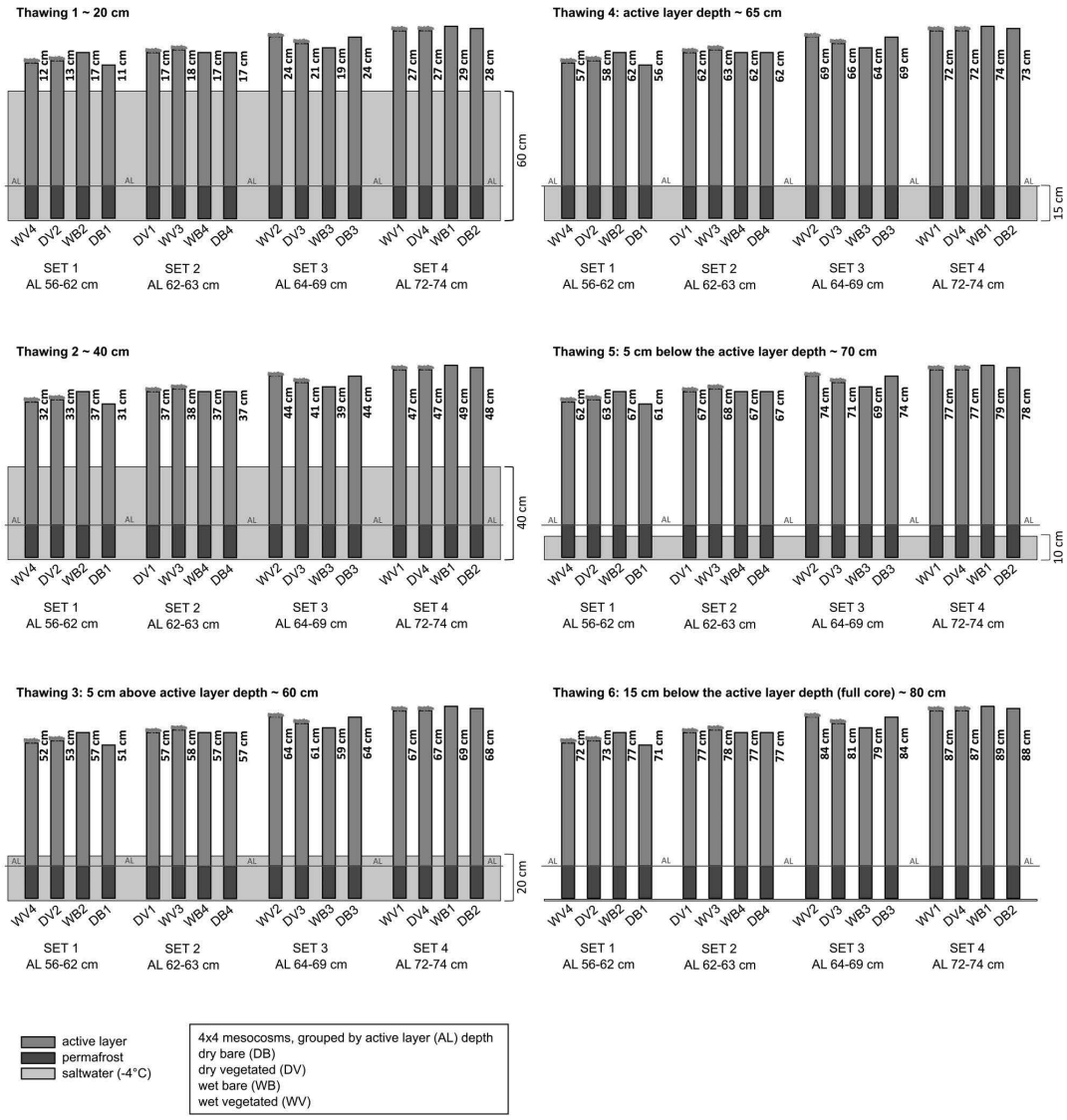

Fig. S4. Set-up of sequential thawing of the peat mesocosms. Mesocosms were grouped, lengthwise, by their respective maximum seasonal thaw depth (active layer) measured in the field. Each set of mesocosms was split into the four treatments: dry bare, dry vegetated, wet bare, wet vegetated.

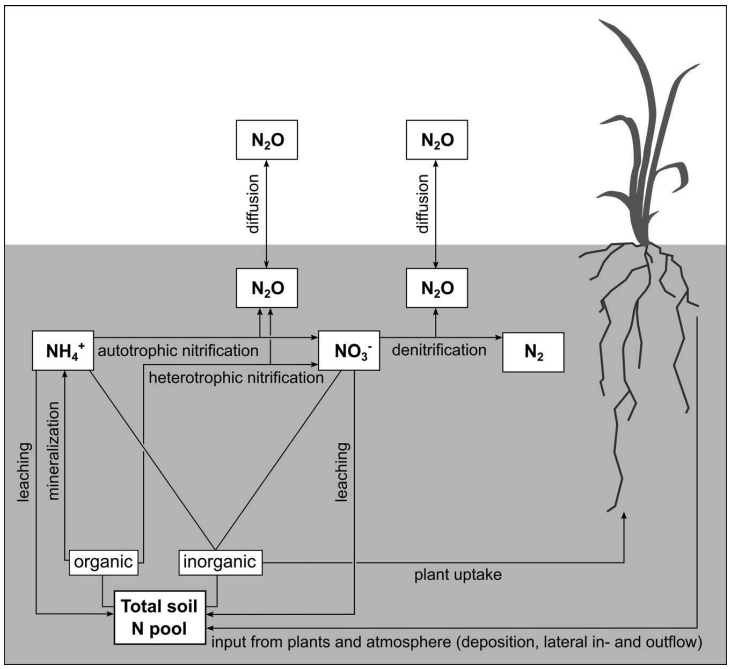

Fig. S5. Soil characteristics of the bare and vegetated mesocosms along the profile. Figure panels show bulk density, pH, soil organic matter (SOM), carbon (C), nitrogen (N), C: N ratio and water-filled pore space (WFPS). Values are shown as mean ± SE, n = 4. Soil characteristics were determined from soil slices at the respective depths, after thawing of the full core. Values are shown for the dry cores only, since leaking of water from wet mesocosms after thawing of the soil slices might have altered soil physical-chemical properties, not representing conditions during the experiment.

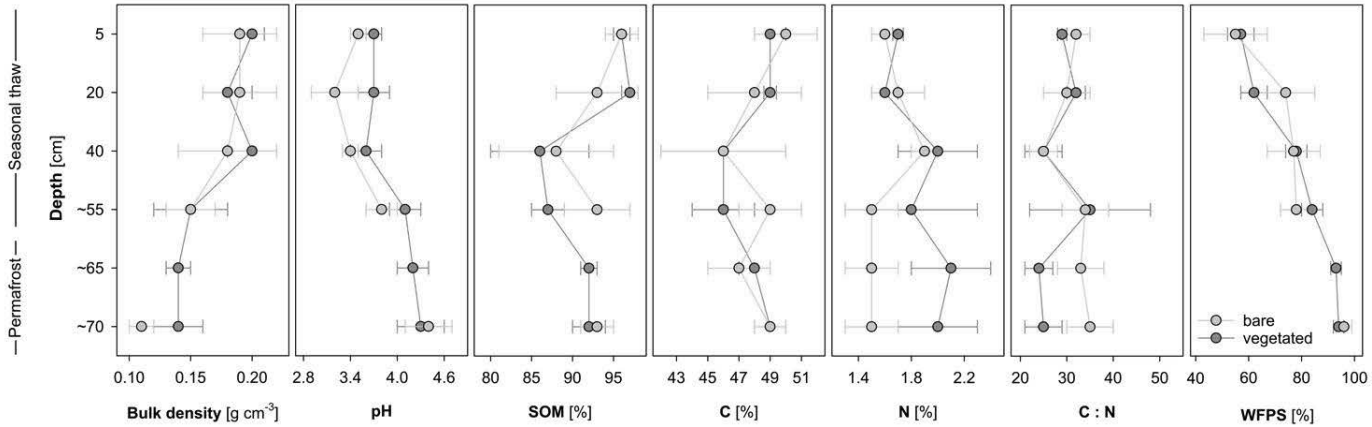

Fig. S6. Nitrous oxide (N_2O) fluxes from the four replicates of dry, bare cores (DB). Fluxes were measured 2–3 times per week. Note deviating scale for DB1 and DB2. Dashed lines represent thawing steps. Week 0: Thawing down to 20 cm, week 4: thawing down to 40 cm, week 8: thawing down to 5 cm above the maximum seasonal thaw depth; week 12: thawing down to the maximum seasonal thaw depth; week 16: thawing down to 5 cm below the maximum seasonal thaw depth; week 20: thawing of the full core (15 cm below the maximum seasonal thaw depth).

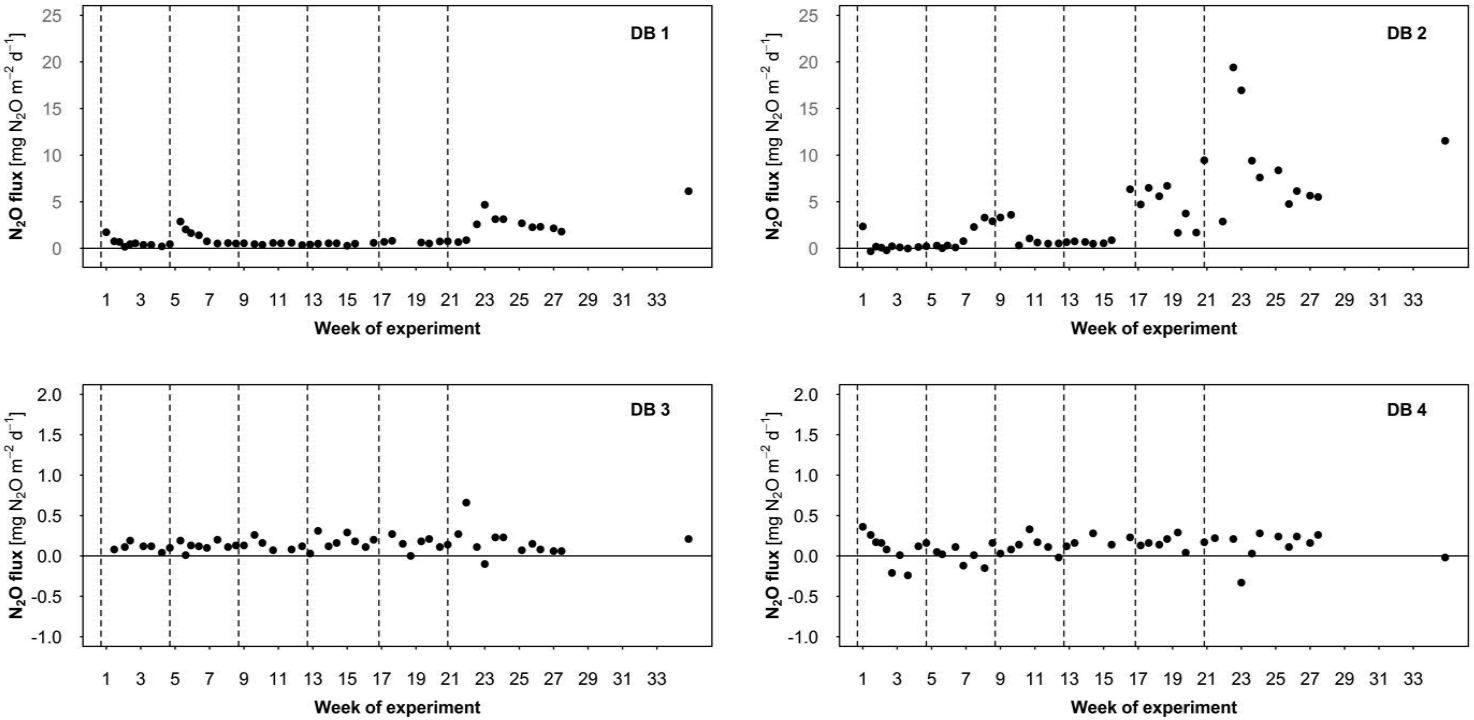

Fig. S7. Nitrous oxide (N_2O) fluxes from the four replicates of dry, vegetated cores (DV). Fluxes were measured 2–3 times per week. Dashed lines represent thawing steps. Week 0: Thawing down to 20 cm, week 4: thawing down to 40 cm, week 8: thawing down to 5 cm above the maximum seasonal thaw depth; week 12: thawing down to the maximum seasonal thaw depth; week 16: thawing down to 5 cm below the maximum seasonal thaw depth; week 20: thawing of the full core (15 cm below the maximum seasonal thaw depth).

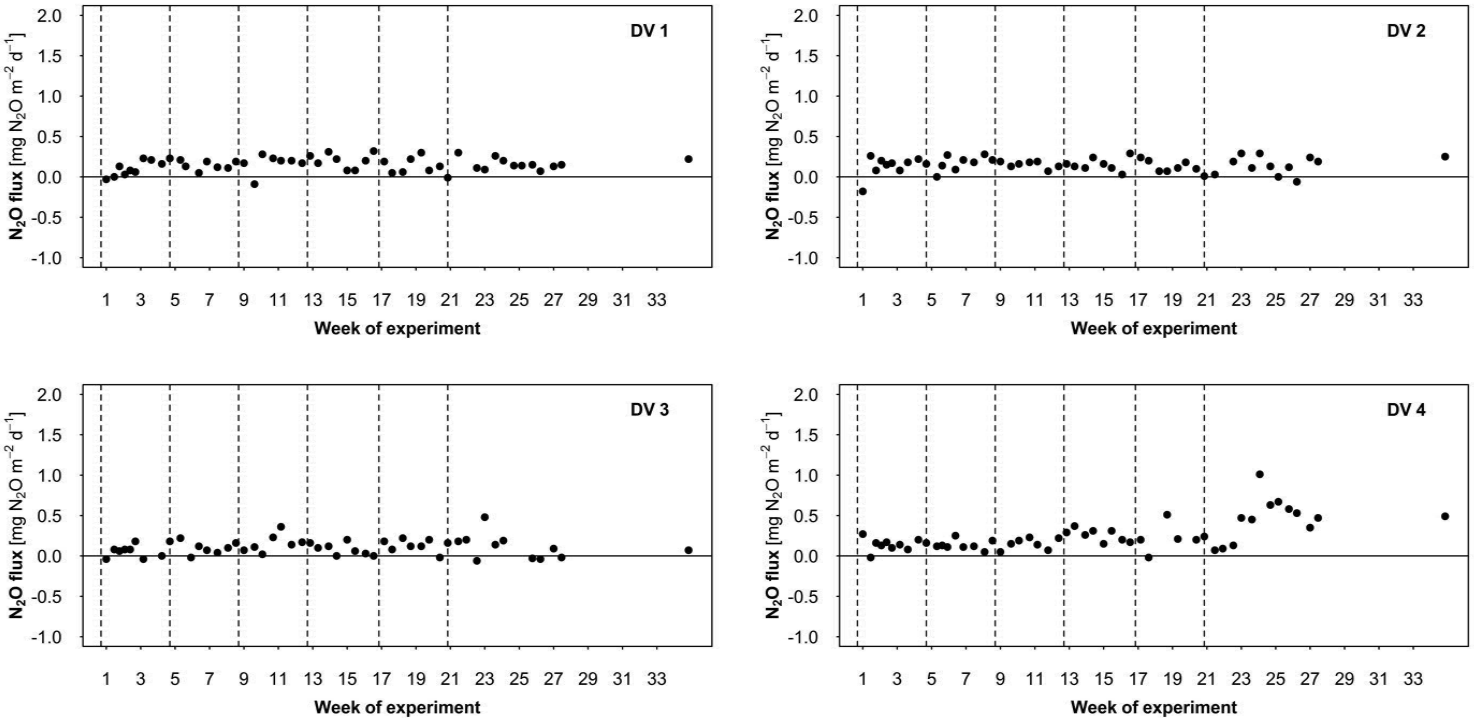

Fig. S8. Nitrous oxide (N_2O) fluxes from the four replicates of wet, bare cores (WB). Fluxes were measured 2–3 times per week. Dashed lines represent thawing steps. Week 0: Thawing down to 20 cm, week 4: thawing down to 40 cm, week 8: thawing down to 5 cm above the maximum seasonal thaw depth; week 12: thawing down to the maximum seasonal thaw depth; week 16: thawing down to 5 cm below the maximum seasonal thaw depth; week 20: thawing of the full core (15 cm below the maximum seasonal thaw depth).

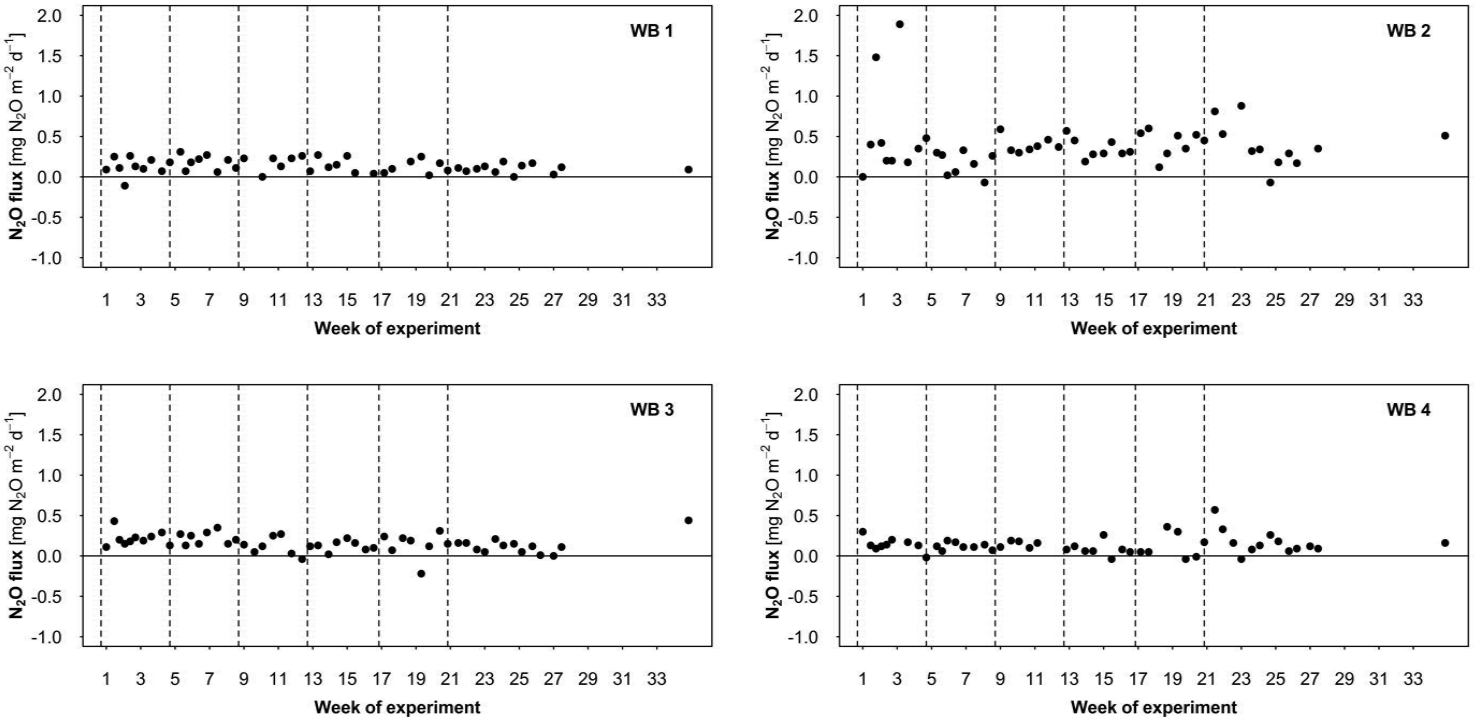

Fig. S9. Nitrous oxide (N_2O) fluxes from the four replicates of wet, vegetated cores (WV). Fluxes were measured 2–3 times per week. Dashed lines represent thawing steps. Week 0: Thawing down to 20 cm, week 4: thawing down to 40 cm, week 8: thawing down to 5 cm above the maximum seasonal thaw depth; week 12: thawing down to the maximum seasonal thaw depth; week 16: thawing down to 5 cm below the maximum seasonal thaw depth; week 20: thawing of the full core (15 cm below the maximum seasonal thaw depth).

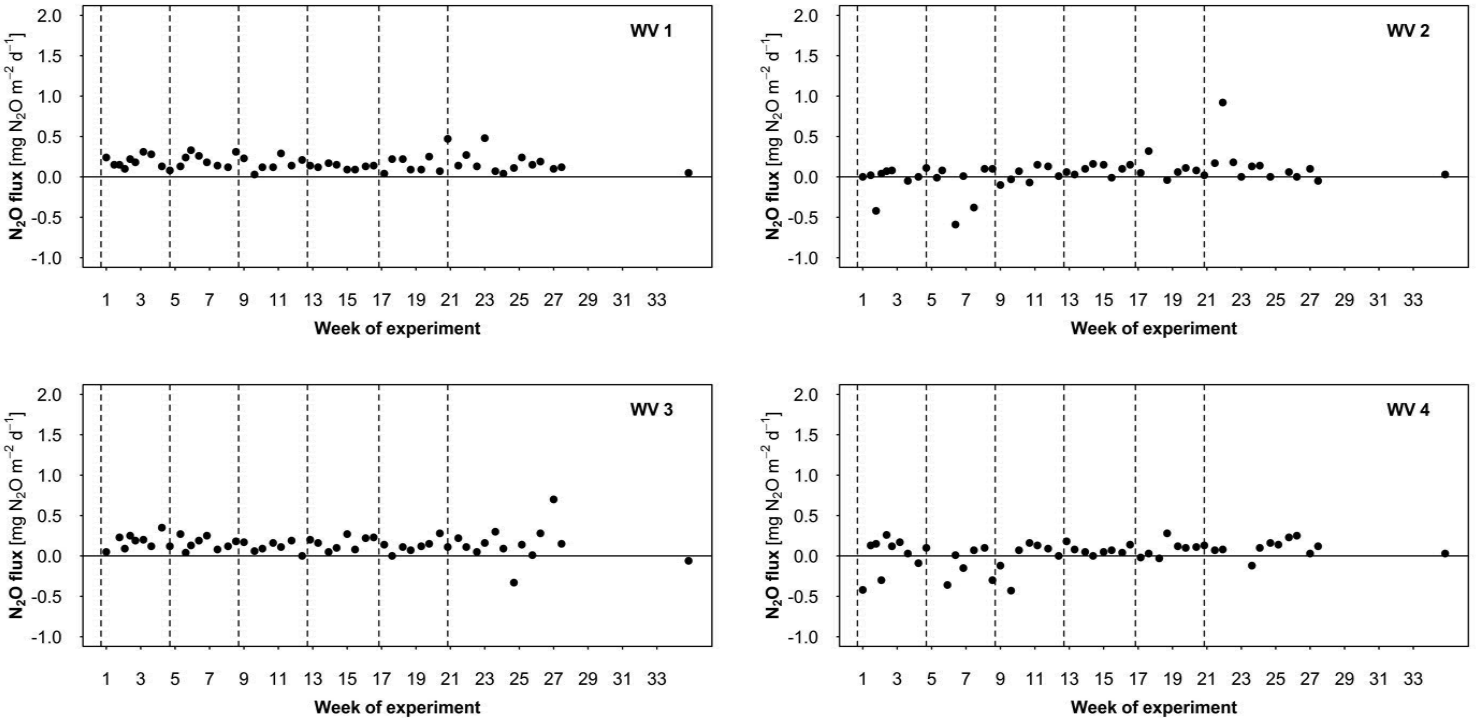

Fig. S10. Amounts of extractable nitrogen (N) and microbial biomass N in the soil profile of the four treatments. Treatment abbreviations: DB = dry bare, DV = dry vegetated, WB = wet bare, WV = wet vegetated. Concentrations were determined from soil slices at the respective depths (mean ± SE, n = 4), after thawing of the full core. Significant differences between depths, as well as the inorganic N pool split into nitrate (NO_3^-) and ammonium (NH_4^+) are shown in Table S4, Table S5.

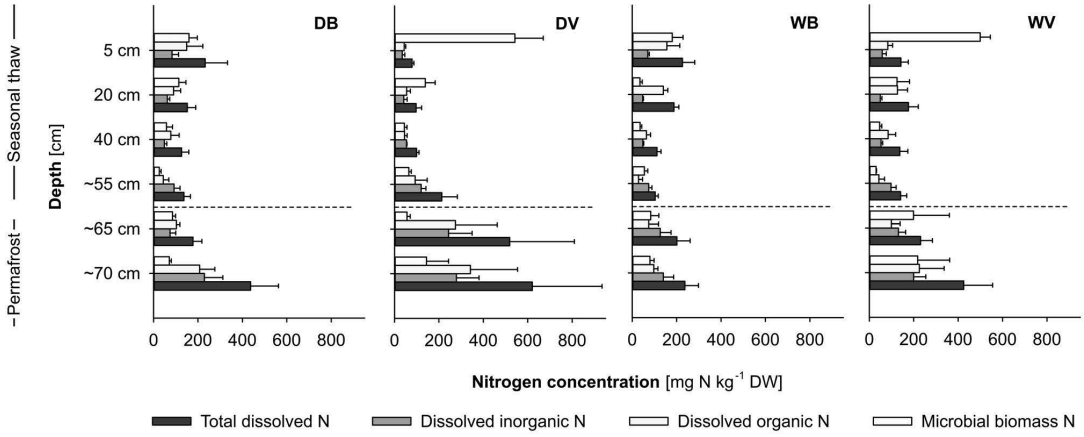

Fig. S11. Soil profile concentration of nitrous oxide (N_2O) in dry mesocosms. The panels show the N_2O concentration (atmospheric concentration = 0.3 ppm) of individual cores (dry treatment; DB = dry bare, DV = dry vegetated). Contour plots were created by linear interpolation between measurement points (n = 26). White areas: no data available due to frozen soil. Thick black line indicates thaw depths and dashed lines indicate thawing steps. Week 1: Thawing down to 20 cm, week 5: thawing down to 40 cm, week 9: thawing down to 5 cm above the maximum seasonal thaw depth; week 13: thawing down to the maximum seasonal thaw depth; week 17: thawing down to 5 cm below the maximum seasonal thaw depth; week 21: thawing of the full core (15 cm below the maximum seasonal thaw depth). Note the logarithmic scaling of colour legends.

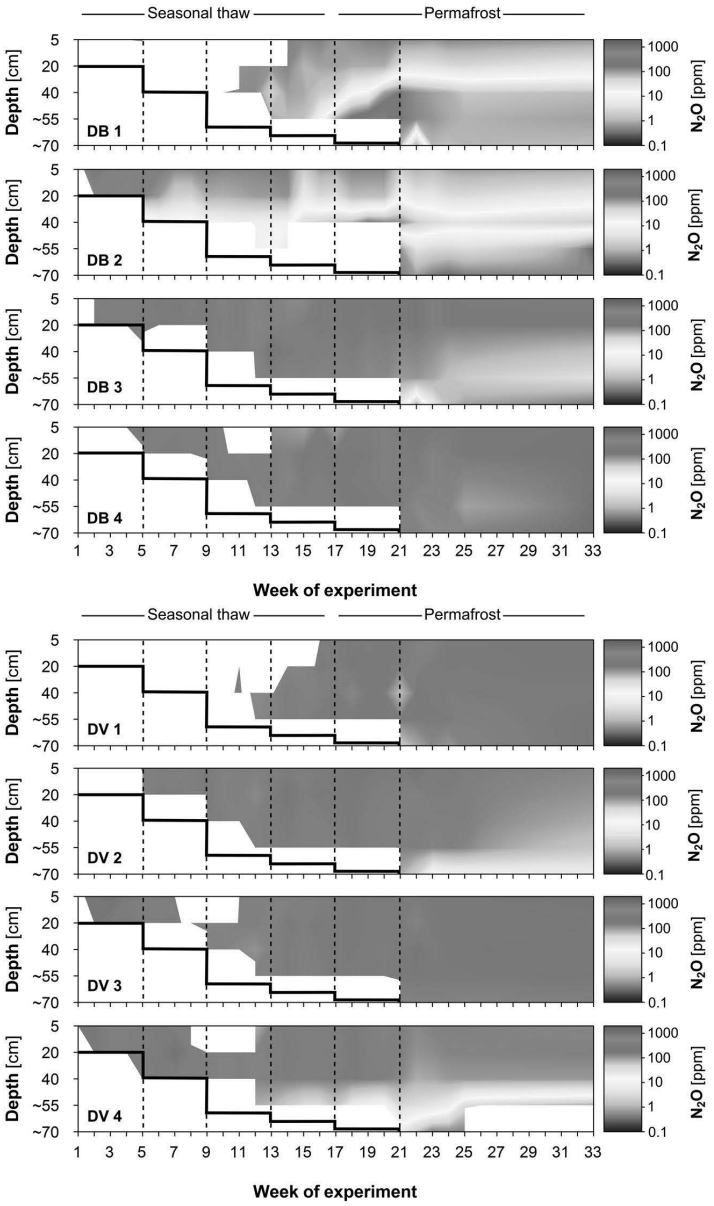

Fig. S12. Soil profile concentration of nitrous oxide (N_2O) in wet mesocosms. The panels show the N_2O concentration (atmospheric concentration = 0.3 ppm) of individual cores (dry treatment; DB = dry bare, DV = dry vegetated). Contour plots were created by linear interpolation between measurement points (n = 26). White areas: no data available due to frozen soil. Thick black line indicates thaw depths and dashed lines indicate thawing steps. Week 1: Thawing down to 20 cm, week 5: thawing down to 40 cm, week 9: thawing down to 5 cm above the maximum seasonal thaw depth; week 13: thawing down to the maximum seasonal thaw depth; week 17: thawing down to 5 cm below the maximum seasonal thaw depth; week 21: thawing of the full core (15 cm below the maximum seasonal thaw depth). Note the logarithmic scaling of colour legends.

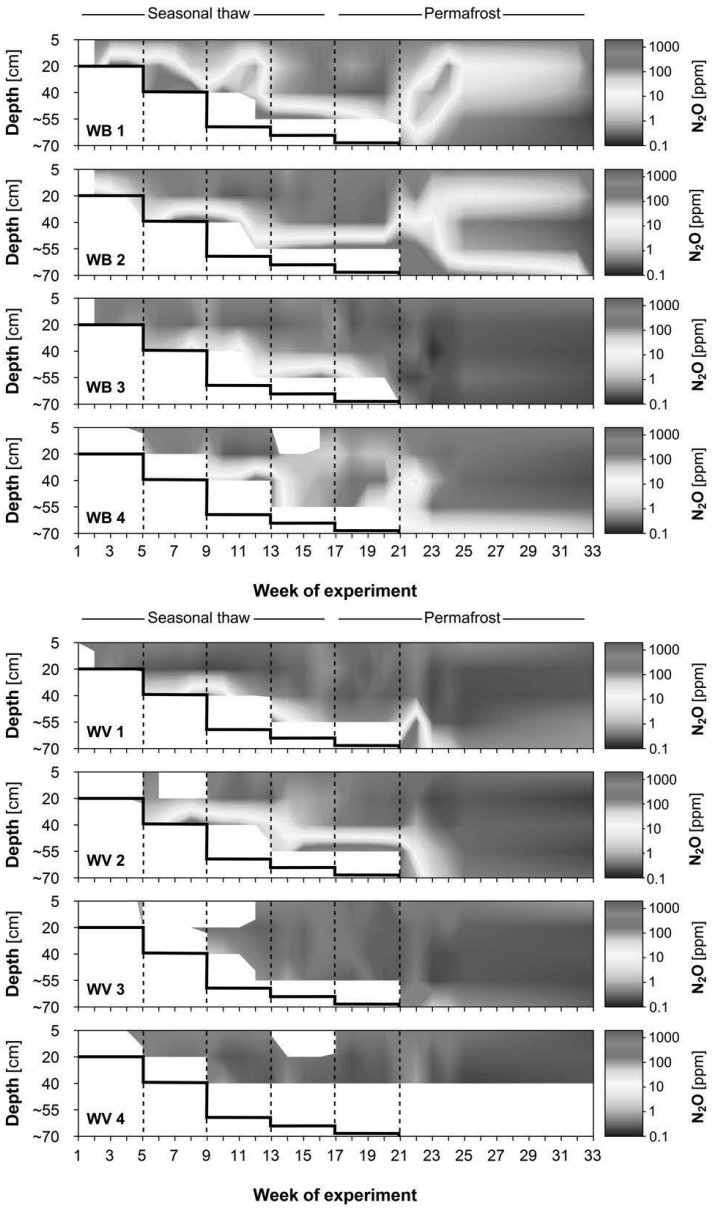

Fig. S13. Soil profile concentration of nitrous oxide (N_2O) in wet mesocosms. The panels show the N_2O concentration (atmospheric concentration = 0.3 ppm) of individual cores (wet treatment; WB = wet bare, WV = wet vegetated). Contour plots were created by linear interpolation between measurement points (n = 26). White areas: no data available due to frozen soil. Thick black line indicates thaw depths and dashed lines indicate thawing steps. Week 1: Thawing down to 20 cm, week 5: thawing down to 40 cm, week 9: thawing down to 5 cm above the maximum seasonal thaw depth; week 13: thawing down to the maximum seasonal thaw depth; week 17: thawing down to 5 cm below the maximum seasonal thaw depth; week 21: thawing of the full core (15 cm below the maximum seasonal thaw depth). Note the logarithmic scaling of colour legends.

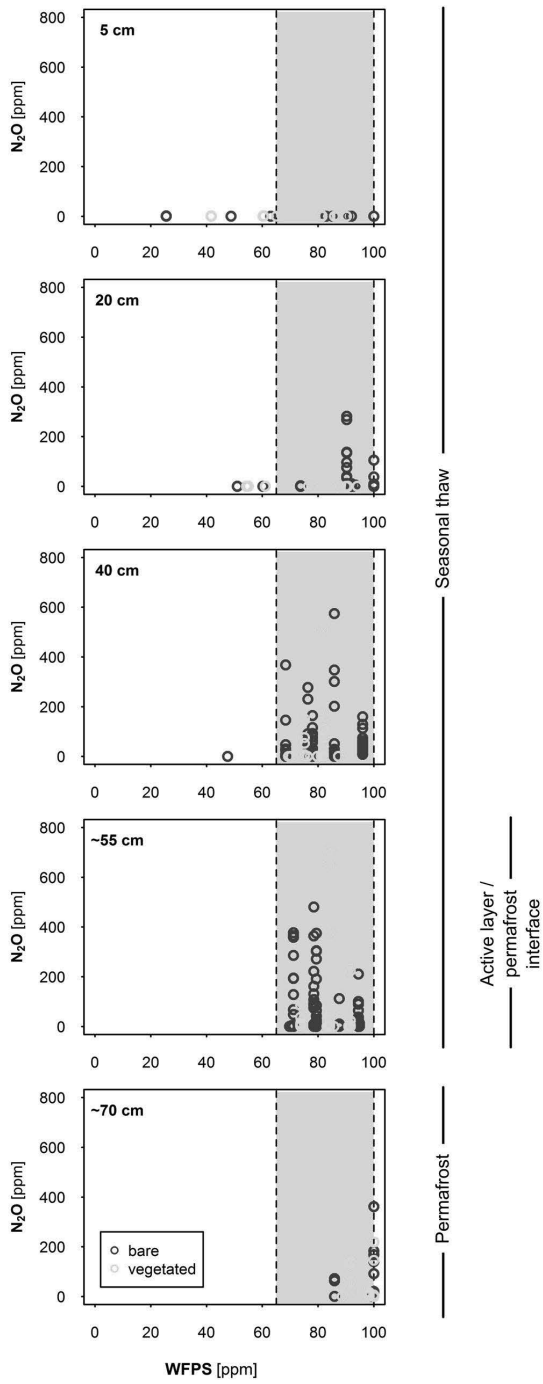

Fig. S14. Soil profile concentration of nitrous oxide (N_2O) vs. soil moisture. Different panels show concentrations in 5 depths (below surface) along the soil profile of bare and vegetated cores vs. water-filled pore space (WFPS) at the same depth. Dashed lines and grey area mark the ideal WFPS range for N_2O production from denitrification (65–100 %).

Table S1. Overview of thawing stages, thaw depths, and duration of thawing stages

Start of thawing	Thaw depth below surface [cm]	Unfrozen permafrost [cm]	Duration [weeks]
week 1	~20 cm	0	4
week 5	~40 cm	0	4
week 9	~60 cm	0	4
week 13	~65 cm	0	4
week 17	~70 cm	5	4
week 21	~80 cm	15	12

Average maximum seasonal thaw depth of the cores: 65 cm, thickness of sampled permafrost layer: 15 cm, average total length of cores: 80 cm.

Table S2. Soil physical chemical characteristics of the mesocosms. Peat characteristics in the active layer (AL) part and the permafrost (PF) part of bare and vegetated cores (mean ± SE, n = 4): bulk density (BD), pH, soil organic matter (SOM) content, carbon (C) and nitrogen (N) content, C:N ratio and water-filled pore space (WFPS).

Core type Depth	BD (g cm $^{-3}$)	pH	SOM (%)	C (%)	N (%)	C:N	WFPS (%)
Bare							
AL (0–65 cm)	0.18 ± 0.01	3.5 ± 0.1	92 ± 2	48 ± 1	1.7 ± 0.1	30 ± 2	71 ± 5
PF (65–80 cm)	0.11 ± 0.01*$^{(-)}$	4.4 ± 0.3**$^{(+)}$	93 ± 2	48 ± 2	1.5 ± 0.2	34 ± 5	96 ± 3***$^{(+)}$
Vegetated							
AL (0–65 cm)	0.18 ± 0.01	3.8 ± 0.1	92 ± 2	48 ± 1	1.7 ± 0.1	30 ± 3	70 ± 4
PF (65–80 cm)	0.14 ± 0.01*$^{(-)}$	4.2 ± 0.2*$^{(+)}$	92 ± 1	48 ± 1	2.1 ± 0.2	25 ± 2	94 ± 1***$^{(+)}$

Values are shown for the dry cores only, since leaking of water from wet mesocosms after thawing of the soil slices might have altered soil physical-chemical properties, not representing conditions during the experiment. Asterisks indicate significant differences between active layer and permafrost and $^{(+)}$ and $^{(-)}$ show whether the values in the permafrost part are significantly higher or lower compared to the active layer, respectively. Levels of significance: ***significant at $P \leq 0.001$, **significant at $P \leq 0.01$, *significant at $P \leq 0.05$. Exact *P*-values are listed in Table S3.

Table S3. *P*-values for soil physical chemical characteristics of the mesocosms

Core type	BD *P*-value	pH *P*-value	SOM *P*-value	C *P*-value	N *P*-value	C:N *P*-value	WFPS *P*-value
Bare (DB)	***0.030***	***0.003***	0.929	0.786	0.367	0.369	***0.029***
Vegetated (DV)	***0.023***	***0.015***	0.864	0.645	0.170	0.260	***<0.001***

P-values for peat characteristics are given for bare (n = 4) and vegetated (n = 4) mesocosms (dry treatment only): bulk density (BD), pH, soil organic matter (SOM) content, carbon (C) and nitrogen (N) content, C:N ratio and water-filled pore space (WFPS). *P*-values are derived from two-sample Student's t-test and show differences between the active layer and the permafrost part of the core. Measured values for peat characteristics are listed in Table S2.

Table S4. Nitrogen (N) pools in the mesocosms

Core type Depth	Total dissolved N (mg N kg $^{-1}$ DW)	NO_3^- (mg NO_3^- –N kg $^{-1}$ DW)	NH_4^+ (mg NH_4^+ –N kg $^{-1}$ DW)	Microbial Biomass N (mg N kg $^{-1}$ DW)	n
			DRY		
Bare					
AL (0–65 cm)	162 ± 28	5.4 ± 2.0	66 ± 11	90 ± 19	16
PF (65–80 cm)	307 ± 111*$^{(+)}$	2.0 ± 0.5	150 ± 70*$^{(+)}$	79 ± 12	8
Vegetated					
AL (0–65 cm)	122 ± 22	4.8 ± 0.9	58 ± 11	197 ± 60	16
PF (65–80 cm)	570 ± 199**$^{(+)}$	1.3 ± 0.4*$^{(-)}$	260 ± 68***$^{(+)}$	101 ± 49$^{)}$	8
			WET		
Bare					
AL (0–65 cm)	158 ± 20	2.1 ± 0.7	58 ± 5	79 ± 20	16
PF (65–80 cm)	219 ± 40	1.9 ± 0.7	132 ± 31**$^{(+)}$	81 ± 18	8
Vegetated					
AL (0–65 cm)	150 ± 17	2.0 ± 0.5	61 ± 8	185 ± 54	15
PF (65–80 cm)	314 ± 75**$^{(+)}$	1.9 ± 0.7	159 ± 33***$^{(+)}$	207 ± 107	7

Amounts of extractable nitrogen (N). Amounts of extractable nitrogen (N) in the active layer (AL) and the permafrost (PF) part of the bare and vegetated cores: Total dissolved N (sum of organic and inorganic N), nitrate (NO_3^-), ammonium (NH_4^+), and microbial biomass N. Values are calculated on a dry weight basis, given per kg of dried soil. Asterisks indicate significant differences between active layer and permafrost and $^{(+)}$ and $^{(-)}$ show whether the values in the permafrost part are significantly higher or lower compared to the active layer, respectively. Levels of significance: ***significant at $P \leq 0.001$, **significant at $P \leq 0.01$, *significant at $P \leq 0.05$. Exact *P*-values are listed in Table S5.

Table S5. *P*-values of nitrogen (N) pools of the mesocosms

Core type	Total N *P*-value	NO_3^- *P*-value	NH_4^+ *P*-value	Microbial Biomass N *P*-value
DB	***0.043***	0.258	***0.036***	0.723
DV	***0.004***	***0.017***	***<0.001***	0.309
WB	0.129	0.860	***0.004***	0.951
WV	***0.008***	0.976	***<0.001***	0.840

P-values are given for amounts of extractable nitrogen (N) of bare and vegetated cores, dry and wet treatment: Total N (sum of organic and inorganic N), nitrate (NO_3^-), ammonium (NH_4^+), and microbial biomass N. *P*-values are derived from two-sample Student's t-test and show differences between the active layer and the permafrost part of the core. Measured values for amounts of extractable N are listed in Table S4.

Table S6. Mean nitrous oxide (N_2O) emissions

Core type	N_2O flux, mean ± SE ($mg\ N_2O\ m^{-2}\ d^{-1}$)	MIN	MAX	n
	DRY			
Bare				
week 1–16	0.56 ± 0.11	-0.31	6.49	104
week 17–33	2.81 ± 0.6***$^{(+)}$ ($P < 0.001$)	-0.33	19.41	52
Vegetated				
week 1–16	0.14 ± 0.01	-0.18	0.37	128
week 17–33	0.20 ± 0.03*$^{(+)}$ ($P = 0.034$)	-0.06	1.01	56
	WET			
Bare				
week 1–16	0.20 ± 0.02	-0.11	1.48	120
week 17–33	0.21 ± 0.03 ($P = 0.643$)	-0.22	0.88	60
Vegetated				
week 1–16	0.08 ± 0.01	-0.59	0.35	120
week 17–33	0.13 ± 0.02 ($P = 0.062$)	-0.33	0.92	60

Nitrous oxide fluxes from bare and vegetated cores, dry and wet treatment (mean ± SE, minimum and maximum fluxes). Fluxes are averaged over week 1–16 (sequential thawing down to the maximum seasonal thaw depth) and week 17–33 (sequential thawing of the permafrost part). Asterisks indicate significant differences between week 1–16 and week 17–33 and $^{(+)}$ and $^{(-)}$ show whether the values during thawing of the permafrost are significantly higher or lower compared to fluxes measured during thawing of the active layer, respectively. Levels of significance: ***significant at $P \leq 0.001$, **significant at $P \leq 0.01$, *significant at $P \leq 0.05$. *P*-values are derived from Welch's two-sample t-test.

Table S7. Soil profile concentrations of nitrous oxide (N_2O)

Core type	5 cm		20 cm		40 cm		~55 cm (AL-10 cm)		~70 cm (AL+5 cm)	
	N_2O (ppm, mean ± SE)	**N**	**N_2O** (ppm, mean ± SE)	**n**	**N_2O** (ppm, mean ± SE)	**N**	**N_2O** (ppm, mean ± SE)	**n**	**N_2O** (ppm, mean ± SE)	**n**
	DRY									
Bare										
week 1–16	0.50 ± 0.03	51	0.83 ± 0.14	49	6.88 ± 2.01	37	2.73 ± 1.00	17	n. d.	0
week 17–33	0.58 ± 0.04	40	1.86 ± 0.34**$^{(+)}$	40	36.36 ± 7.70***$^{(+)}$	40	52.13 ± 18.34*$^{(+)}$	35	18.60 ± 6.38 $^{n. d.}$	24
Vegetated										
week 1–16	0.47 ± 0.03	45	0.44 ± 0.01	46	0.45 ± 0.01	36	0.90 ± 0.22	20	n. d.	0
week 17–33	0.42 ± 0.01	39	0.43 ± 0.01	40	0.50 ± 0.03	40	4.73 ± 2.34	39	25.05 ± 10.13 $^{n. d.}$	22
	WET									
Bare										
week 1–16	0.46 ± 0.01	59	19.61 ± 7.48	57	137.92 ± 51.92	43	138.74 ± 26.62	19	n. d.	0
week 17–33	0.42 ± 0.01**$^{(-)}$	40	5.14 ± 3.71	37	6.42 ± 2.72*$^{(-)}$	39	67.66 ± 20.72*$^{(-)}$	38	45.10 ± 20.21 $^{n. d.}$	21
Vegetated										
week 1–16	0.51 ± 0.06	50	0.44 ± 0.03	53	35.29 ± 14.33	39	107.45 ± 55.33	13	n. d.	0
week 17–33	0.40 ± 0.01	40	0.32 ± 0.02**$^{(-)}$	40	0.32 ± 0.02*$^{(-)}$	40	130.12 ± 57.88	29	18.44 ± 12.16 $^{n. d.}$	21

Nitrous oxide (N_2O) concentration in 5 depths (below surface) along the soil profile of bare and vegetated cores, dry and wet treatment (mean ± SE). Concentrations are averaged over week 1–16 (sequential thawing down to the maximum seasonal thaw depth) and week 17–33 (sequential thawing of the permafrost part). Asterisks indicate significant differences between week 1–16 and week 17–33 and $^{(+)}$ and $^{(-)}$ show whether the values during thawing of the permafrost are significantly higher or lower compared to fluxes measured during thawing of the active layer, respectively. Levels of significance: ***significant at $P \leq 0.001$, **significant at $P \leq 0.01$, *significant at $P \leq 0.05$. Exact *P*-values are listed in Table S8.

Table S8. *P*-values for nitrous oxide (N_2O) concentration of the mesocosms

Core type	5 cm	20 cm	40 cm	~55 cm (AL-10 cm)	~70 cm (AL+5 cm)
	N_2O *P*-value	N_2O *P*-value	N_2O *P*-value	N_2O *P*-value	N_2O *P*-value
DB	0.185	***0.008***	***<0.001***	***0.011***	n. d.
DV	0.174	0.787	0.138	0.111	n. d.
WB	***0.003***	0.087	***0.015***	***0.042***	n. d.
WV	0.114	***0.002***	***0.019***	0.779	n. d.

P-values are given for 5 depths (below surface) along the soil profile of bare and vegetated cores, dry and wet treatment: *P*-values are derived from Welch's two-sample t-test and show differences between the active layer and the permafrost part of the core. Measured values for N_2O soil profile concentrations are shown in Table S7.

Table S9. Linear mixed-effects model results

Fixed effects	Estimate	SE	2.5 % CI	97.5 % CI	t-value	P-value	Signif.
Intercept	3.49×10^{-1} (-1.97×10^{-2})	1.91×10^{-1}	-3.21×10^{-2}	7.27×10^{-1}	1.823	0.109	
N_2O_{AL}	3.73×10^{-2} (4.37×10^{-1})	5.22×10^{-3}	2.69×10^{-2}	4.81×10^{-2}	7.050	<0.001	***
$N_2O_{AL} : N_2O_{PF}$	-3.29×10^{-4} (-3.69×10^{-3})	5.75×10^{-5}	-4.43×10^{-4}	-2.16×10^{-4}	-5.680	<0.001	***
$N_2O_{PF} : {NH_4^+}_{PF}$	3.51×10^{-4} (-5.95×10^{-6})	1.73×10^{-4}	-1.43×10^{-5}	6.81×10^{-4}	1.978	0.055	×

Linear mixed effects model estimates of fixed effects, their standard error (SE), t-value, lower (2.5 %) and upper (97.5 %) confidence intervals (derived from bootstrapping techniques with 1000 iterations), t- and *P*-values (using Kenward-Roger approximation for the degrees of freedom) for nitrous oxide (N_2O) fluxes from dry, bare mesocosms (DB). N_2O_{AL} = N_2O soil profile concentration in the active layer part of the core, N_2O_{PF} = N_2O soil profile concentration in the permafrost part of the core, ${NH_4^+}_{PF}$ = ammonium (NH_4^+) concentration in the pore water of the permafrost part of the core. Level of significance: ***significant at $P \leq 0.001$, **significant at $P \leq 0.01$, *significant at $P \leq 0.05$, ×marginally significant at $P \leq 0.1$. Data for N_2O fluxes were log transformed prior to model parametrization. The estimate for non-transformed data is shown in brackets.

Table S10. Coverage of areas vulnerable for nitrous oxide (N_2O) emissions

	Coverage (km^2)	Coverage (% of Northern circumpolar permafrost region)
Permafrost	18.41×10^6	100
Peatlands	3.60×10^6 (2.06×10^6)	19.5 (11.2)
Thermokarst	3.82×10^6 (3.64×10^6)	20.8 (19.7)
Peatland thermokarst	2.48×10^6 (1.91×10^6)	13.5 (10.3)
Total area with high potential for N_2O emissions	4.94×10^6 (3.79×10^6)	26.8 (20.6)

Estimated areal distribution of regions with high potential for nitrous oxide (N_2O) emissions across the Northern circumpolar permafrost region: Peatlands, thermokarst, and "hot spot" areas peatland thermokarst. Peatlands include polygons with landcover classes Histels and Histosols with >15% coverage (20, 21). Thermokarst includes polygons with high (30–60%) and very high (60–100%) thermokarst coverage (24). The areas given in brackets provide the actual areas, taking into account the peatland and thermokarst coverage (1–100%) within each polygon. The area of the Northern circumpolar permafrost region (24) is based on the extent of continuous, discontinuous, sporadic and isolated permafrost (21) in Canada, Finland, Denmark, Iceland, Norway, Russia, Sweden and the United States.

References for SI Appendix

1. Borge AF, Westermann S, Solheim I & Etzelmüller B (2017) Strong degradation of palsas and peat plateaus in Northern Norway during the last 60 years. *The Cryosphere* 11(1): 1-16.

2. Sannel A & Kuhry P (2011) Warming-induced destabilization of peat plateau/thermokarst lake complexes. *Journal of Geophysical Research: Biogeosciences* 116: G03035.

3. Zoltai S (1972) Palsas and peat plateaus in central Manitoba and Saskatchewan. *Canadian Journal of Forest Research* 2(3): 291-302.

4. Seppälä M (2006) Palsa mires in Finland. *The Finnish Environment* 23: 155-162.

5. Zoltai S & Tarnocai C (1975) Perennially frozen peatlands in the Western Arctic and Subarctic of Canada. *Canadian Journal of Earth Sciences* 12(1): 28-43.

6. Seppälä M (2005) Dating of palsas. Quaternary Studies in the Northern and Arctic Regions of Finland. *Geological Survey of Finland, Special Paper* 40: 79-84.

7. Seppälä M (2003) Surface abrasion of palsas by wind action in Finnish Lapland. *Geomorphology* 52(1): 141-148.

8. Kohout T, Bućko MS, Rasmus K, Leppäranta M & Matero I (2014) Non-Invasive geophysical investigation and thermodynamic analysis of a palsa in Lapland, Northwest Finland. *Permafrost Periglacial Processes* 25(1): 45-52.

9. Pirinen P*, et al* (2012) Tilastoja suomen ilmastosta 1981–2010. The Finnish Meteorological Institute.

10. Hutchinson GL, Livingston GP, Healy RW & Striegl RG (2000) Chamber measurement of surface-atmosphere trace gas exchange: Numerical evaluation of dependence on soil, interfacial layer, and source/sink properties. *J Geophys Res-Atmos* 105(D7): 8865-8875.

11. Voigt C*, et al* (2016) Warming of subarctic tundra increases emissions of all three important greenhouse gases–carbon dioxide, methane, and nitrous oxide. *Global Change Biol.* DOI: 10.1111/gcb.13563.

12. Lide D & Frederikse H (1995) CRC handbook of chemistry and physics, vol. 76. Boca Raton: CRC Press.

13. Miranda K, Espey M & Wink D (2001) A rapid, simple spectrophotometric method for simultaneous detection of nitrate and nitrite. *Nitric Oxide: Biology and Chemistry* 5(1): 62-71.

14. Fawcett JK & Scott JE (1960) A rapid and precise method for the determination of urea. *J Clin Pathol* 13: 156-159.

15. Marushchak ME*, et al* (2011) Hot spots for nitrous oxide emissions found in different types of permafrost peatlands. *Global Change Biol* 17(8): 2601-2614.

16. Brookes PC, Landman A, Pruden G & Jenkinson D (1985) Chloroform fumigation and the release of soil nitrogen: A rapid direct extraction method to measure microbial biomass nitrogen in soil. *Soil Biol Biochem* 17(6): 837-842.

17. Vidal M & Amigo JM (2012) Pre-processing of hyperspectral images. Essential steps before image analysis. *Chemometrics Intellig Lab Syst* 117: 138-148.

18. R Core Team (2015) R: A language and environment for statistical computing. R Foundation for Statistical Computing.

19. Bates D, Maechler M, Bolker B & Walker S (2014) Lme4: Linear mixed-effects models using eigen and S4. R Package Version 1.

20. Zuur A, Ieno E, Walker N, Saveliev A & Smith G (2009) Mixed effects models and extensions in ecology with R. New York: Springer. *574 P.*

21. Brown J, Ferrians Jr O, Heginbottom J & Melnikov E (2014) Circum-Arctic map of permafrost and ground-ice conditions. National Snow and Ice Data Center.

22. Hugelius G*, et al* (2013) The Northern Circumpolar Soil Carbon Database: Spatially distributed datasets of soil coverage and soil carbon storage in the northern permafrost regions. *Earth System Science Data* 5(1): 3-13.

23. Hugelius G*, et al* (2014) Estimated stocks of circumpolar permafrost carbon with quantified uncertainty ranges and identified data gaps. *Biogeosciences* 11(23): 6573-6593.

24. Olefeldt D*, et al* (2016) Circumpolar distribution and carbon storage of thermokarst landscapes. *Nat Commun* 7: 13043.

CAROLINA VOIGT

The Arctic is warming faster than the rest of the globe, causing permafrost soils to thaw, thereby increasing greenhouse gas release to the atmosphere. Using environmental manipulation experiments, this work examines fluxes of carbon dioxide, methane, and nitrous oxide from subarctic tundra ecosystems. Besides showing enhanced release of all three greenhouse gases, this study identifies permafrost peatlands as important source of the strong greenhouse gas nitrous oxide in a future, warmer world.

UNIVERSITY OF
EASTERN FINLAND

uef.fi

PUBLICATIONS OF
THE UNIVERSITY OF EASTERN FINLAND
Dissertations in Forestry and Natural Sciences

ISBN 978-952-61-2720-0
ISSN 1798-5668